Deciphering additional mechanisms of mTORC1 signaling in skeletal muscle

Inauguraldissertation

zur

Erlangung der Würde eines Doktors der Philosophie

vorgelegt der

Philosophisch-Naturwissenschaftlichen Fakultät

der Universität Basel

von

Kathrin Chojnowska

aus Deutschland

Basel, 2019

Genehmigt von der Philosophisch-Naturwissenschaftlichen Fakultät

auf Antrag von

Prof. Dr. Markus A. Rüegg

Prof. Dr. Christoph Handschin

Basel, den 19.02.2019

Prof. Dr. Martin Spiess

Dekan der Philosophisch-Naturwissenschaftlichen Fakultät

Table of Content

1 Acknowledgements

First and foremost, I would like to express my thanks to Prof. Dr. Markus Rüegg for giving me the opportunity to develop scientific expertise and subsequently obtaining my PhD in his laboratory. I am very grateful for your continuous support in my PhD studies and all the related research projects that I have been conducting. I very much cherished your guidance and immense knowledge, the freedom to develop my own ideas and to gain expertise but also to develop my professional, as well as personal skills. I am glad for your patience, in particular throughout our sometimes rocky path and that you accepted and appreciated me as an individual with all my strength and weaknesses in your laboratory.

Besides my advisor, I would also like to thank the rest of my thesis committee: Prof. Dr. Christoph Handschin and Prof. Dr. Susan Treves for their insightful comments and encouragement, their critical questions throughout my committee meetings and other presentations. I also would like to thank both for their unique support when acquiring new techniques and utilizing their laboratory specialization. I appreciated the collaborations and I am very grateful for the teamwork. Frankly speaking, I enjoyed working with both of you and your lab members as a team a lot. Thanks to your support, I was able to widen my knowledge, and horizon on skeletal muscle research.

Sincere gratitude goes to Dr. Perrine Castets and Dr. Nathalie Rion. You have not just been incredibly helpful within the first year of my PhD by teaching me various techniques to improve precision to a very high quality standard, but you also always had an open ear, be it for scientific discussions or giving me food for thought and expertise in general.

I would also like to thank my fellow labmates for the stimulating discussions and for all the fun we have had throughout the four years. I had a wonderful time with you and I am grateful for the immense support. Special thanks to Dr. Daniel Jacob Ham for his support and expertise in lab animal handling and statistics. Thanks goes to Dr. Shuo Lin for the continuous support and knowhow be it force measurements or microscopy. I do not know whether I would still sit in front of the microscope, if it was not for your support throughout the years.

I would also like to mention the support of the “coffee gang”. You were a great sanction and I appreciated the fruitful discussions we always had. Special thanks goes to my lab-buddy, sitting next to me. You were the best support and friend I could hope for in a busy, professional work environment.

I would also like to thank the members of Prof. Dr. Bernhard Bettler’s and Prof. Dr. Michael Hall’s laboratory for their continuous support, for any technical or theoretical questions. Special thanks go to Diana Weissenberger for all the emotional support during the countless nights that I have been working. Many thanks go to Dr. Martin Gassmann for answering all my questions regarding the world of academia — which is, frankly speaking, sometimes still a mystery to me. I hope you know how much I appreciated your help, especially during the last phase of my PhD. I am certain that there is no amount of chocolate, which can possibly compensate for what you have done for me.

I thank all my friends, from school, from University, from my time at the Biozentrum and from life itself. I am proud to have an amazing chosen family that I can count on. I am in the lucky position of receiving great support from all of you. Thank you for always finding encouraging and motivating words to cheer me up when skies are grey.

Special thanks go to my family for their tremendous support throughout my PhD and my professional career in general. I would not have been able to stand here today, if it was not for you. Thank you for always being supportive, no matter which ideas I have had, what I wanted to become or where I wanted to go next. I truly appreciate your never-ending support.

Lastly, I cannot express how thankful I am for having Claude Chautems by my side. You were the best support and help I could wish for. Thank you for always being patient with me and for your ability of calming me down during this emotional and challenging chapter of my life. I very much appreciated your help, and I cannot wait to start our new chapter in Zurich and to see what the future holds for us.

2 List of Abbreviations

4E- BP1	Eukaryotic initiation factor 4E-binging protein 1
ACh	Acetylcholine
Akt/PKB	Protein Kinase B
AMP	Adenosine monophosphate
AMPK	AMP-activated protein kinase
Atg	Autophagy-related protein
ATP	Adenosine triphosphate
Ca^{2+}	Calcium
CAIN	Calcineurin inhibitor protein
CaM	Calmodulin
CaMKII	Ca^{2+}/calmodulin-dependent protein kinase II
CaN	Calciuneurin
CLAMS	Comprehensive Lab Animal Monitoring System
CR	Calorie restriction
CREB	cAMP response element-binding protein
Ctrl	Control
COX	Cyclooxygenase
CSQ	Calsequestrin
CyA	Cyclosporine A
DEPTOR	DEP domain containing mTOR-interacting protein
DHE	Dihydroethidium
DHPR	Dihydropyridine receptor
DM1	Myotonic dystrophy type 1
DMD	Duchenne muscular dystrophy
DMPK	Dystrophin myotonia protein kinase
DR	Dietary restriction
DRP1	Dynamin-related protein 1
ECC	Excitation-contraction coupling
ECRE	Elementary calcium release events
EDL	Extensor digitorum longus
EM	Electron microscope
ETC	Excitation-transcription coupling
FAO	Fatty acid oxidation
FDB	Flexor digitorum brevis
FFA	Free fatty acids

FGF-21	Fibroblast growth factor 21
FIP2000	Focal adhesion kinase family integrating protein
FIS1	Mitochondrial fission 1 protein
FKBP12	FK506 binding protein
FoxO	Forkhead box O
GAS	Gastrocnemius
GCLC	Glutamate-cysteine ligase catalytic subunit
GCLM	Glutamate-cysteine ligase regulatory subunit
GCN2	General control nonderepressible 2
GP-1	Glycogen phosphorylase, muscle specific
Gpx-1	Glutathione peroxidase 1
GS	Glycogen synthase
GSH	Reduced glutathione
GSS	Glutathione synthetase
GSSG	Oxidized glutathione
Gsta1	Glutathione S-transferase alpha 1
HSA	Human skeletal actin
HRT	Half relaxation time
H&E	Haematoxylin and eosin
IGF	Insulin-like growth factor
IMF	Intramyofibrillar mitochondria
IMM	Inner mitochondrial membrane
IRS-1	Insulin-receptor substrate 1
IP3	Inositol 1, 4 ,5,-trisphosphoate
LC3b	Microtubule-associated proteins 1A/1B light chain 3B
MAPK	Mitogen-activated protein kinase
Map1LC3B	Gene coding for LC3b (see LC3b)
Mef2a	Myocyte enhancer factor 2A
MFN	Mitofussin
mLST8	Mammalian lethal with sec-13 protein 8
MM	Mitochondrial myopathy
MRI	Magnetic resonance imaging
mRNA	Messenger ribonucleic acid
mSin1	Mammalian stress-activated map kinase-interacting protein 1
mtDNA	Mitochondrial deoxyribonucleic acid
mTOR	Mammalian/ mechanistic target of rapamycin

mTORC1/mTORC2	Mammalian/ mechanistic target of rapamycin complex 1/2
Myh	Myosin heavy-chain
MyHC	Myosin heavy-chain
Myl	Myosin light-chain
Mylk	Myosin light-chain kinase
MyoD	Myogenic factor 3
MyoG	Myogenin
nAChR	Nicotinic acetylcholine receptors
NAD+	Oxidized nicotinamide adenine dinuleotide (NAD)
NADH	Reduced nicotinamide adenine dinuleotide
NADPH	Reduced nicotinamide adenine dinucleotide phosphate
N.D.	Not detectable
nDNA	nucleic DNA
NFAT	Nucleic factor of activated T-cell
NMJ	Neuromuscular junction
NRF2	NF-E2-related factor 2
OMM	Outer mitochondrial membrane
OPA1	Mitochondrial dynamin like GTPase
OXPHOS	Oxidative phosphorylation
p62	Sequestosome 1
PAS	Periodic acid schiff
PDK1	Phosphoinositide-dependent kinase 1
PGC-1α	Peroxisome proliferator-activated receptor γ coactivator 1α
PGM-2	Phosphoglucomutase 2
PI3K	Phosphoinositide 3-kinase
PLN	Phospholamban
PRAS40	Proline-rich Akt substrate 40kDa
PTEN	Phosphatase and tensin homolog
PV	Parvalbumin
PYGM-1	Glycogene phosphorylase, muscle associated
RAPA	Rapamycin
RLC	Regulatory light chain
ROS	Reactive oxygen species
RyR	Ryanodine receptor 1
SDH	Succinate dehydrogenase

SIRT1	Sirtuin-1
SS	Subsarcolemmal mitochondria
qPCR	quantitiative polymerase chain reaction
RAmKO	*Raptor* muscle-specific knockout mice
Raptor	Regulatory-associated protein of mTOR
Rheb	Ras homolog enriched in brain
ROS	Reactive oxygen species
RT	Room temperature
SEM	Standard error of the mean
SERCA	Sarcoplasmic/endoplasmic reticulum calcium ATPase
SOL	Soleus
SR	Sarcoplasmic reticulum
SREBP	Sterol responsive binding protein
S6	Ribosomal protein S6
S6K	Ribosomal protein S6 kinase
TA	Tibialis anterior
TF	Transcription factor
TFEB	Transcription factor EB
TPT	Time-to-peak tension
Trib3	Tribbles pseudokinase 3
TSC1/TSC2	Tuberous sclerosis 1/2
TSCmKO	*Tsc1* muscle-specific knockout mice
ULK1	Unc-51-like autophagy activating kinase 1

3 Aim of the Study

Skeletal muscle comprises about 40% of the body mass and plays an essential role in metabolism and movement. It is a highly plastic tissue that adapts to its use and is modulated in disease and aging. The gradual age-associated loss of muscle mass and muscle force or strength, known as sarcopenia, greatly decreases the quality of life for it results in immobility and subsequently morbidity. The causes of sarcopenia are multifactorial and can include genetic and environmental factors. In mice and humans, reducing the mammalian target of rapamycin complex 1 (mTORC1) signaling increases longevity and reduces age-associated pathologies. This suggests that the inhibition of mTORC1 may be a useful therapeutic strategy to maintain muscle mass and strength, and a promising therapeutic strategy to delay the progression of sarcopenia.

mTORC1 is a serine-threonine kinase that senses stress, growth factors, and nutrients to initiate translation and regulate cell growth and cell size; it also negatively regulates autophagy. The mTOR pathway is therefore crucial for maintaining cell homeostasis by balancing protein synthesis and protein degradation.

Several years ago, muscle-specific TSC1 knockout (TSCmKO) mice were generated and characterized by Castets et al. (Castets et al, 2013). These mice develop a severe late-onset myopathy, kyphosis, and ER stress due to sustained activation of the mTORC1 signaling pathway in skeletal muscle tissue. Specifically, these TSCmKO mice show a severe loss of muscle mass and muscle strength, an increase in ER stress, impaired autophagy, and premature death (Castets et al, 2013; Guridi et al, 2016). Some of these characteristics are signs and symptoms of sarcopenia.

The aim of this study was to further characterize and understand the development of the myopathy of the TSCmKO mice by focusing on mechanisms that are directly or indirectly regulated by mTORC1. I particularly focused on the mitochondrial phenotype to identify whether this phenotype is a cause of the myopathy or a consequence triggered through accumulating damage and impairing autophagy. Additionally, I aimed to find a way to decrease

myopathic features in the skeletal muscle of TSCmKO mice and to increase muscle function. Therefore, calorie restriction was used to decrease sarcopenic features and to induce positive effects on skeletal muscle pathophysiology in TSCmKO mice.

4 Outline of the Thesis

Chapter I: Introduction

Chapter I briefly introduces the composition and function of skeletal muscle as a plastic organ in health and disease. This chapter also outlines the importance of the mammalian target of rapamycin in skeletal muscle homeostasis.

Chapter II: Sustained activation of mTORC1 in skeletal muscle causes impaired mitophagy with a subsequent increase in mitochondrial size but without altering mitochondrial homeostasis

As they age, TSCmKO mice revealed a gradually developing mitochondrial phenotype in skeletal muscle. The increase in mitochondrial density is associated with increased oxidative stress and a concomitant increase in the antioxidative stress response. This suggests that mitochondrial and oxidative changes remain balanced in muscle from old TSCmKO mice. Further characterization of the muscle phenotype validated TSCmKO mice as a potential model for sarcopenia.

Chapter III: Long-term calorie restriction reduces skeletal muscle myopathy in TSCmKO mice

The effects of calorie restriction (CR) on skeletal muscle of TSCmKO mice was investigated. Long-term CR treatment significantly reduced sarcopenic and myopathic features in TSCmKO mice without altering the activity of mTORC1. This indicates that the TSC1-mTORC1 signaling pathway is not essential for mediating the beneficial effects of CR in skeletal muscle physiology.

Chapter IV: Sustained activation of mTORC1 in skeletal muscle disturbs calcium homeostasis and excitation-transcription coupling

In this part of the thesis, by using various biochemical and electrophysiological techniques, I identified that the excitation-contraction coupling and excitation-transcription coupling was directly influenced by sustained mTORC1 activation in TSCmKO mice. It is very likely that the disruptions in calcium signaling are responsible for the loss in muscle isometric forces, as well as for influencing various transcriptional signaling pathways within skeletal muscle.

5 Introduction

5.1 Skeletal muscle in health and disease- a metabolic organ

Skeletal muscle plays a fundamental role in mobility, disease prevention, and quality of life as it is the biggest metabolic organ in the human body, comprising 40% of the body lean mass. Muscle is a highly plastic tissue. It is subdivided into smooth muscle and striated muscle (cardiac muscle and skeletal muscle). Skeletal muscle is responsible for the coordination and the movement of the organism/body, innervated via the somatic nervous system, and is also important for the control of breathing and thermogenesis (Merrell & Kardon, 2013; Periasamy et al, 2017). The smallest units of striated muscle are the muscle fibers (Figure I), which build muscle fiber bundles surrounded by a perimysium. The so-called fascicles are again bundled together surrounded by an epimysium, building the full muscle as a unit. A tendon anchors muscle to the bone or cartilage to enable a proper and directed muscle function (Apostolakos et al, 2014). Nevertheless, muscle can also be directly connected to the skeletal system (Apostolakos et al, 2014).

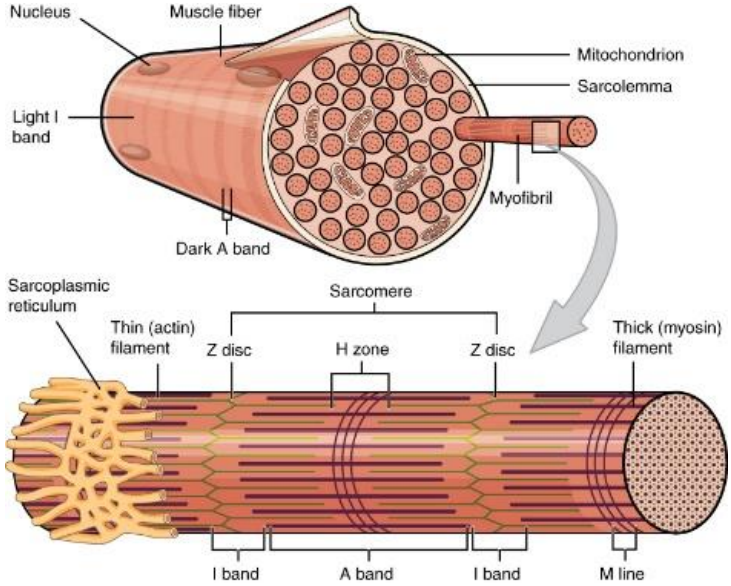

Figure I: Illustrated depiction of a muscle fiber, with its subunits. (Betts, 2018)

On a smaller scale, due to the density of particular proteins differentially expressed in certain areas, striated muscle reveals its striation in electron microscopic (EM) pictures. The A-band represents the overall myosin filament area, including an H-band (myosin without actin) and an M-line, which is the area in which only transverse myosins are present. Additionally, there is a lighter I-band, predominantly containing actin filaments, including the Z-line, exclusively containing actin-binding proteins. The overall unit from one Z-line to another is termed

sarcomere, and it contains all the important contractile elements of the striated muscle (Frontera & Ochala, 2015). In order to generate muscle contraction and subsequently muscle force, a nerve signal (action potential) triggers the release of acetylcholine into the synaptic cleft at the endplate of the neuromuscular junction (NMJ) (Kuo & Ehrlich, 2015). This initiates an action potential propagating across the sarcolemma into the t- (or transverse) tubules. A cascade of different voltage sensitive receptors is activated, leading to a subsequent release of calcium (Ca^{2+}) from the sarcoplasmic reticulum (SR) into the cytosol, where Ca^{2+} binds to troponin, which exposes myosin-binding sites. More details on the excitation-contraction coupling can be found in chapter 3. Troponin then forms a cross bridge with the actin filaments and initiates a contraction. Ca^{2+} is then actively transported back into the SR and troponin blocks the myosin binding sites, leading to muscle fiber relaxation (Kuo & Ehrlich, 2015).

Mammalian skeletal muscles are composed of two different types of fibers: slow fibers, mainly containing myosin heavy chain I; and fast fibers, which are divided into three subgroups: Type IIa, Type IIx and Type IIb (Schiaffino & Reggiani, 2011). Slow-twitch muscle (e.g. soleus) contracts more slowly, due to smaller NMJs, an increased amount of mitochondria, and their reliance on aerobic metabolism. Fast fibers (e.g. extensor digitorum longus (EDL), tibialis anterior (TA) and gastrocnemius (GAS)) contract more rapidly thanks to the presence of faster myosins (Schiaffino & Reggiani, 2011). More on this subject can be found in chapter 3.

As mentioned above, skeletal muscle coordinates muscle force generation, function and movement, but it is also a very important metabolic organ. Therefore, it has to maintain its function upon extrinsic and intrinsic stimuli. For this purpose, a defined balance between protein synthesis and degradation is of major importance to regulate muscle homeostasis. This includes various mechanisms to regulate protein synthesis, through translation and transcriptional processes, but also post-translational modifications, protein folding, and subsequently protein degradation through macro- and micro-autophagy and the proteasome system (Mitch & Goldberg, 1996; Sandri, 2010; Tipton et al, 2018).

Skeletal muscle dystrophies or skeletal muscle myopathies have been shown to affect skeletal muscle function, muscle force and muscle coordination and whole body metabolism (Allen et al, 2010; Menazza et al, 2010; Tarnopolsky, 2016). Subsets of specific organelles are affected in certain myopathies, such as mitochondria, the powerhouse of the cell (Jongpiputvanich et al, 2005; Komulainen et al, 2015). A change in mitochondrial size and/or number can have either beneficial effects, as seen for example in exercise studies (Axelrod et al, 2018; Baldwin et al, 1972; Holloszy, 1967; Hood et al, 2018) or detrimental effects, as known from certain mitochondrial myopathies (Ahmed et al, 2018). Also, the inability to use certain fuels, such as glycogen, can lead to muscle myopathy, as seen in Pompe disease (Kohler et al, 2018). It was additionally shown that the myokine FGF-21, a hormone excreted by skeletal muscle upon cellular stress, effects whole body metabolism (Guridi et al, 2015).

5.2 mTORC1 and its role in skeletal muscle

One of the major regulators of protein synthesis and degradation in skeletal muscle is the mammalian (or mechanistic) target of rapamycin (mTOR). mTOR exists in two distinct complexes: mTOR complex 1 (mTORC1), which is responsible for the regulation of cell growth, cell size, translation and also protein degradation (Castets et al, 2013; Holz et al, 2005; Saxton & Sabatini, 2017); and mTOR complex 2 (mTORC2), which is mainly responsible for the organization of the cytoskeleton, cell proliferation, and survival (Garcia-Martinez & Alessi, 2008; Jacinto et al, 2004; Oh & Jacinto, 2011). mTORC1 and 2 are assembled from various subunits. Both contain the DEP domain containing mTOR-interacting protein (DEPTOR), an endogenous kinase inhibitor (Peterson et al, 2009), the mammalian lethal with sec-13 protein 8 (mLST8) — whose distinct function is currently unknown — and the Tti1/Tel2 complex (Laplante & Sabatini, 2012b). Whereas mTORC1 contains an additional proline-rich Akt substrate 40kDa (PRAS40) and the regulatory-associated protein of mTOR (raptor) (Laplante & Sabatini, 2012b), mTORC2 contains the rapamycin-insensitive companion of mTOR (rictor), as well as the mammalian stress-activated map kinase-interacting protein 1 (mSin1) (Laplante & Sabatini, 2012b).

As a key player in regulating cellular homeostasis, mTORC1 and its activity are controlled by several upstream pathways sensing nutrients, growth factors, and stress hormones. mTORC1 additionally senses energy availability and amino acids (Bar-Peled & Sabatini, 2014; Goberdhan et al, 2016; Xu et al, 2012). Upon an upstream stimulus, in particular insulin, a downstream cascade is activated (Figure II). Binding of insulin or insulin-like growth factors (IGFs) to their receptors initiates the recruitment and phosphorylation of the insulin-receptor substrate 1 (IRS-1) and finally leads to the activation of the lipid kinase phosphatidylinositol-4, 5-bisphosphate 3-kinase (PI3K) signaling pathway (Laplante & Sabatini, 2009; 2012a). <<

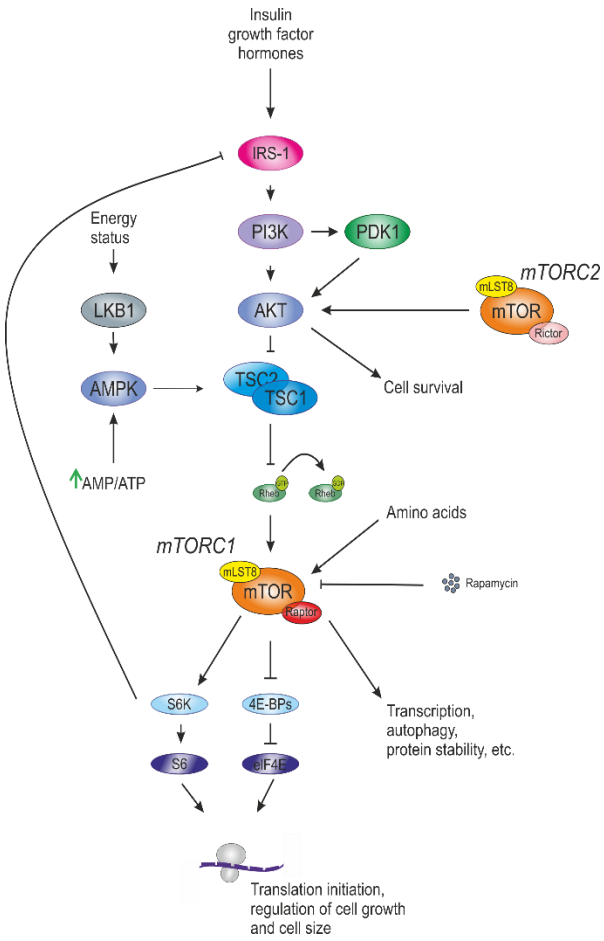

Figure II: mTOR-signaling pathway at a glance

This activation includes the recruitment of the serine/threonine protein kinase B (PKB/Akt) to the membrane and the following auto-phosphorylation of the phosphoinositite-dependent kinase 1 (PDK1). Activating the PKB/Akt axis disturbs the interaction of the tuberous sclerosis complex 1 (TSC1) and tuberous sclerosis complex 2 (TSC2), which is directly phosphorylated by AKT (Inoki et al, 2002; Manning et al, 2002). Subsequently, the TSC1/TSC2 complex, functioning as a GTPase-activating protein, inhibits the small GTPase Ras homolog enriched in brain (Rheb) (Inoki et al, 2003; Tee et al, 2003). GTP-Rheb is a direct activator of mTORC1. Protein kinase B (AKT) can also a activate mTORC1 in a TSC1/2 independent manner through phosphorylation of PRAS40 (Sancak et al, 2007; Thedieck et al, 2007; Vander Haar et al, 2007). Another mechanism of mTORC1 activation, and one, which is independent of the PKB/AKT-axis, is the activation of adenosine monophosphate-activated protein kinase (AMPK) (Gwinn et al, 2008; Shaw et al, 2004). Cells

with low energy levels and a high AMP/ATP ratio activate AMPK, which subsequently phosphorylates TSC2, directly increases Rheb and subsequently inhibits mTORC1. AMPK can also inhibit the binding of raptor through its direct phosphorylation. Lastly, mTORC1 is known to sense amino acids, such as arginine and leucine (Jewell et al, 2015; Jung et al, 2015; Rebsamen et al, 2015). Precise, studies have revealed that both amino acids are crucial for mTORC1 activation (Chantranupong et al, 2016; Wolfson et al, 2016). Extracellular amino acids are transported into the cell by the vacuolar proton pump H^+-ATPase (v-ATPase), which is responsible for the acidification of the lysosome and for the integration of various lysosomal transmembrane proteins. v-ATPase is assembled into a complex with the pentameric protein complex Ragulator and the Rag GTPases, which are located closely to the lysosomal surface (Shimobayashi & Hall, 2016). Due to increasing levels of amino acids, Ragulator and v-ATPase undergo conformational changes, activating the heterodimeric protein Rag, and recruiting mTORC1 to the lysosomal membrane. Through this translocation of mTORC1 and the final activation through Rheb-GTP, mTORC1 initiates, on the one hand, anabolic programs, such as translation and cell size determination. On the other hand, it represses catabolic processes, e.g. autophagy (Jung et al, 2010; Rabanal-Ruiz et al, 2017).

mTORC1 is an atypical serine threonine kinase which, upon activation, phosphorylates the ribosomal protein S6 p70 kinase 1 (S6K1, Threonine 389 residue), thereby controlling nucleotide and ribosome synthesis, and activating several proteins involved in mRNA translation initiation (Holz et al, 2005). mTORC1 also phosphorylates eukaryotic initiation factor 4E-binging protein 1 (4E-BP1, Serine 65 residue), negatively regulating 5'cap-dependent mRNA translation by sequestering eIF4E. Both aforementioned phosphorylations trigger catabolic processes (Gingras et al, 1999). mTORC1 is additionally involved in the regulation of lipid synthesis through the sterol responsive binding protein (SREBP), a master regulator of lipo- and sterolgenic gene transcription (Duvel et al, 2010; Saxton & Sabatini, 2017). As a final point, mTORC1 also negatively regulates degradative processes such as autophagy, over the phosphorylation of Unc-51-like autophagy activating kinase 1 (ULK1, Serine 757 residue) (Castets et al, 2013).

Autophagy is the autophago-lysosomal degradation of defective material, such as organelles, aggregate-prone proteins and toxins. Activation of autophagy through starvation or other cellular stressors leads to the mTORC1 dependent activation of transcription factor EB (TFEB). TFEB translocates into the nucleus and initiates translation of autophagy-related genes, such as *Atg4*, *Atg9B* and *Map1LC3B,* to only name three (Settembre et al, 2011). On the other hand, TFEB functions as a master regulator of lysosomal biogenesis (Sardiello et al, 2009). Upon ubiquitination and the subsequent recruitment of the ubiquitin binding protein p62 to defective organelles and proteins, ULK1 forms a complex with ATG13, ATG101 and FIP2000, thus initiating the formation of the pre-autophagosome (Ganley et al, 2009; Hara et al, 2008; Hosokawa et al, 2009). The autophagosome is assembled upon recruitment of additional factors such as ATG3, ATG7, the lipidation of the cytosolic protein LC3I to LC3II, and the subsequent translocation to the outer membrane of the pre-autophagosome (Mizushima et al, 2011; Weidberg et al, 2011). The autophagosome fuses with the lysosome, containing acid hydrolases, for the degradation of defective material. Through the phosphorylation and inactivation of ULK1 by mTORC1, autophagy is impaired (Castets et al, 2013).

As a key regulator of muscle homeostasis, mTORC1 plays an important role in defining muscle health. To elucidate the role of mTORC1 in skeletal muscle, a mouse line, specifically lacking TSC1 in skeletal muscle, termed TSCmKO, was previously generated (Castets et al, 2013). TSCmKO mice were obtained by crossing mice with a conditional *Tsc1* allele, in which exon 16 and 17 were flanked by loxP sites, with mice expressing Cre-recombinase under the control of the human skeletal actin promotor (HAS) (Cre-LoxP system). The deletion of TSC1 leads to sustained activation of mTORC1, exclusively in skeletal muscle tissue. Several studies have shown that the disruption of mTORC1 signaling in skeletal muscle can have detrimental consequences not only for muscle performance but also for the health and lifespan of the animal. For example, Bentzinger et al. have shown that *Rptor* deletion in mouse skeletal muscle tissue (RAmKO) results in smaller muscle fibers, skeletal muscle myopathy, and a lethal dystrophy, with a premature death around the age of 5-6 months (Bentzinger et al, 2008). Short-term activation of mTORC1 through denervation induced muscle fiber hypertrophy and

was able to reverse the atrophic phenotype (Bentzinger et al, 2013). Surprisingly, sustained activation of mTORC1 in mouse skeletal muscle tissue through the knockout of *Tsc1* lead to muscle atrophy and an increase in oxidative capacity (Castets et al, 2013). Later, it was also shown that *Tsc1* deletion in skeletal muscle leads to an impairment in autophagy and a severe late onset myopathy, which are characterized by a loss in isometric muscle force and subsequent death around the age of 9-12 months. In addition, protein synthesis was significantly increased in TSCmKO mice (Castets et al, 2013). Rapamycin, an allosteric inhibitor of mTORC1, was sufficient to restore skeletal muscle composition and function in TSCmKO mice.

Studies of both TSCmKO and RAmKO mice clearly demonstrate that the balance between mTORC1 activation and suppression is important to maintain muscle homeostasis, and, lastly muscle function. For example, it has been shown that the deletion of *Tsc1* in mouse skeletal muscle affects whole-body metabolism (Guridi et al, 2015). TSCmKO mice were leaner, showed an increase in insulin sensitivity, and an increase in fatty acid oxidation (FAO). Changes in other metabolic tissues, such as browning of white adipose tissue, as well as the increase in liver FAO and increased ketogenesis, were also observed (Guridi et al, 2015). Those effects were triggered by the increase in ER stress in TSCmKO mice, which led to the release of the myokine fibroblast growth-factor 21 (FGF-21), a hormone stimulating glucose uptake and fatty acid oxidation. In addition, RAmKO mice have been analyzed for their metabolic phenotype. A study in 2016 has shown that RAmKO mice have a lean phenotype, develop insulin resistance, and display an increase in energy expenditure already at a young age (ten weeks) (Guridi et al, 2016). Suppression of mTORC1 activity, as well as a sustained activation, both have detrimental consequences, not just on skeletal muscle, but also other organs and metabolism at the whole-body level.

6 Chapter 1: Sustained activation of mTORC1 in skeletal muscle causes impaired mitophagy with a subsequent increase in mitochondrial size but without altering mitochondrial homeostasis

6.1 Summary

Several myopathic and sarcopenic characteristics were previously described in the TSCmKO mice, including an impairment in autophagy and certain pathological features of mitochondrial myopathies. Therefore, the mitochondrial phenotype in TSCmKO mice was further investigated. To determine whether the mitochondrial phenotype is a direct consequence of the sustained mTORC1 activation in skeletal muscle, or rather a consequence of the progressive myopathy and the impairment in autophagy, the mitochondrial phenotype was analyzed in 3- and 9-month-old TSCmKO mice. Throughout my investigations, I discovered a progressive enlargement of mitochondria, which was barely evident in 3-month-old mice. The increase in mitochondrial density and size in 9-month-old mice is accompanied by an increase in ROS production as well as the antioxidative stress response, which reveal an additional sarcopenia feature not yet investigated in the TSCmKO mouse model. I established the mitochondrial phenotype to be rather a consequence than a primary cause of the TSCmKO mice phenotype, as only 9-month-old TSCmKO mice show an increase in mitochondrial size/density, and oxidative stress. Increased mitochondrial dynamics or the impairment in mitophagy show a strong correlation with enlargement of mitochondria. Additionally, impairment in glycogen utilization was detected.

6.2 Introduction

6.2.1 Mitochondria- the powerhouse of the cell

Mitochondria are considered the powerhouse of the cell, able to respond to extrinsic and intrinsic signals in an autonomous manner by remodeling their morphology. Their key function is to use oxygen to generate ATP, which is the primary source of energy in both plant and animal cells.

Mitochondria have a very distinct structure, distinguishing them from other organelles. They consist of a double-layered membrane comprising the outer mitochondrial membrane (OMM) and the inner mitochondrial membrane (IMM). The OMM serves as a barrier, but at the same time, it builds the exchange platform between mitochondrion and cytosol for smaller molecules and ions. It additionally protects the cell from noxious mitochondrial products, such as death signals and reactive oxygen species (ROS), and it maintains mitochondrial membrane potential (Hood et al, 2018). The IMM builds cristae to increase mitochondrial inner membrane surface area, which is the place where mitochondrial respiration takes place. Cristae are highly sensitive to extra- and intra-mitochondrial stimuli by adapting their length, width, rigidity and angularity. Under high-energy demands, mitochondria increase the import of newly translated ATP synthases, which could result in an increase in proliferation of cristae folds. This is usually associated with an increase in respiratory chain components and a subsequent boost in oxidative phosphorylation (OXPHOS), through which ATP is produced.

In detail, the mitochondrial electron transport chain is composed of five multimeric complexes. The nicotinamide adenine dinucleotide hydride (NADH) dehydrogenase oxidizing NADH to NAD^+ (complex 1); the succinate reductase, oxidizing succinate into fumarate (complex 2); and the Cytochrome *c* reductase complex (complex 3) regulating the proton gradient. Next, the Cytochrome *c* oxidase (complex 4) is responsible for completing the electron transport. Complexes one, two and three build the electron gradient, enabling the ATP synthase (complex 5) to produce ATP as the protons reenter the mitochondrial matrix (Sousa et al, 2018).

As an autonomous system, mitochondria contain their own plasmids, the so-called mitochondrial DNA (mtDNA), which are hosted in the mitochondrial matrix. mtDNA codes for 13 proteins, which are all involved in mitochondrial respiration (oxidative phosphorylation). However, the mitochondrial genome is not able to independently produce all proteins needed for functionality. It thus still relies heavily on the import of nuclear gene products (Hood et al, 2018). Cells contain numerous mitochondria and therefore thousands of mtDNA copies. Most mitochondrial disorders are inherited disorders, and are often caused by defects in genes encoded by either mtDNA or nuclear DNA (nDNA) (Gorman et al, 2016; Leonard & Schapira, 2000a; b; Rusecka et al, 2018). mtDNA-associated changes can, for example, cause exercise-induced muscle pain or fatigue, but they are also responsible for the appearance of detrimental pathologies such as rhabdomyolysis. Rhabdomyolysis, includes rapid muscle breakdown, also leading to severe multiorgan dysfunctions such as, for example, the accumulation of myoglobin in the kidney, which could lead to kidney failure (Petejova & Martinek, 2014). mtDNA mutations lead to defects within the reparatory chain through the accumulation of defective respiratory chain components. This increases the intracellular ROS levels, initiating the release of cytochrome C, resulting in apoptosis, but also leading to mitochondrial dysfunction accompanied by dysfunctional cell signaling (Redza-Dutordoir & Averill-Bates, 2016). During intense skeletal muscle contractile activity such as, for example, during exercise, or in response to increased cytokines, mitochondria also produce increased amounts of free radicals and higher ROS. Because of increasing amounts of oxidized proteins, lipids and DNA, the glutathione antioxidative stress response, the major intracellular scavenger of oxidized proteins, is turned on (Redza-Dutordoir & Averill-Bates, 2016; Ribas et al, 2014).

A conserved family of dynamin-like proteins, whose role is critical for human health, mediates mitochondrial remodeling. The fusion of mitochondria is thought to be the key player for maintaining mitochondrial health (El-Hattab et al, 2018; Iqbal & Hood, 2015). This fusion event, which can take less than two minutes, enables the exchange of information through mtDNA, proteins, lipids, and metabolites, but it also enables the cell to cope with defective mitochondria. Three proteins are particularly important for mitochondrial fusion maintenance.

They are mitofusin 1 (MFN1), mitofusin 2 (MFN2) and mitochondrial dynamin like GTPase (OPA1). MFN1 and MFN2 can complement each other to a certain extent, as overexpression of one or the other rescues fusion in mouse embryonic fibroblasts deficient for either $Mfn1^{-/-}$ or $Mfn2^{-/-}$ (Chen et al, 2003).

However, while mutations in *Mfn2* are responsible for ~20% of cases of Charcot-Marie-Tooth disease, a hereditary motor and sensory neuropathy, mutations in *Mfn1* have not been reported to cause diseases (Ranieri et al, 2013; Rocha et al, 2018; Zuchner et al, 2004). OPA1 is the mediator of inner mitochondrial membrane fusion (Romanello & Sandri, 2015). Genetic ablation of OPA1 causes increased fragmentation of the mitochondrial system, whereas overexpression causes elongation (Cipolat et al, 2004). OPA1 is cleaved into long and short isoforms. The role of specific OPA1 isoforms is elusive; however, short isoforms are abundant during mitochondrial depolarization events. The division or fission of mitochondria is more complex than mitochondria fusion. It requires the coordinated separation of cytoplasmic, cytoskeletal and organellular elements and is regulated by dynamin-related protein 1 (DRP1) and Fissin 1 (Fis1) (Iqbal & Hood, 2015; Romanello & Sandri, 2015). Fis1 is dispensable for fission even though its knockdown increases elongation, and its overexpression leads to an increase in mitochondrial fragmentation (Iqbal & Hood, 2015; Stojanovski et al, 2004).

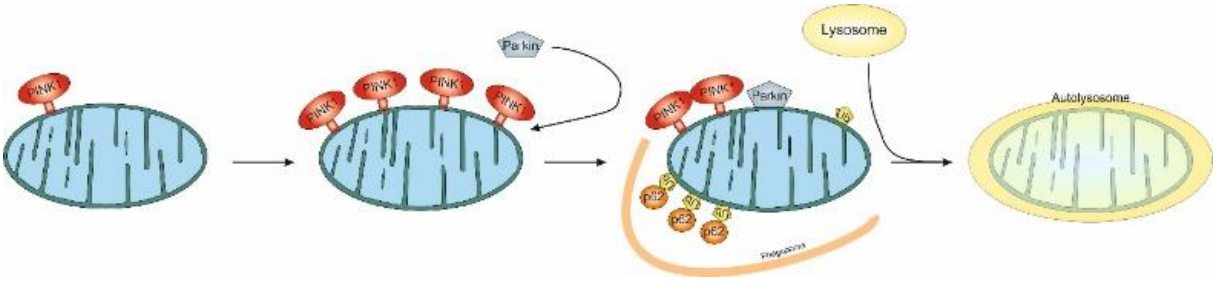

Figure III: Simplified overview of breakdown of defective mitochondria, mitophagy

Defects in the maintenance in mitochondrial dynamics, associated with accumulation of defective mitochondria, activate the autophagolysosomal system. The autophagolysosomal degradation of defective mitochondria is called mitophagy. Usually, depolarized or unhealthy mitochondria are rapidly targeted by the system for degradation. During this process, Parkin, an E3 ubiquitin ligase, is recruited to the surface of dysfunctional mitochondria in a PINK

dependent manner, marking them for degradation (Figure III). After recruitment and marking of the defective mitochondria, other E3 ubiquitinases are recruited and initiate the autophagolysosomal degradation of the organelles.

Importantly, two distinct sub-populations of mitochondria exist in skeletal muscle: First, intramyofibrillar mitochondria (IMF) account for 80% of the total mitochondria in the muscle fibers. They have higher amounts of proteins involved in oxidative phosphorylation, superior mitochondrial coupling, and are specialized in energy production to support force generation. Second, subsacrolemmal mitochondria (SS) are responsible for supplying energy for membrane-associated events (Hood et al, 2018; Picard et al, 2013). SS mitochondria demonstrate a greater sensitivity to both positive (e.g. endurance training) and negative stimuli (inactivity) than the intramyofibrillar population, and they also produce higher amounts of ROS.

6.2.2 Mitochondria in skeletal muscle

Mitochondria, whose major function is the production of ATP, are involved in various cellular functions. Particularly in skeletal muscle, mitochondria play an important role in myonuclear apoptosis and serve as an important source of calcium. Increasing mitochondrial size and mitochondrial number can have beneficial effects as reported during exercise, but it can also have detrimental consequences for the muscle, its metabolism, and subsequently for human health (Hood et al, 2018; Iqbal & Hood, 2015; Russell et al, 2014).

Exercise largely induces mitochondrial remodeling through the peroxisome proliferator-activated receptor γ coactivator 1α (PGC-1α) (Safdar et al, 2011). PGC-1α is a transcriptional coactivator that enhances lipid oxidation and lipogenesis through the promotion of fatty acid oxidation (FAO). It additionally remodels calcium signaling, altering Ca^{2+} reuptake, switches fiber types towards more slower ones, but most importantly it increases mitochondrial numbers by increasing mitochondrial biogenesis, mitochondrial respiration, and decreases ROS biogenesis (Lin et al, 2002; Ventura-Clapier et al, 2008). PGC-1a overexpression during aging was reported to improve muscle endurance and mitochondrial remodeling by phenocopying exercise effects (Gill et al, 2018).

Mitochondrial dysfunction has also been shown to play a role in the development of atrophying skeletal muscle. Expression of the fission machinery is sufficient to cause muscle wasting in adult skeletal muscle triggered through AMPK activation (Romanello et al, 2010). In addition, the mTOR pathway was shown to be involved in regulating mitochondrial activity, biogenesis, mitochondrial oxygen consumption, and oxidative capacity (Morita et al, 2013; Schieke et al, 2006). It selectively promotes translation of nucleus-encoded mitochondria related mRNAs through 4E-BP1 inhibition, which increases the ATP production capacity (Morita et al, 2013). In skeletal muscle, it was shown that *Rptor* ablation, resulting in suppression of mTORC1 activity, decreases oxidative capacity, with a subsequent decrease of genes involved in mitochondrial biogenesis, such as PGC-1a, thereby altering skeletal muscle metabolic properties (Romanino et al, 2011).

More strikingly, the magnitude of malfunctioning mitochondria is visible in the pathology of mitochondrial myopathies (MM). These are progressive muscle diseases, characterized by the impairment of oxidative phosphorylation, leading to a subsequent deficit in energy production, and resulting in decreased levels of ATP (Houstek et al, 2006; Shepherd et al, 2006). However, patients suffering from MM often show additional multisystemic symptoms, such as liver failure, cardiomyopathies, and diabetes, to only name a few (Ahmed et al, 2018; Gorman et al, 2016). MMs are diagnosed by cyclooxygenase (COX) deficiency in immunohistochemistry, but also spectrometric evaluations of the components of the mitochondrial respiratory chain can be performed. Khan et al. reported that mTORC1 is activated by mtDNA replication defects, which leads to the upregulation of the one-carbon- (1C-) cycle, thus stimulating fibroblast growth-factor 21 (FGF-21) through the activation of the ATF4 mediated integrated stress response (Khan et al, 2017). This results in a subsequent increase in mitochondrial myopathy progression (Khan et al, 2017). The MM progression was reverted by the application of rapamycin, which directly inhibits mTORC1 activity. Additionally, it was shown that suppressing autophagy in skeletal muscle leads to an accumulation of enlarged and dysmorphic mitochondria (Carnio et al, 2014).

Moreover, ROS is known to be involved in the progression of certain inherited muscular dystrophies. Dystrophic muscle is prone to stress, which can be enhanced through exercise-induced damage. On dystrophic muscle membranes, exercise provokes micro-lesions, disrupting the intracellular Ca^{2+} homeostasis. The increased influx of Ca^{2+}, affects the mitochondria as a Ca^{2+} buffering organelle, leading to mitochondrial swelling and functional alterations, which results in an increase in apoptosis and necrosis (Allen et al, 2010; Bellinger et al, 2009; Robert et al, 2001; Shkryl et al, 2009).

Many mitochondrial therapies so far have been developed for diseases caused by mutations in mitochondrial DNA or by mutations in nuclear genes that encode mitochondrial proteins. However, mitochondrial dysfunction has also been found to contribute to many other disorders. For example, it contributes to diabetes and some skeletal muscle myopathies, as mentioned above. Because these are highly prevalent diseases, mitochondria are thus an important drug target. Much evidence has shown that mTORC1 is indirectly involved in the progression of myopathic phenotypes associated with alterations of mitochondria (Romanino et al, 2011). It would be interesting to find out whether or not the mitochondrial phenotype is altered in skeletal muscle upon sustained activation of mTORC1, and how the mitochondria might contribute to the pathophysiology of the transgenic mice.

6.3 Results

Sustained activation of mTORC1 increases oxidative capacity in young TSCmKO mice and reveals signs of a mild mitochondrial myopathy

TSCmKO mice were shown to develop a late-onset myopathy accompanied by skeletal muscle alterations already at young age (Castets et al, 2013). Constant activation of mTORC1 in skeletal muscle promoted increased mitochondrial oxidative capacity in slow (SOL) and fast (TA and GAS) skeletal muscle already in 3-month-old TSCmKO mice (Castets et al, 2013). By using COX and SDH staining, I first confirmed the increased oxidative capacity of TA muscle in 3-month-old TSCmKO mice compared to control littermates (Figure 1A). To evaluate whether or not the increased oxidative capacity is due to an increased number of mitochondria, I determined the amount of mitochondrial DNA (mtDNA) in TA muscle homogenates (Figure 1B). The mtDNA/gDNA ratio was similar in both genotypes for all examined mitochondrial genes (Figure 1B). Direct quantification of mitochondrial number (mitochondria/μm^2), density and relative mitochondrial size in electron microscopy (EM) pictures (Figure 1C) also did not reveal any significant changes (Figure 1D). In line with these findings, the expression of proteins involved in mitochondrial fusion (Mfn1/2, OPA1) and fission (Fis1, Drp1) was mostly similar in TSCmKO and control muscle (Figure 1E). Only an induction in Opa1 expression was observed.

The unchanged expression of fusion/fission regulated proteins, in combination with the similar mitochondrial density and size compared to control muscle, indicates that the mitochondrial dynamics of TSCmKO skeletal muscle is not greatly disturbed. Further analysis of EM pictures of TSCmKO TA muscle revealed an accumulation of intermyofibrillar mitochondria in certain areas (Figure 1F), a pathology that was not observed in control muscle (not shown). The distinct function of such mitochondrial herds is currently unknown, but it could be responsible for altering the excitation-contraction profile of the skeletal muscle (Miragoli et al, 2016). The presence of mitochondrial herds/accumulations is a feature often observed in human

mitochondrial myopathies, as visualized by ragged-red fibers (RRF) revealed by the modified Gomori trichrome stain (DiMauro, 2004; Pant et al, 2015a; Vogel, 2001).

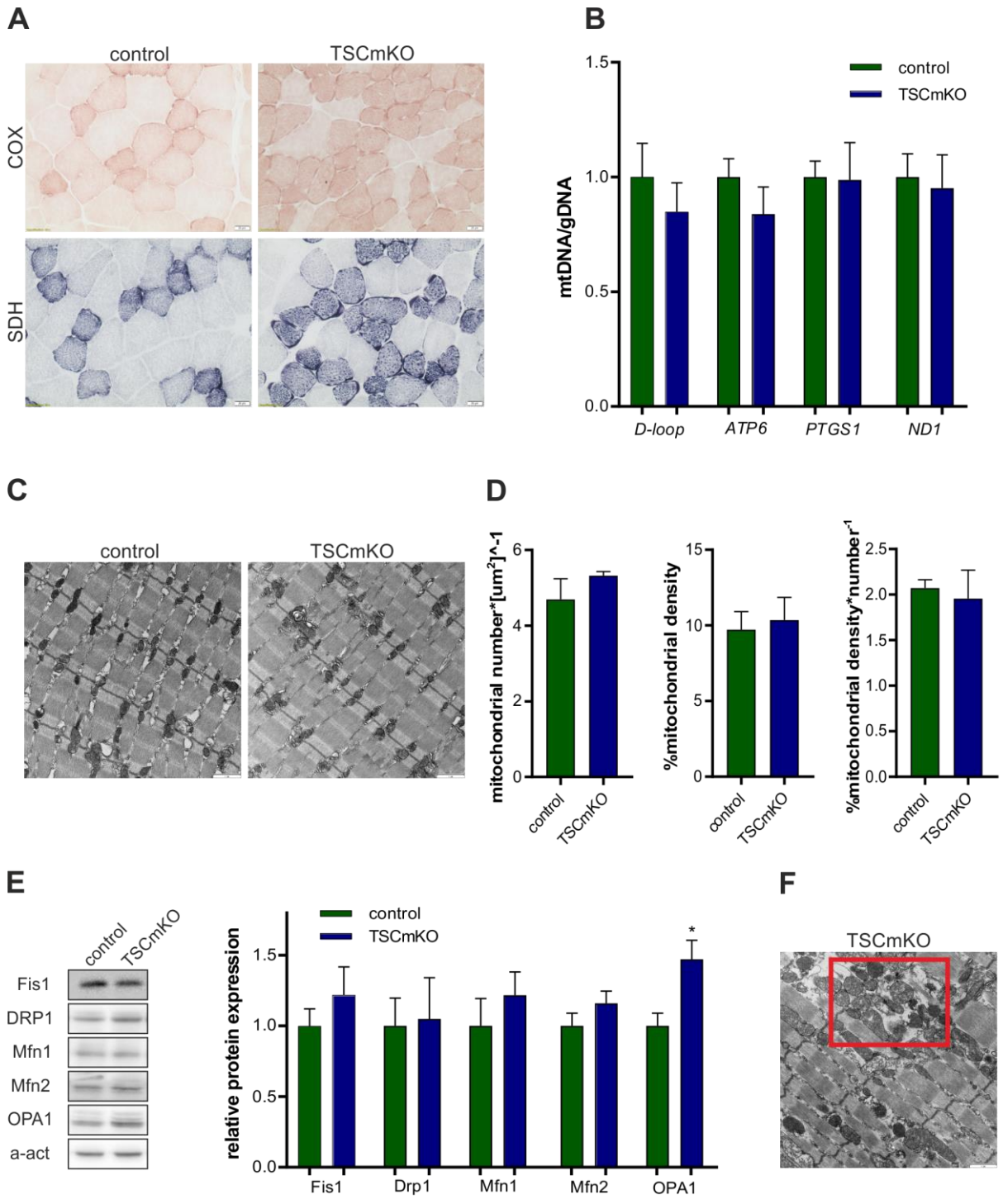

Figure 1: Sustained activation of mTORC1 does increase oxidative capacity of skeletal muscle in young mice, without changing mitochondrial number and dynamics

(A) Enzymatic SDH and COX staining of 3-month-old control and TSCmKO TA muscle, oxidative fibers (darker). Scale bar = 20 µm. **(B)** Indirect quantification of mitochondrial number using qPCR in 3-month-old TSCmKO

mice. Values are mean ± SEM. Data normalized to *β-globulin* levels; *p < 0.05. n ≥ 4. **(C)** Electron micrograph of 4-month-old control and TSCmKO mice. Scale bar = 1 µm. **(D)** Quantification of mitochondrial number, density and average size using electron micrographs of control and TSCmKO littermates. Values represent mean ± SEM. *p < 0.05, **p < 0.01, ***p < 0.001. n = 3. **(E)** Immunoblots and quantification of TA whole muscle lysate of 3-month-old controls and TSCmKO mice and subsequent quantification of proteins involved in mitochondrial fusion and fission. Data normalized to α–actinin. Values represent mean ± SEM. *p < 0.05, **p < 0.01, ***p < 0.001. n ≥ 3. **(F)** Electron micrograph of 4-month-old TSCmKO mouse. Representative picture. Scale bar = 1 µm.

Muscle from young TSCmKO mice do not show malfunctioning mitochondria

The increase in oxidative capacity in TSCmKO mice, as described above, is not caused by an increase in mitochondrial biogenesis or by disrupting mitochondrial dynamics. However, I wondered whether or not the increase in oxidative capacity in 3-month-old TSCmKO mice is caused by an increase in mitochondrial function. Whereas defective mitochondria are prone to produce more mitochondrial stress and reactive oxygen species (Baumann et al, 2016; Powers et al, 2011; Zorov et al, 2014), an increase in mitochondrial function is usually accompanied by an increased expression of proteins involved in the mitochondrial respiration, thus leading to elevation of oxidative phosphorylation. The amount of the five major protein complexes of the respiratory chain can be assessed by western blot analysis using a cocktail of five antibodies (OXPHOS blot). This analysis did not reveal any significant changes in the assembly of the five complexes in TA total muscle lysates of 3-month-old TSCmKO mice compared to wild-type (Figure 2A). Also, analyzing mitochondrial oxidative stress did not reveal any significant changes (Figure 2B). These results are in line with the normal levels of ROS observed by performing DHE staining on TA muscle cross sections (Figure 2C), and the subsequent quantification by using staining intensity measurements (Figure 2C, right).

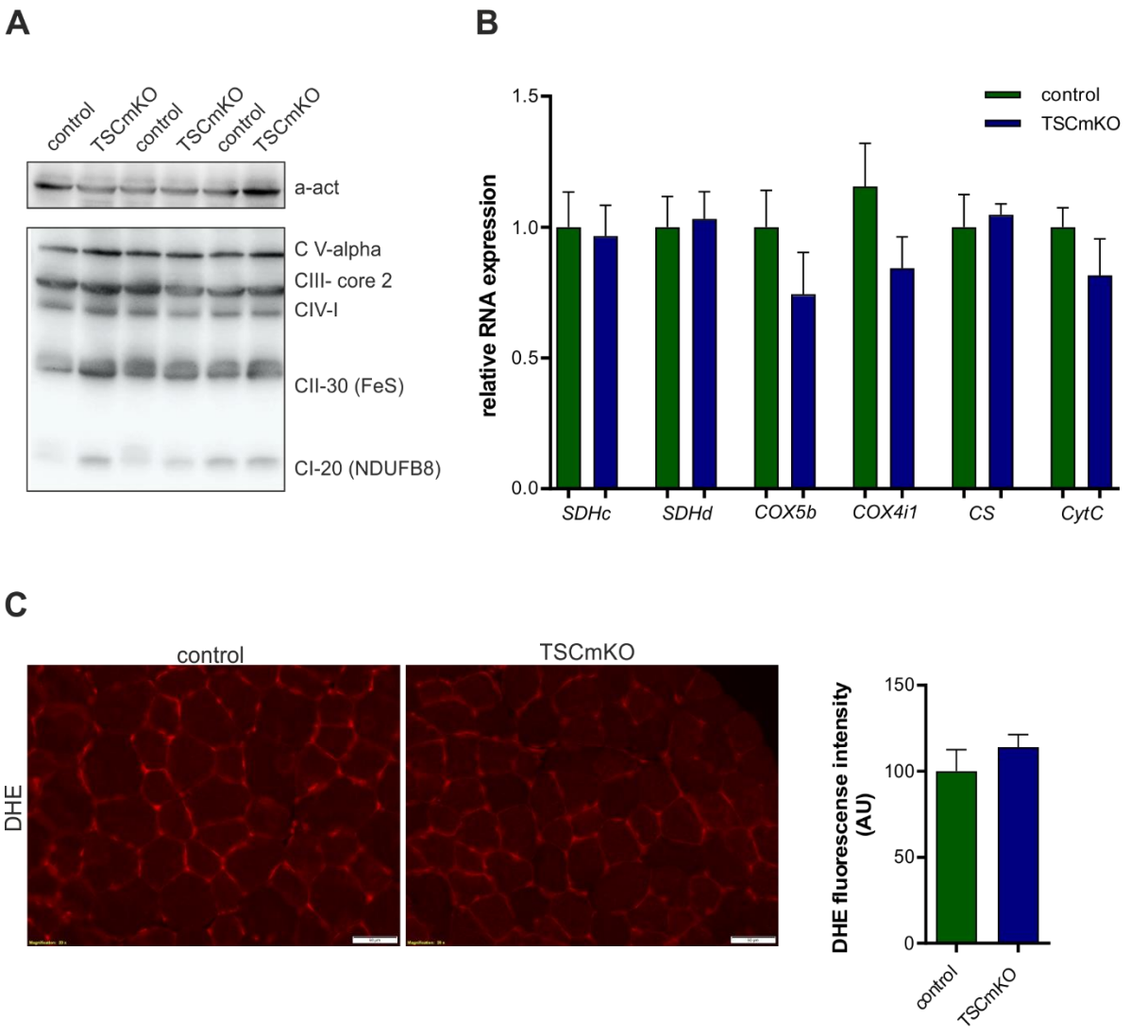

Figure 2: Young TSCmKO mice do not reveal mitochondrial stress or increase in reactive oxygen species

(A) Expression of genes involved in mitochondrial stress does not show any significant changes in TA muscle of 3-month-old TSCmKO mice. Values are mean ± SEM. Data normalized to *β-actin* levels; $^{*}p \leq 0.05$. $n \geq 3$. **(B)** OXPHOS Blot of total protein lysates from 3-month-old control and TSCmKO littermates. α–actinin used as loading control. Values represent mean ± SEM. $^{*}p < 0.05$, $^{**}p < 0.01$, $^{***}p < 0.001$. $n \geq 3$. **(C)** Dihydroethidium immunostaining and subsequent quantification of 3-month-old TA muscle cross sections of control and TSCmKO mice. Values are mean ± SEM. $^{*}p \leq 0.05$. $n = 6$.

Young TSCmKO mice show signs of impaired glucose utilization and glycogen storage

Skeletal muscle can generate energy from various sources, depending on the amount of force required and the duration of the activity. TSCmKO mice have previously shown a decrease in skeletal muscle ATP (Guridi et al, 2015). One of the energy sources in mouse skeletal muscle is glucose. Glucose is stored in skeletal muscle as glycogen, and it is broken down through the activation of so-called debranchers. Excessive glycogen can also be degraded via the autophagolysosomal system (Zhao et al, 2018). Accumulation of glycogen in skeletal muscle has been shown to have detrimental consequences (e.g. Pompe disease) (Kohler et al, 2018). PAS staining used to detect polysaccharides — in this case glycogen accumulations — on TA muscle cross sections, did not reveal any significant changes (Figure 3A). This indicates normal glycogen storage in TSCmKO skeletal muscle.

In order to confirm these results, I used a more quantitative approach directly measuring glycogen levels. In line with the PAS staining, I detected normal glycogen levels in TA muscle lysates from TSCmKO mice (Figure 3A and B). Additionally, I analyzed glycogen brancher and debrancher. While glycogen phosphorylase (*PYGM-1*) mRNA levels were normal, phosphoglucomutase (*PGM*) mRNA levels were significantly downregulated in TSCmKO TA muscle (Figure 3C). PGM is responsible for converting glucose-1-phosphate into glucose-6-phosphate. Glucose-6-phosphate is an important metabolite for the pentose phosphate pathway and, subsequently, for the purine pyrimidine metabolism. However, it is also upstream the gluconeogenesis and is converted to pyruvate in the cytosol, and lastly in the mitochondria to Acetyl-CoA, thus entering the citric acid cycle. By further analyzing protein levels of proteins responsible for the glycogen synthesis, I observed an upregulation of the glycogen synthase (GS) activity (Figure 3D). Glycogen synthase is phosphorylated by glycogen kinases inhibiting its activity. Whereas GS levels are increased in TSCmKO, the relative phospho-GS levels are unchanged in TSCmKO mice compared to control littermates.

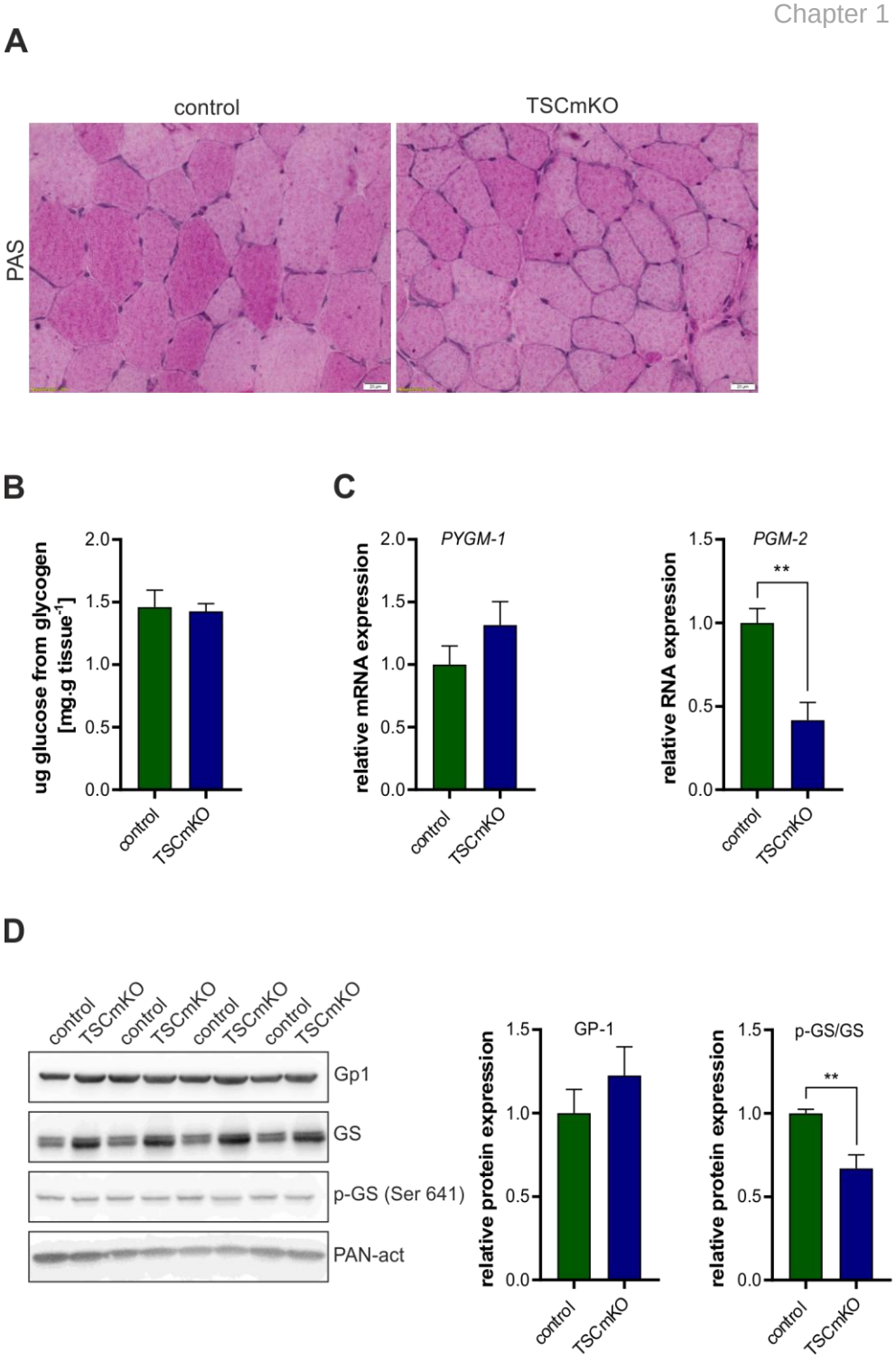

Figure 3: Glycogen breakdown is impaired in young TSCmKO mice

(A) Periodic Acid-Schiff (PAS) staining of 3-month-old TA muscle cross-sections of control and TSCmKO mice. Scale bar = 20µm. **(B)** Hexokinase-assay to determine free glucose and glycogen content of TA muscle lysates of 3-month-old TSCmKO and control littermates. Values represent mean ± SEM. $^{*}p < 0.05$, $^{**}p < 0.01$, $^{***}p < 0.001$. n = 4. **(C)** Expression of *PYGM-1 (*Glycogen phosphorylase, muscle associated) and *PGM* (Phosphoglucomutase), genes involved in the breakdown of glycogen in 3-month-old TSCmKO and control littermates. Values are mean ± SEM. Data normalized to *β-actin* levels. $^{*}p < 0.05$, $^{**}p < 0.01$, $^{***}p < 0.001$. n ≥ 3. **(D)** Immunoblots and subsequent quantification of TA whole muscle lysate for Glycogen phosphorylase (GP-1) and Glycogen synthase (GS), phospho-sites indicated in brackets. Data normalized to α–actinin. Values represent mean ± SEM. $^{*}p < 0.05$, $^{**}p < 0.01$, $^{***}p < 0.001$. n = 4.

Sustained mTORC1 activation in skeletal muscle leads to increase mitochondria size without changing mitochondrial respiration with age

In skeletal muscle, constantly activating mTORC1 by deleting its upstream inhibitor, TSC1, impairs autophagy (Castets et al, 2013). Autophagy is the primary means of degrading and removing defective organelles, such as mitochondria (mitophagy). PINK and Parkin bind defective mitochondria, thereby marking them for autophagic breakdown. I observed a significant increase in PINK and Parkin protein levels in 10.5-month-old TSCmKO mice compared to control littermates (Figure 4A). Additionally, I confirmed that muscle from TSCmKO mice display an increase in oxidative capacity, compared to control muscle, as visualized by COX and SDH staining (Figure 4B). To determine whether or not this increase in oxidative capacity is due to an increase in mitochondrial number, I compared the ratio of mitochondrial DNA (mtDNA) with genomic DNA (gDNA) between the genotypes. The amounts of mitochondrial genes, such as *D-loop1, Atp6*, *Ptgs1*, and *Nd1*, were all significantly increased in the muscle of TSCmKO mice compared to controls (Figure 4C). To investigate whether or not this increase in mtDNA reflects an increase in mitochondrial number and/or mass, I next used electron microscopy with subsequent contrast staining (Figure 4D). While the number of intermyofibrillar mitochondria/μm^2 did not change (Figure 4E, left), mitochondrial size and density significantly increased in TSCmKO muscle compared to control muscle (Figure 4E). This increase in mitochondrial mass is consistent with the increased mtDNA/gDNA ratio.

An increase in mitochondrial size might derive from an imbalance in the fusion to fission ratio (Scott & Youle, 2010; Westermann, 2012; Youle & van der Bliek, 2012). Therefore, I next analyzed genes involved in mitochondrial fusion (*Mfn2, Opa1*) and fission (*Drp1, Fis1*) dynamics. While the expression of these genes was not changed at transcriptional levels (Figure 4F), Mfn1 and DRP1 amounts strongly increased at the protein level in 10.5-month-old TSCmKO muscle (Figure 4G), thus indicating increased mitochondrial fusion and fission activity. However, the TSCmKO muscle appear to exhibit unbalanced mitochondrial dynamics, which results in the accumulation of enlarged mitochondria (Figure 4D). To address whether

or not the enlarged mitochondria in TSCmKO muscle were functional, I evaluated parameters of mitochondrial respiration in isolated mitochondria by using the Seahorse XF24 Analyzer. I did not detect changes in basal oxidative consumption rates in mitochondria from TSCmKO TA muscle, compared to mitochondria from control muscle (Figure 4H). Similarly, mitochondrial basal respiration, proton leak, ATP-linked respiration, maximal respiration, reserve capacity, and non-mitochondrial respiration were similar in mitochondria from both genotypes (Figure 4I). In conclusion, the mTORC1-mediated block in autophagy and subsequently impaired mitophagy, confirmed by the increased PINK and Parkin levels, is associated with an increase in fusion/fission dynamics, enlarged mitochondria, and an increase in oxidative capacity.

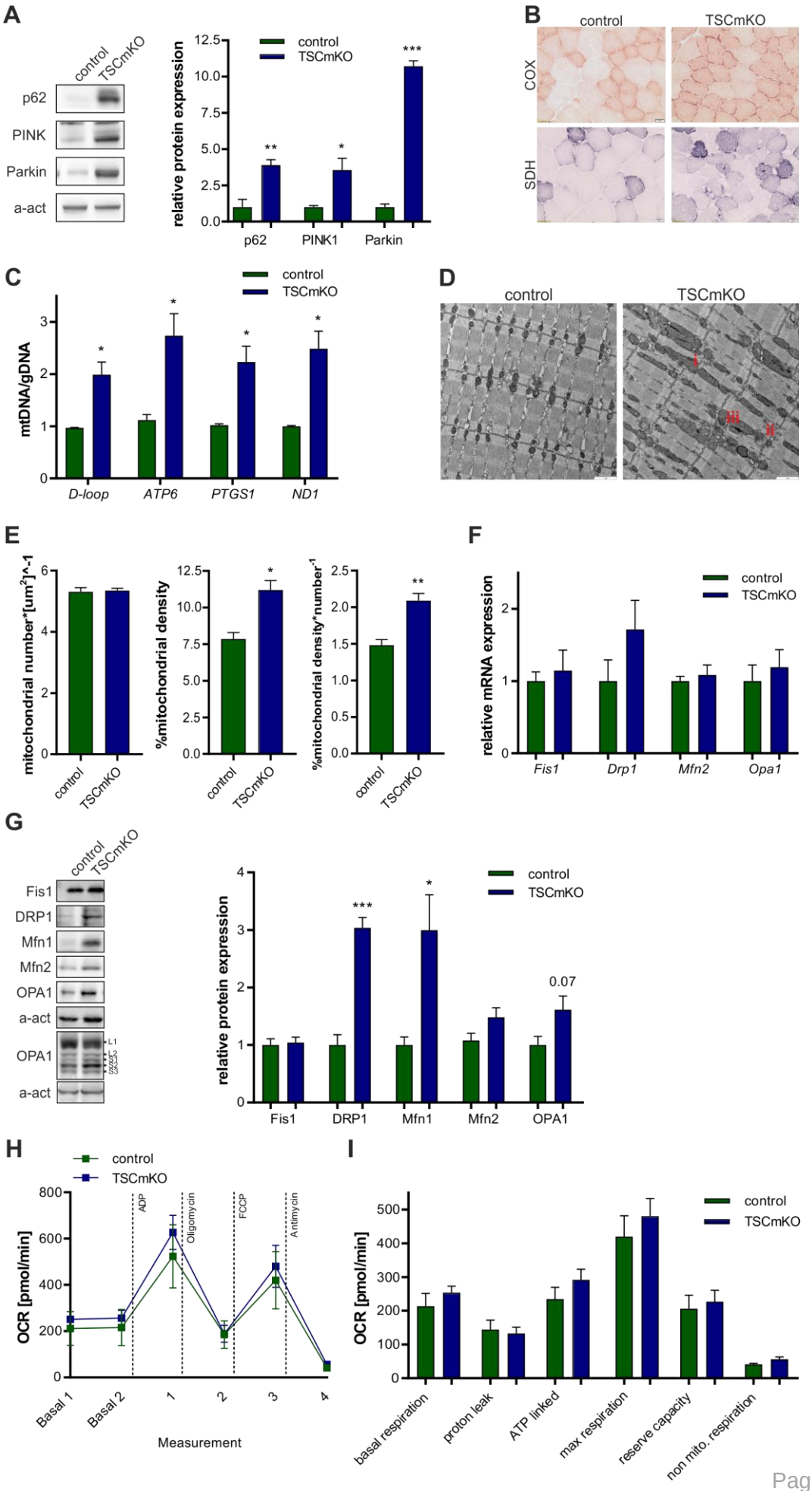
A
control
TSCmKO
p62
PINK
Parkin
a-act
relative protein expression
control
TSCmKO
p62
PINK1
Parkin
B
control
TSCmKO
COX
SDH
C
control
TSCmKO
mtDNA/gDNA
D-loop
ATP6
PTGS1
ND1
D
control
TSCmKO
E
mitochondrial number*[um²]^-1
%mitochondrial density
%mitochondrial density*number⁻¹
F
control
TSCmKO
relative mRNA expression
Fis1
Drp1
Mfn2
Opa1
G
control
TSCmKO
Fis1
DRP1
Mfn1
Mfn2
OPA1
a-act
OPA1
a-act
relative protein expression
0.07
H
control
TSCmKO
OCR [pmol/min]
ADP
Oligomycin
FCCP
Antimycin
Basal 1
Basal 2
Measurement
I
control
TSCmKO
OCR [pmol/min]
basal respiration
proton leak
ATP linked
max respiration
reserve capacity
non mito. respiration

Figure 4: Sustained mTORC1 activation leads to increase mitochondria size in old TSCmKO mice without changing mitochondrial respiration

(A) Immunoblots of TA whole muscle lysate for autophagy (p62) and mitophagy (PINK, Parkin) markers of 10.5-month-old controls and TSCmKO TA muscle lysate and subsequent quantification. α–actinin used as loading control. Values represent mean ± SEM. $^{*}p < 0.05$, $^{**}p < 0.01$, $^{***}p < 0.001$. n ≥ 3. **(B)** Enzymatic SDH and COX staining of 10.5-month-old control and TSCmKO TA muscle cross-sections. Oxidative fibers (darker). Scale bar = 20 µm. **(C)** Indirect quantification of mitochondrial number by using qPCR in 10.5-month-old TSCmKO mice. Values are mean ± SEM. Data normalized to *β-globulin* levels; $^{*}p < 0.05$, $^{**}p < 0.01$, $^{***}p < 0.001$. n = 3. **(D)** Electron micrograph of 10.5-month-old control and TSCmKO mice show an increase in mitochondrial density, showing (i) enlarged mitochondria; (ii) disruption of the contraction apparatus; (iii) delocalization of the tirade. Scale bar = 1 µm. **(E)** Quantification of mitochondrial number, density and average size by using electron micrographs reveals enlarged mitochondria in 10.5-month-old TSCmKO mice compared to control littermates. Values represent mean ± SEM. $^{*}p < 0.05$, $^{**}p < 0.01$, $^{***}p < 0.001$. n = 3. **(F)** Relative expression of genes encoding for proteins involved in mitochondrial fusion and fission. Values represent mean ± SEM. Data normalized to *β-actin* levels. $^{*}p < 0.05$, $^{**}p < 0.01$, $^{***}p < 0.001$. n ≥ 3. **(G)** Immunoblots and quantification of TA whole muscle lysate of 10.5-month-old controls and TSCmKO mice and subsequent quantification of proteins involved in mitochondrial fusion and fission. Data normalized to α–actinin. Values represent mean ± SEM. $^{*}p < 0.05$, $^{**}p < 0.01$, $^{***}p < 0.001$. n ≥ 3. **(H)** Measurement of the oxidative consumption rate by the Seahorse approach in 10.5-month-old control and TSCmKO mice. Values represent mean ± SEM. Data normalized to total protein of the mitochondrial fraction by using BCA for protein determination. n ≥ 3. **(I)** Quantitative analysis of the seahorse measurement. Values represent mean ± SEM. n ≥ 3.

Oxidative stress and the anti-oxidative stress response are upregulated in aged TSCmKO mice

An accumulation of mitochondria can be beneficial; however, they are also a major contributor to the production of reactive oxygen species (Hood et al, 2018; Murphy, 2009; Sena & Chandel, 2012). To determine whether or not the higher mitochondrial mass in TSCmKO muscle leads to increased oxidative stress, I measured levels of the reduced (GSH) and oxidized (GSSG) forms of glutathione, a major endogenous antioxidant, as a readout of redox balance. I detected a parallel increase in both GSSG and GSH levels (Figure 5A) in TSCmKO muscle compared to controls, such that the ratio remained unchanged. This suggests an increase in both ROS production and endogenous buffering capacity in TSCmKO mice. Consistent with higher GSH levels, I observed higher mRNA and protein expression of key mediators of GSH production, including glutathione synthetase (GSS), and the catalytic subunit of γ-glutamate-cysteine ligase (GCLC) (Figure 5B and C). The observed increase in both ROS production and antioxidant buffering capacity could arise from increased mitochondrial stress. However, mRNA expression of mitochondrial stress markers were not altered in TSCmKO mice (Figure 5D). These results suggest that muscle of TSCmKO mice counteract higher ROS production by promoting endogenous antioxidant systems. The balance between cellular stress and endogenous buffering systems designed to counteract oxidative stress is a critical determinant of the muscle's physiological condition.

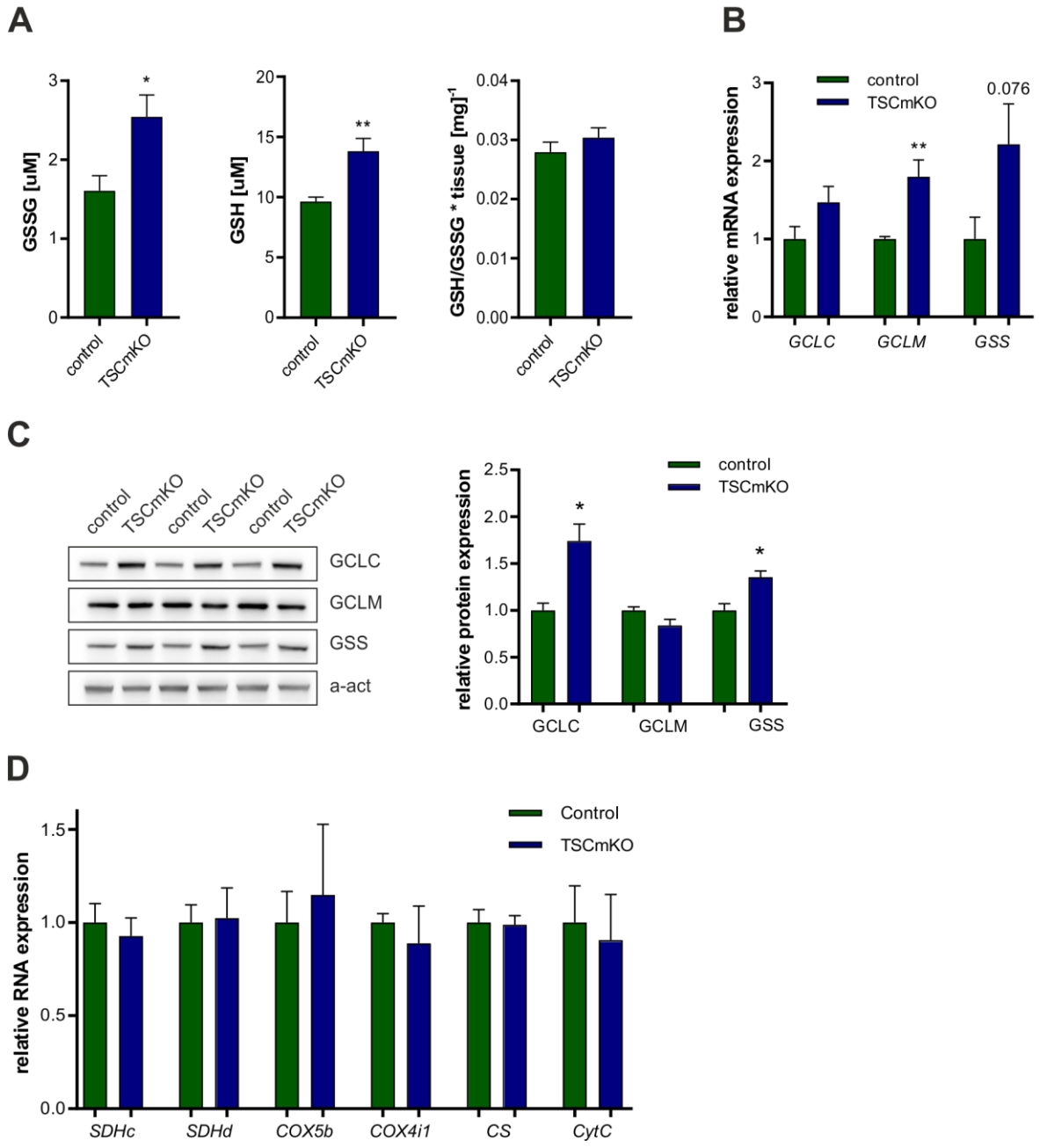

Figure 5: Oxidative stress and the antioxidative stress defense are upregulated in old TSCmKO mice

(A) Measurement of the levels of reduced an oxidized glutathione (GSH and GSSG) in gastrocnemius fresh muscle lysates of 10.5-month-old controls and TSCmKO mice. Values represent mean ± SEM. $^{*}p < 0.05$, $^{**}p < 0.01$, $^{***}p < 0.001$. **(B)** Relative expression of genes encoding proteins involved in glutathione production. Values represent mean ± SEM. $^{*}p < 0.05$, $^{**}p < 0.01$, $^{***}p < 0.001$. n ≥ 3. **(C)** Immunoblot and quantification of GCLC (Glutamate-cysteine ligase catalytic subunit), GCLM (Glutamate-cysteine ligase regulatory subunit), and GSS (Glutathione synthetase) in TA total muscle lysate. α–actinin used as loading control. Values represent mean ± SEM. $^{*}p < 0.05$, $^{**}p < 0.01$, $^{***}p < 0.001$. n ≥ 3. **(D)** Expression of genes involved in mitochondrial stress does not show any significant changes in TA muscle of 10.5-month-old TSCmKO mice. Values are mean ± SEM. Data normalized to *β-actin* levels; $^{*}p \leq 0.05$. n ≥ 3.

6.4 Discussion

mTORC1 plays a pivotal role in protein synthesis and protein degradation in skeletal muscle (Goodman, 2014; Morita et al, 2013). Mice with depleted *Tsc1* specifically in skeletal muscle have been previously described and characterized as suffering from a late-onset myopathy, resulting in death around the age of 9-12 months (Castets et al, 2013). Apart from the late-onset myopathy, the impairment in autophagy, and the loss of muscle mass and muscle strength, I identified an increase in oxidative stress in mutant muscle and further characterized the severity of the myopathy of the transgenic mouse model. The increase in cellular oxidative stress is accompanied, however, by a similar increase in the antioxidative buffering response. Here, I observed a mitochondrial myopathy-like phenotype with a gradual age-related increase in mitochondrial density and size in the transgenic mice. The previously described impaired autophagy is accompanied by impaired mitophagy and by an increase in mitochondrial dynamics. Presumably, these mitochondrial changes also contribute to the severity of the muscle pathology observed in old TSCmKO mice. I also found the mitochondrial phenotype to gradually develop with age, which is a consequence of sustained activation of mTORC1 in the skeletal muscle because the development of the mitochondrial phenotype clearly coincides with the development of other myopathic features (e.g. loss of muscle force). Therefore, the increase in oxidative stress might be a consequence of the progressive mitochondrial phenotype.

Sustained activation of mTORC1 gradually leads to pathological alterations observed in mitochondrial myopathies

Mitochondria are regarded as key players in the pathogenesis of muscular dystrophies (Jongpiputvanich et al, 2005; Komulainen et al, 2015; Pant et al, 2015b). However, it is unclear whether they serve a primary or secondary role in the onset of the pathology. Rapamycin has been recently discovered to reverse the progression of mitochondrial myopathy, even in old age (Khan et al, 2017), thus emphasizing the role mTORC1 plays in the development of

skeletal muscle mitochondrial phenotypes. By characterizing the mitochondrial phenotype in young (3-month-old) transgenic mice, I confirmed the previously observed increase in oxidative capacity in TSCmKO glycolytic muscle (Castets et al, 2013) (Figure 1A). Analysis of other mitochondrial characteristics, such as mitochondrial number, size, density and mitochondrial dynamics, do not show alterations in 3-month-old transgenic mouse muscle. However, EM analysis detected so-called intermyofibrillar mitochondrial herds in the skeletal muscle of 3-month-old TSCmKO mice that were not present in the muscle of age-matched controls (Figure 1F). This is a strong indication of an onset of a mitochondrial myopathy often seen in humans diagnosed with the disease (DiMauro, 2004; Pant et al, 2015a; Vogel, 2001). However, certain limitations do exist when analyzing mitochondria in EM pictures from mice. Compared to humans, mouse muscle is less homogenous. The medial part of mouse skeletal muscle shows glycolytic but more type IIa fibers, whereas the lateral part is slightly faster (Schiaffino & Reggiani, 2011). This leads to higher variability in mitochondrial distribution in murine skeletal muscle.

Impaired mitochondrial function can directly influence skeletal muscle atrophy and contribute to disease severity (Russell et al, 2014). Myopathic features were already observed in 3-month-old TSCmKO mice, such as skeletal muscle atrophy and lower isometric forces (Castets et al, 2013). These signs are much more pronounced in the transgenic mice at an older age. The evidence was striking for I found mitochondrial density, average size, and oxidative capacity to increase exclusively in muscle from old TSCmKO mice (Figure 4B, C, D, and E). Mitochondrial morphology is determined by the fusion to fission ratio. After determining the amount of fusion and fission proteins in TA muscle lysates of old TSCmKO mice, I found elevated levels of proteins involved in mitochondrial dynamics (Figure 4G). Increased fusion would be in line with the observed increase in mitochondrial density (Figure 4E). The correct arrangement of the skeletal muscle architecture is important for maintenance of the skeletal muscle contractile apparatus. For example, mitochondrial elongation in the heart muscle has been described as causing alterations of the contractile apparatus, by disrupting the sarcomere arrangement (Miragoli et al, 2016). Therefore, the elongation of mitochondria and the presence

of mitochondrial herds might be partly responsible for the loss in skeletal muscle isometric force and for alterations occurring within the muscle contraction profile observed in the TSCmKO mice (Chapter 3, (Castets et al, 2013)). In line with the progression of the mitochondrial phenotype with age, the reduction in isometric forces was more prominent in old TSCmKO mice (Chapter 2, Figure 2B and C (Castets et al, 2013)).

It was shown that starvation-induced Mfn1 dependent mitochondrial elongation protects against myopathy and enables mitochondria to maximize their energy production through mobilization of fatty acids (Rambold et al, 2015). Mfn1 is upregulated in old TSCmKO mice, suggesting that FAO might be the primary energy source of the mitochondria for energy production. The oxidative metabolism, or the generation of ATP through free fatty acids (FFA) or glucose, occurs at a much slower rate than the generation of ATP through phosphocreatine and muscle glycogen, although overall yields of ATP are much higher (38 ATP per glucose molecule) (Egan et al, 2016).

Accumulating defective or enlarged mitochondria can overwhelm the system and have detrimental effects. Although our oxygen consumption measurements have limitations regarding their quantification, our data nevertheless suggest that enlarged mitochondria in old TSCmKO mice function at normal levels (Figure 4H and I). This was rather surprising since the mTOR-Raptor complex formation has been shown to correlate in Jurkat cells with the overall mitochondrial activity. This suggested that mTORC1 might be directly involved in the ATP synthetic capacity (Schieke et al, 2006). However, by measuring the oxidative consumption rate of isolated skeletal muscle mitochondria, one removes the organelles from their microenvironment, which might again influence the organelle's function. The oxygen consumption rate I measured in isolated mitochondria from muscle of TSCmKO mice may yet suggest that bigger mitochondria act similar to the "normal" sized mitochondria observed in control mice. Normal mitochondrial function is also reflected in the normal expression levels of proteins involved in OXPHOS (Figure 2A). However, decreased cristae density were observed in EM pictures of TSCmKO muscle (data not shown). To concretely evaluate cristae defects,

cristae density would have to be analyzed and calculated. In conclusion, old TSCmKO mice have an increase in mitochondrial density and size in skeletal muscle. However, it appears that the function of the enlarged mitochondria is normal, at least *in vitro*. To elucidate mitochondrial function *in vivo* or within their microenvironment requires further investigation. Concluding, the development of the mitochondrial phenotype progresses with age and appears to contribute to the severity of the myopathy in old TSCmKO mice.

Elevated ROS in TSCmKO skeletal muscle with an increase in ROS buffering system

Increases in oxidative stress and molecular inflammation, through exogenous and endogenous stimuli, may lead to mitochondrial dysfunction (Meng & Yu, 2010). Disturbed mitochondrial function or shape has effects on energy production and might increase ROS. By investigating the glutathione pathway, which is responsible for the antioxidative stress response, I observed an upregulation of the oxidized form (GSSG) of glutathione in old TSCmKO mouse muscle, which is an indirect measurement for increased cellular oxidative stress (Figure 5A). At the same time, the reduced form of glutathione (GSH), which functions as an oxidative stress scavenger, was elevated to the same extent. This indicates that TSCmKO skeletal muscle is able to cope with the elevated oxidative stress by boosting its antioxidative stress response. Oxidative stress can induce low-grade inflammation (Howard et al, 2007; Meng & Yu, 2010). This subtle increase in inflammation is thought to blunt anabolic and promote catabolic pathways. TSCmKO mice display a skeletal muscle atrophy (Castets et al, 2013), potentially linking inflammation/oxidative stress and catabolic pathways. I could not detect mRNA expression for any pro-inflammatory markers in TA total muscle lysates of TSCmKO mice (results not shown), indicating inflammation was very subtle, if there was any at all. However, by using H&E staining on TA cross sections, I observed an accumulation of nuclei in the intermyofibrillar space in TSCmKO mice, which indicates inflammatory herds and subtle inflammation. Of note, oxidative stress also increases the contingency of damaged proteins and DNA and activates atrophic pathways. TSCmKO mice revealed an increased amount of

damaged proteins/organelles, which was visualized by the accumulation of p62 (Bjorkoy et al, 2009; Castets et al, 2013). Further experiments are needed to validate whether or not the amount of damaged DNA, and/or subtle inflammation is changed or present, respectively.

3-month-old TSCmKO mice show perturbations in glycolysis

The metabolism in TSCmKO mice, with the increase in fatty acid oxidation (FAO) and the observed loss in fat mass (Guridi et al, 2015), seems to rely heavily on FAO for energy generation. FAO does indeed yield the most energy; however, it yields some energy, but to a slower extent then the energy anaerobic metabolism produces. This can have detrimental effects during an increase in energy expenditure, as the production/utilization ratio would drop below zero. By depleting GATOR1, an mTORC1 inhibitor, Dutchak et al. were able to show that chronic mTORC1 activity increases anaplerotic pathways, replacing the TCA cycle intermediates needed for energy production (Dutchak et al, 2018). Fast glycolytic muscle heavily relies on glucose/glycolysis for energy production. TSCmKO mice have decreased cellular ATP levels (Guridi et al, 2015). In order to meet ATP demands, TSCmKO cells would have to increase glycolysis. Therefore, the glycolytic flux is of major importance for low energy cells to maintain energy balance and function. Glycogen phosphorylase, the enzyme converting glycogen to glucose-1-phosphate was not changed in mRNA and protein expression level. However, phosphoglucomutase mRNA expression was significantly downregulated in TSCmKO mice. This is another important enzyme involved in the breakdown of glycogen for energy and fuel usage, for it converts glucose-1-phosphate into glucose-6-phosphate. A deficit in the so-called debranchers of glycogen has been shown to lead to glycogen storage diseases that have severe consequences for the skeletal muscle (Kohler et al, 2018; Martinuzzi et al, 1999). However, I did not observe glycogen accumulation in the muscle of young transgenic mice. Upon carbohydrate intake, glucose can be converted into glucose-6-phosphate via the hexokinase enzyme. This would suggest a direct usage of glucose during feeding periods (night) and FAO during periods when mice consume less food

(diurnal cycle — day). It is however interesting that without increased levels in glycogen storage, TA muscle from TSCmKO mice show an increase in activated glycogen synthase.

The results reveal an increased expression of genes involved in glycogenesis and a decreased expression of genes involved in glycolytic flux in TSCmKO muscle. The resulting inability of muscle to break down glycogen and the impairment in glycogenolysis might be responsible for the shift towards alternative fuel utilization. This might lead to a gradual increase in mitochondria size, to overcome the previously observed increase in energy expenditure (Guridi et al, 2015). This is because alternative fuels provide “slower” energy availability. Why the mitochondria increase in size, but do not increase their respiratory capacity still has to be elucidated.

7 Chapter 2: Long-term calorie restriction reduces skeletal muscle myopathy in TSCmKO mice

7.1 Summary

Calorie restriction (CR) without malnutrition is a promising non-invasive intervention, successfully proven to increase health and lifespan. A large body of evidence has shown that CR has positive effects on sarcopenia, the age-associated loss of muscle mass and strength. CR increases cellular stress resistance, induces autophagy, and increases health and lifespan. One pathway thought to be responsible for mediating the positive effects of CR is the downregulation of mTORC1 activity. I used TSCmKO mice to address whether or not CR has beneficial effects on sarcopenia induced by a sustained activation of the mTORC1 pathway in the muscle. CR did not only decrease the oxidative and antioxidative stress response, but also increased skeletal muscle cellular stress resistance by shifting skeletal muscle fiber metabolism towards a slow phenotype. Significant downregulation of fibers, with an aggregation of p62 and ubiquitinated proteins in TSCmKO mice undergoing CR compared to their *ad libitum* fed littermates, was accompanied by a decrease in the percentage of centro-nucleated fibers and normalization of plasma creatine kinase levels. Hence, CR decreased muscle damage and increased physiological parameters, without reducing mTORC1 activity.

7.2 Introduction

7.2.1 Calorie restriction and its beneficial effects

Sarcopenia, the loss of skeletal muscle mass and function, is a hallmark of aging. Calorie restriction (CR), defined as the reduction in food intake without malnutrition, is known as a non-invasive intervention. It has been successfully shown to increase health, and subsequently lifespan in various organisms and animals (Anton & Leeuwenburgh, 2013; Golbidi et al, 2017; Mattison et al, 2017; Yang et al, 2016). CR has additional pleiotropic and largely positive effects for metabolism. Already in 1935, McCay discovered that CR increases life-span in rodents (McCay, 1935). Fifty years later, Weindruch and colleagues described the same finding and showed that this increase in lifespan depends on the amount of CR (Weindruch et al, 1986). Other studies performed in primates were able to show that CR decreased mortality rates (Mattison et al, 2017). Those studies clearly suggest that a mild life-long CR, at least in animals, reveals mostly beneficial effects. Moreover, CR has been shown to improve metabolic fitness and beneficially affects dietary related diseases, such as cardiovascular diseases and diabetes (Colman et al, 2009). Furthermore, CR has expedient effects in certain cancer types, mainly through the downregulation of oxidative stress and an increase in stress resistance. Even dietary interventions and nutritional supplements were recently reported to trigger beneficial effects on neuronal inflammation and depression (Kafami et al, 2010; Martin et al, 2016; Piccio et al, 2008; Redman et al, 2008).

For a long time, it was thought that CR was less easy implementable in humans, as it is said to be impractical for humans to experience life-long calorie restriction. However, recent studies have shown that short-term CR also has major beneficial effects. Four weeks of 40% food reduction or fasting (100% CR for 1-3 days) significantly reduced organ damage and dysfunction, and even fasting overnight can already protect against post-surgery renal failure (Chandrasekar et al, 2001; Verweij et al, 2011). Certain diseases are however, incompatible with preconditioning approaches, such as stroke, traumatic injuries, and heart attacks. In rats, a 24h fast or the delivery of ketones, an important energy supplier upon carbohydrate reduction/deprivation, were sufficient to promote the rats' recovery (Davis et al, 2008;

Robertson & Mitchell, 2013). Molecular changes upon short-term CR in metabolic tissue, e.g. liver, have been reported to be similar to the metabolic changes observed in long-term CR (Cao et al, 2001).

Not only does CR decrease fat mass, it also increases autophagy and improves glucose homeostasis, insulin sensitivity, and resistance to cellular stressors (Bagherniya et al, 2018; Kemnitz et al, 1994; Yang et al, 2016). Studies so far do not point to a single gene or molecular pathway yielding the beneficial effects of CR, but rather pin down several potential mechanisms. On a molecular level, CR enables a fuel switch or more efficient utilization (Anderson & Weindruch, 2010). CR also decreases apoptosis and subsequently increases survival (Phillips & Leeuwenburgh, 2005). Furthermore, CR induces expression of genes that are responsible for the cells stress resistance (Omodei et al, 2013; Yang et al, 2016; Yu & Chung, 2001). Additionally, CR has been shown to increase key mediators of nutrient and energy sensing such as AMPK, general control nonderepressible 2 (GCN2), mTORC1 and Sirtuin 1 (SIRT1).

7.2.2 Calorie restriction and mTORC1

Interestingly, although CR was previously described as having beneficial effects on certain cancers, Kalaany et al. have found that tumors with constitutive activation of the phosphatidylinositol-3-kinase (PI3K) pathway fail to respond to CR (Kalaany & Sabatini, 2009). However, restoring PI3K and PTEN function allows them to respond to the mediated CR effects (Kalaany & Sabatini, 2009). Furthermore, a very striking study was performed on hepatic ischemia reperfusion injury to determine the roles of TSC1 and GCN2, both nutrient sensors, on the cells' resistance to stress. For example, the group of Mitchell used Liver *Tsc1* KO mice and saw that through the upregulation of hepatic mTORC1, cell death in the mice was increased and protective CR mediated mechanisms were lost. Therefore, TSC1, at least in liver, is required to sense dietary restriction mediated protection (Harputlugil et al, 2014).

With robust effects on health and lifespan, but limitations regarding long-term adherence in human populations, there is enormous interest in understanding the underlying mechanisms

responsible for the positive effects of CR. To date, several randomized clinical studies have revealed that humans on dietary restriction (DR) for between six months and two years show similarities to animal models with regards to blood pressure, body weight loss, serum triglycerides and glucose metabolism (Redman et al, 2007; Rochon et al, 2011). Yang et al. were able to show that CR in humans inhibits inflammation by increasing serum cortisol concentrations (Yang et al, 2016). Additionally, CR increased the expression of genes coding for proteins involved in protein quality control by increasing proteostasis via the AKT/FoxO (Forkhead box protein) signaling axis (Yang et al, 2016).

7.2.3 Calorie restriction and its benefits on skeletal muscle

CR had previously been reported to not only have beneficial effects on metabolism and overall health, but also to affect metabolic organs. As early as 2004, it was shown that mitochondrial insults and oxidative stress in old *ad. libitum* fed rats was reversed through the reduction of protein levels in their diet (Usuki et al, 2004). Besides, those rats retained their motor activity at old age, suggesting that even mild CR is enough to attenuate age-related changes in skeletal muscle (Usuki et al, 2004). One suggested mechanism responsible for the positive effects of CR is the suppression of mTORC1 and autophagy induction (Harputlugil et al, 2014; Martinez-Lopez et al, 2017). I therefore addressed the question of whether or not CR would also mediate beneficial effects in TSCmKO mice, independent of mTORC1. Additionally, I was interested in analyzing whether CR is able to improve the myopathy observed in the transgenic mouse model.

7.3 Results

Long-term calorie restriction improves muscle physiology in TSCmKO mice

Elevated cellular stress is frequently observed in several types of muscle myopathies (MM), as well as sarcopenia. In healthy cells or organisms, ROS accumulation can be counteracted through an upregulation of the endogenous ROS buffering system, the antioxidative stress response. CR is a potent promoter of endogenous ROS defense systems and is thought to act largely via the suppression of mTORC1 signaling. For example, in the liver, mTORC1 suppression is necessary to induce stress protective mechanisms sensed by CR (Harputlugil et al, 2014). Next to test whether or not CR beneficial effects can be mediated in skeletal muscle in the absence of TSC1 as an upstream inhibitor of mTORC1, I calorie restricted TSCmKO and control mice for six months as outlined in Sup. Figure 1A. CR lowered body mass by ~15-20% in both control and TSCmKO mice. *Ad. libitum*-fed TSCmKO mice were already lighter (leaner and decreased in fat mass) than their control littermates (Figure 1A) at the beginning of the experiment. As expected, percent whole-body fat mass as measured by EchoMRI was lower in both CR groups than their respective *ad. libitum*-fed littermates (Figure 1B). In control mice, CR resulted in a 25.8% ± 7.1% lower fat mass, whereas in TSCmKO mice, CR resulted in a 10.9% ± 7.2% lower fat mass (Sup. Figure 1B). By using CLAMS, an open circuit indirect calorimeter for mice, I could observe that CR reduces energy consumption in both control and TSCmKO mice (Figure 1C and D). Furthermore, CR particularly changed the energy consumption pattern of control and TSCmKO mice, displaying an increase in activity just before feeding (5 pm) and peaking shortly thereafter. Overall, both CR groups remained less active than *ad. libitum*-fed littermates. The respiratory exchange ratio (RER), monitored during day and night, showed the same pattern as energy consumption levels (Figure 1E). Compared to control mice, RER was significantly higher in TSCmKO mice during the day, but not during the night indicating a greater reliance on glucose metabolism and an increase in energy consumption. Long-term CR normalized daytime RER to control levels (Figure 1E and F). To assess the functional consequences of CR, I measured muscle endurance by using the inverted hangtest.

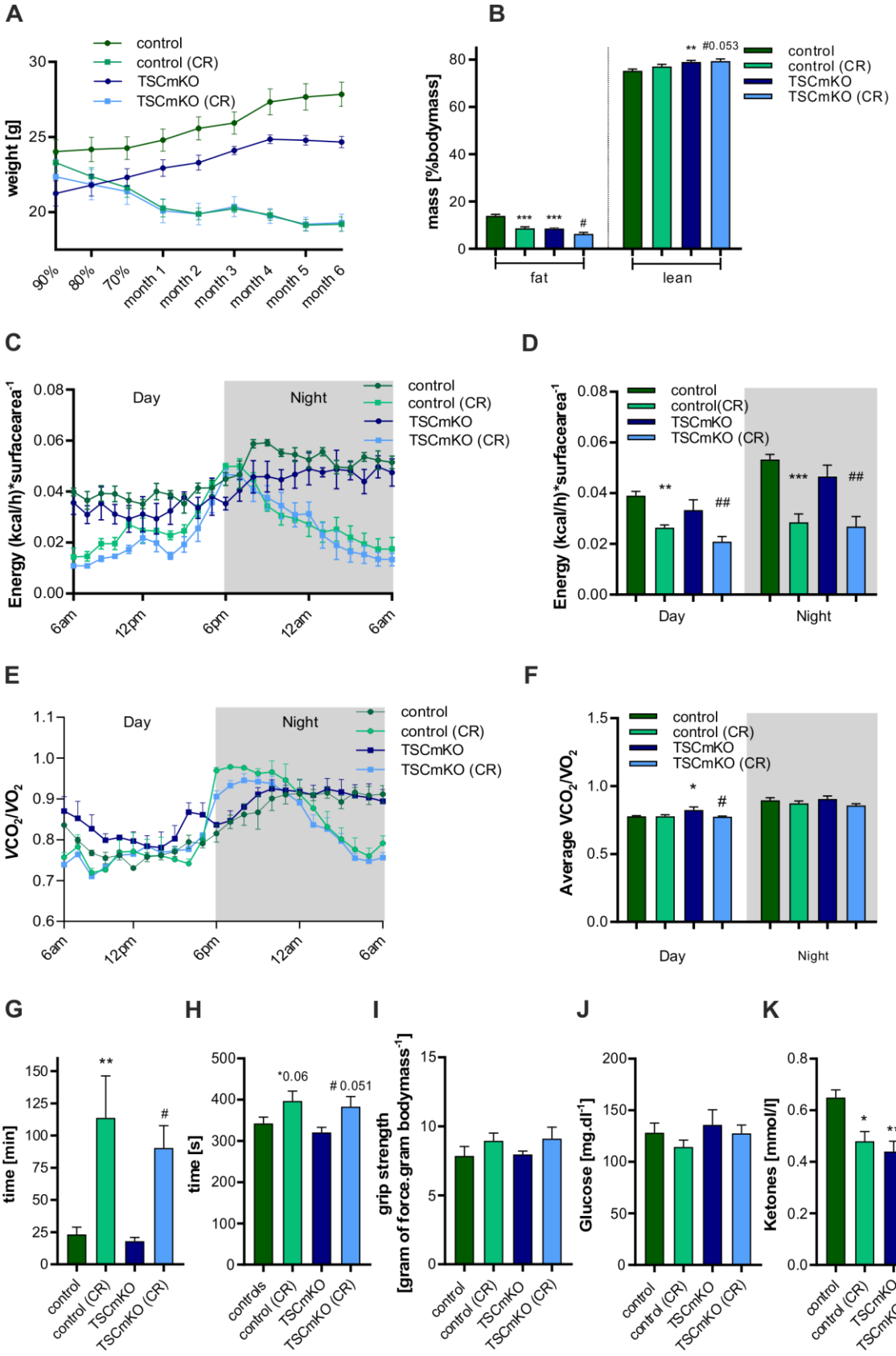
A
control
control (CR)
TSCmKO
TSCmKO (CR)
weight [g]
30
25
20
90%
80%
70%
month 1
month 2
month 3
month 4
month 5
month 6
B
mass [%bodymass]
80
60
40
20
0
**
#0.053
***
***
#
fat
lean
control
control (CR)
TSCmKO
TSCmKO (CR)
C
Energy (kcal/h)*surfacearea-1
0.08
0.06
0.04
0.02
0.00
Day
Night
6am
12pm
6pm
12am
6am
control
control (CR)
TSCmKO
TSCmKO (CR)
D
Energy (kcal/h)*surfacearea-1
0.08
0.06
0.04
0.02
0.00
control
control(CR)
TSCmKO
TSCmKO (CR)
**
##
***
##
Day
Night
E
VCO2/VO2
1.1
1.0
0.9
0.8
0.7
0.6
Day
Night
6am
12pm
6pm
12am
6am
control
control (CR)
TSCmKO
TSCmKO (CR)
F
Average VCO2/VO2
1.5
1.0
0.5
0.0
control
control (CR)
TSCmKO
TSCmKO (CR)
*
#
Day
Night
G
time [min]
150
125
100
75
50
25
0
**
#
control
control (CR)
TSCmKO
TSCmKO (CR)
H
time [s]
500
400
300
200
100
0
*0.06
0.051
controls
control (CR)
TSCmKO
TSCmKO (CR)
I
grip strength
[gram of force.gram bodymass-1]
15
10
5
0
control
control (CR)
TSCmKO
TSCmKO (CR)
J
Glucose [mg.dl-1]
200
150
100
50
0
control
control (CR)
TSCmKO
TSCmKO (CR)
K
Ketones [mmol/l]
0.8
0.6
0.4
0.2
0.0
*
**
control
control (CR)
TSCmKO
TSCmKO (CR)

Figure 1: Long-term calorie restriction improves muscle physiology in TSCmKO mice

(A) Weight curve during the period of 7months. Displayed average of 4 weeks. n ≥ 6. **(B)** Echo MRI analysis of body composition (excluding water content). Values represent mean ± SEM. $^{*}p < 0.05$, $^{**}p < 0.01$, $^{***}p < 0.001$. $^{\#}$ = statistical comparison to TSCmKO. $^{\#}p < 0.05$, $^{\#\#}p < 0.01$, $^{\#\#\#}p < 0.001$. n ≥ 6. **(C)** Graphical representation of the day and night energy consumption as measured by CLAMS (Comprehensive Lab Animal Monitoring System). Values relative to body surface area (weight^0.75). Data averaged for every hour. n = 3. **(D)** Average energy expenditure during light (day) and dark (night) cycle. Average of 12 hours. Values relative to body surface area. Values are mean ± SEM. $^{*}p < 0.05$, $^{**}p < 0.01$, $^{***}p < 0.001$, $^{\#}$ = statistical comparison to TSCmKO. $^{\#}p < 0.05$, $^{\#\#}p < 0.01$, $^{\#\#\#}p < 0.001$. n = 3. **(E)** Graphical representation of RER during day and night as measured by CLAMS (Comprehensive Lab Animal Monitoring System). Data averaged for every hour. n = 3. **(F)** Average respiratory exchanges ratio during light (day) and dark (night) cycles. Average of 12 hours. Values represent mean ± SEM. $^{*}p < 0.05$, $^{**}p < 0.01$, $^{***}p < 0.001$, $^{\#}$ = statistical comparison to TSCmKO. $^{\#}p < 0.05$, $^{\#\#}p < 0.01$, $^{\#\#\#}p < 0.001$. n = 3. **(G)** Inverted hangtest was used to analyze muscle endurance. Endpoint measurements, average of three measurements on three consecutive days. Values are mean ± SEM of data. $^{*}p < 0.05$, $^{**}p < 0.01$, $^{***}p < 0.001$, $^{\#}$ = statistical comparison to TSCmKO. $^{\#}p < 0.05$, $^{\#\#}p < 0.01$, $^{\#\#\#}p < 0.001$. n ≥ 4. **(H)** Rota Rod was used to measure muscle coordination and, somewhat, endurance. Average of three measurements on three consecutive days. Values are mean ± SEM of data. $^{*}p < 0.05$, $^{**}p < 0.01$, $^{***}p < 0.001$, $^{\#}$ = statistical comparison to TSCmKO. $^{\#}p < 0.05$, $^{\#\#}p < 0.01$, $^{\#\#\#}p < 0.001$. n ≥ 6. **(I)** Determination of grip strength. Data represents average of 3 consecutive measurements. Values are mean ± SEM of data. $^{*}p < 0.05$, $^{**}p < 0.01$, $^{***}p < 0.001$, $^{\#}$ = statistical comparison to TSCmKO. $^{\#}p < 0.05$, $^{\#\#}p < 0.01$, $^{\#\#\#}p < 0.001$. n ≥ 4. **(J)** Glucose determination prior to dissection. Values are mean ± SEM of data. $^{*}p < 0.05$, $^{**}p < 0.01$, $^{***}p < 0.001$, $^{\#}$ = statistical comparison to TSCmKO. $^{\#}p < 0.05$, $^{\#\#}p < 0.01$, $^{\#\#\#}p < 0.001$. n ≥ 4. **(K)** Ketone body determination prior to dissection. Values are mean ± SEM of data. $^{*}p < 0.05$, $^{**}p < 0.01$, $^{***}p < 0.001$, $^{\#}$ = statistical comparison to TSCmKO. $^{\#}p < 0.05$, $^{\#\#}p < 0.01$, $^{\#\#\#}p < 0.001$. n ≥ 4.

Long-term CR significantly increased relative muscular endurance in both control and TSCmKO mice (Figure 1G). When calculating muscle endurance relative to body mass, endurance performance was still significantly increased in calorie restricted TSCmKO mice compared to their *ad. libitum* fed littermates (Sup. Figure 1C). CR control and TSCmKO mice performed slightly better in the Rota Rod test compared to their *ad. libitum* fed littermates, indicating increased motor coordination and somewhat endurance (Figure 1H). Furthermore, by measuring physiological performance to evaluate the effect of CR on the physical performance of those mice, I could measure maximal force/tension generated by all four limbs of the mice in a grip strength test (Figure 1I). However, no significant differences were observed. For the metabolic determination of the long-term CR, glucose (Figure 1J) and ketone (Figure 1K) levels were determined from blood plasma prior to sacrifice.

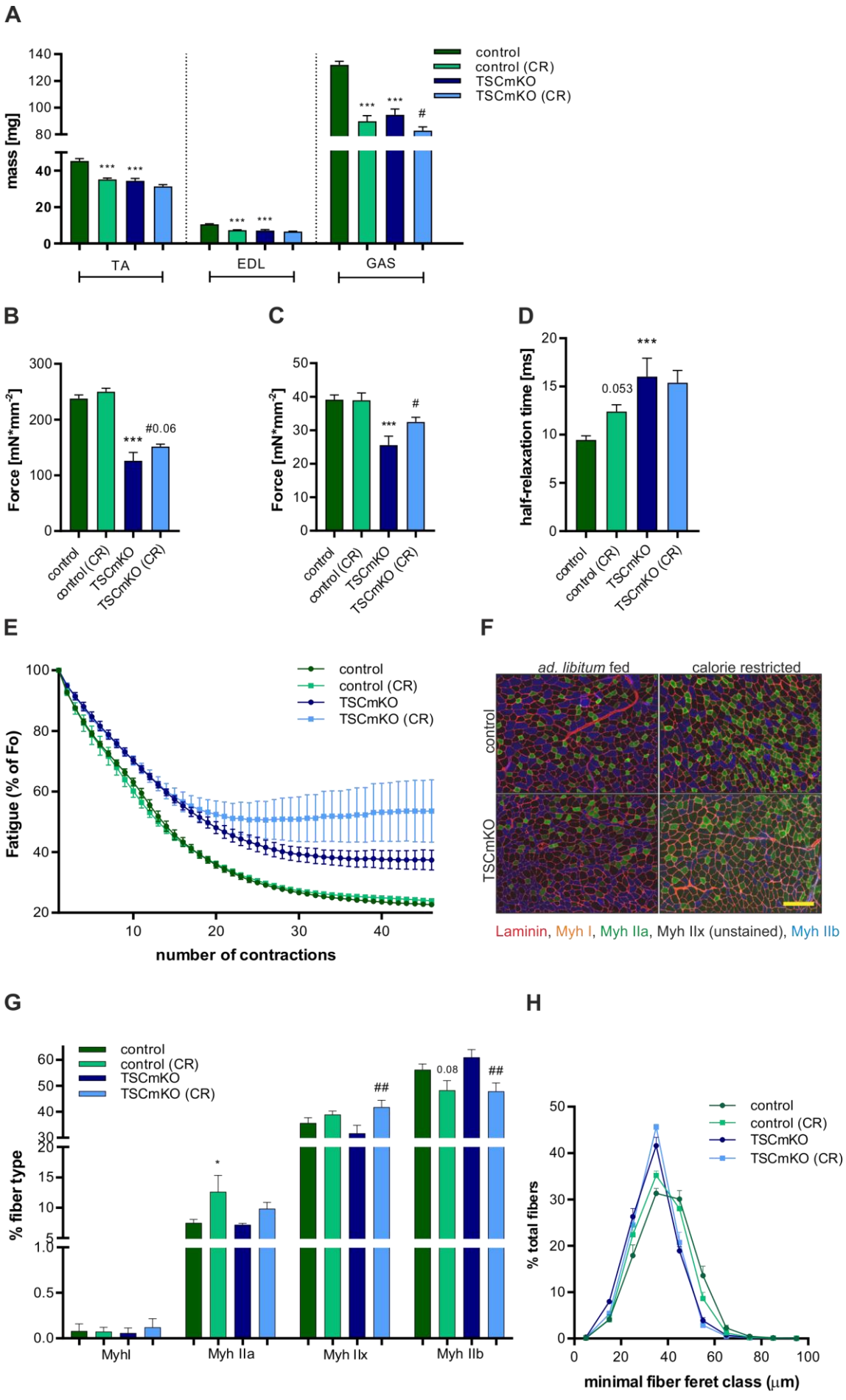
A
mass [mg]
control
control (CR)
TSCmKO
TSCmKO (CR)
TA
EDL
GAS
B
Force [mN*mm-2]
#0.06
C
Force [mN*mm-2]
D
half-relaxation time [ms]
0.053
E
Fatigue (% of Fo)
number of contractions
F
ad. libitum fed
calorie restricted
Laminin, Myh I, Myh IIa, Myh IIx (unstained), Myh IIb
G
% fiber type
Myhl
Myh IIa
Myh IIx
Myh IIb
0.08
H
% total fibers
minimal fiber feret class (µm)

Figure 2: Long-term CR promotes a slower muscle phenotype

(A) Muscle mass of glycolytic hindlimb muscles. n ≥ 6. **(B)** Specific peak force measured in isolated EDL muscle *in vitro* in control and TSCmKO mice with and without long-term CR. Values represent mean ± SEM. $^{*}p < 0.05$, $^{**}p < 0.01$, $^{***}p < 0.001$, $^{\#}$ = statistical comparison to TSCmKO. $^{\#}p < 0.05$, $^{\#\#}p < 0.01$, $^{\#\#\#}p < 0.001$. n ≥ 6. **(C)** Specific twitch force measured in isolated EDL muscle *in vitro* in control and TSCmKO mice with and without long-term CR. Values represent mean ± SEM. $^{*}p < 0.05$, $^{**}p < 0.01$, $^{***}p < 0.001$, $^{\#}$ = statistical comparison to TSCmKO. $^{\#}p < 0.05$, $^{\#\#}p < 0.01$, $^{\#\#\#}p < 0.001$. n ≥ 6. **(D)** Measurement of half relaxation time (HRT) on isolated EDL *in vitro* in TSCmKO mice compared to control mice with and without CR. Values are mean ± SEM. $^{*}p < 0.05$, $^{**}p < 0.01$, $^{***}p < 0.001$, $^{\#}$ = statistical comparison to TSCmKO. $^{\#}p < 0.05$, $^{\#\#}p < 0.01$, $^{\#\#\#}p < 0.001$. n ≥ 6. **(E)** Fatigue analysis of EDL muscle *in vitro* in control and TSCmKO mice with and without long-term CR. Values are mean ± SEM of data. n ≥ 6. **(F)** Immunostaining against laminin-γ1, Myh I, Myh IIa, Myh IIx, and Myh IIb on TA muscle cross sections. Scale bar = 100 µm. **(G)** Quantification of fiber type distribution in controls and TSCmKO *ad. libitum* fed and controls and TSCmKO after long-term CR. Values are mean ± SEM of data normalized to control *ad. libitum* fed. $^{*}p < 0.05$, $^{**}p < 0.01$, $^{***}p < 0.001$, $^{\#}$ = statistical comparison to TSCmKO. $^{\#}p < 0.05$, $^{\#\#}p < 0.01$, $^{\#\#\#}p < 0.001$. n =4. **(H)** Quantification of fiber feret in controls and TSCmKO *ad. libitum* fed, and controls and TSCmKO after long-term CR. Values are mean ± SEM of data normalized to control *ad. libitum* fed. $^{*}p < 0.05$, $^{**}p < 0.01$, $^{***}p < 0.001$, $^{\#}$ = statistical comparison to TSCmKO. $^{\#}p < 0.05$, $^{\#\#}p < 0.01$, $^{\#\#\#}p < 0.001$. n = 4.

Long-term CR did not alter glucose levels in TSCmKO and control mice. Ketone bodies, however, were significantly downregulated in control CR mice, as well as in both TSCmKO groups compared to *ad. libitum* fed controls. EDL muscle weight as well as muscle length were recorded to calculate specific peak and tetanic force. (Sup. Figure 2D and E). I found the muscle weight of the EDL to be similar to the ones isolated for snap frozen muscle tissue (Figure 2A). Skeletal muscle length was significantly reduced in control mice after CR compared to their control littermates. In TSCmKO mice after CR, no significant changes were observed when comparing them to their TSCmKO *ad. libitum* fed littermates. This is because TSCmKO mice already displayed shorter EDL muscle than control mice.

Since CR promotes a fast-to-slow shift in skeletal muscle contractile properties (Russell et al, 1984), I examined twitch half-relaxation time (HRT) and fatigability during repeated tetanic contractions. TSCmKO mice showed a longer HRT as well as greater fatigue resistance (Figure 2D and E), whereas time-to-peak tension (TPT) remained unchanged (Sup. Figure 2F). CR further increased fatigue resistance in TSCmKO mice but did not influence fatigability in the EDL of control mice. I observed a shift in fiber type proportion that was consistent with the CR-induced improvements in fatigue resistance, with more type IIx fibers and fewer type

IIb fibers in calorie-restricted TSCmKO mice (Figure 2F and G). In addition, I observed the previously described atrophy in TSCmKO mice compared to control littermates (Castets et al, 2013). Fiber size was additionally reduced in control mice after CR compared to their *ad. libitum* fed littermates, and it was further reduced in TSCmKO mice after long-term CR compared to TSCmKO *ad. libitum* fed littermates (Figure 2H). In conclusion, CR promotes a slower muscle phenotype in TSCmKO mice as well as control mice.

Long-term CR improves skeletal muscle parameters in slow skeletal muscle

I then investigated effects of CR on soleus (SOL), a muscle largely consisting of slow oxidative fibers. Interestingly, the muscle mass of the SOL significantly increased in TSCmKO mice compared to control littermates, and was resistant to the CR treatment (Figure 3A). In contrast, CR significantly reduced SOL mass in control mice (Figure 3A). However, the CR treatment significantly increased specific peak force of the SOL control as well as TSCmKO mice (Figure 3B). Specific tetanic force in SOL was not increased in TSCmKO mice by long-term CR (Figure 3C). HRT, as well as TPT were increased in the SOL of control and TSCmKO mice after long-term CR (Figure 3D and E). Those results are in line with the increase in fatigue resistance in TSCmKO mice with CR compared to their *ad. libitum*-fed littermates (Figure 3F). SOL is by nature more fatigue resistant than fast skeletal muscle, thanks to its fiber composition and physiological properties. But we should sound a note of caution with regard to such findings as the same protocol as for determining EDL fatigue was utilized for measuring SOL fatigue resistance. Apart from lowering the frequency of the stimulation to 120Hz (200Hz in EDL), the same amount of stimuli was used. Due to the usage of a “weak” fatigue protocol for SOL, only minor changes at the end of the measurement are visible in changes in fatigue resistance. Surprisingly, TSCmKO mice also showed an increase in fatigue resistance compared to control mice without any changes in HRT and TPT.

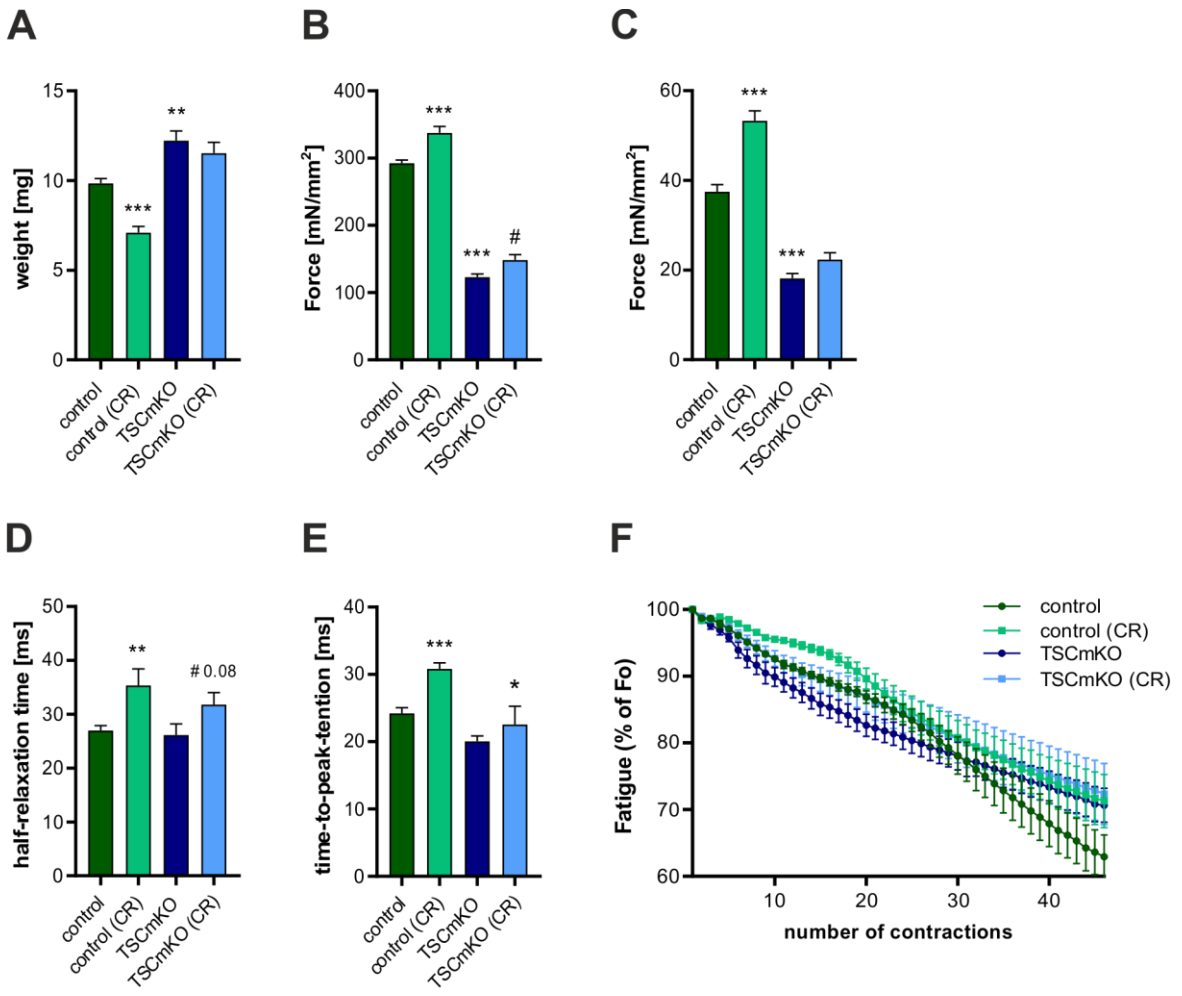

Figure 3: Long-term CR in TSCmKO mice does increase muscle force in slow hindlimb muscle

(A) Muscle mass of oxidative hindlimb muscle soleus. n ≥ 6. **(B)** Specific peak force measured in isolated SOL muscle *in vitro* in control and TSCmKO mice with and without long-term CR. Values represent mean ± SEM. $^{*}p < 0.05$, $^{**}p < 0.01$, $^{***}p < 0.001$, $^{\#}$ = statistical comparison to TSCmKO. $^{\#}p < 0.05$, $^{\#\#}p < 0.01$, $^{\#\#\#}p < 0.001$. n ≥ 6. **(C)** Specific twitch force measured in isolated SOL muscle *in vitro* in control and in TSCmKO mice with and without long-term CR. Values represent mean ± SEM. $^{*}p < 0.05$, $^{**}p < 0.01$, $^{***}p < 0.001$, $^{\#}$ = statistical comparison to TSCmKO. $^{\#}p < 0.05$, $^{\#\#}p < 0.01$, $^{\#\#\#}p < 0.001$. n ≥ 6. **(D)** Measurement of half relaxation time (HRT) on isolated SOL *in vitro* in TSCmKO mice compared to control mice with and without CR. Values are mean ± SEM. $^{*}p < 0.05$, $^{**}p < 0.01$, $^{***}p < 0.001$, $^{\#}$ = statistical comparison to TSCmKO. $^{\#}p < 0.05$, $^{\#\#}p < 0.01$, $^{\#\#\#}p < 0.001$. n ≥ 6. **(E)** Determination of time-to-peak tension (TPT) in isolated SOL *in vitro* in TSCmKO mice compared to control littermates with and without CR. Values are mean ± SEM. $^{*}p < 0.05$, $^{**}p < 0.01$, $^{***}p < 0.001$, $^{\#}$ = statistical comparison to TSCmKO. $^{\#}p < 0.05$, $^{\#\#}p < 0.01$, $^{\#\#\#}p < 0.001$. n ≥ 6. **(F)** Fatigue analysis of EDL muscle *in vitro* in control and in TSCmKO mice with and without long-term CR. Values are mean ± SEM of data. n ≥ 6.

Long-term CR decreases p62 accumulation independent of mTORC1 signaling and without reactivation of autophagy

To test whether CR would eventually blunt mTORC1 signaling in TSCmKO mice, I examined the phosphorylation status of mTOR and its downstream targets — ribosomal protein S6 (S6) and eukaryotic translation initiation factor 4E-binding protein 1 (4E-BP1) — in TA glycolytic muscle (Figure 4A). As expected, the phosphorylation status of mTOR, S6 and 4E-BP1 were significantly higher in TSCmKO than in control mice (Figure 4A). Long-term CR failed to significantly reduce phosphorylation of these proteins in both genotypes (Figure 4A). Similar results were obtained in other glycolytic muscle and the other gender, such as gastrocnemius and females (Sup. Figure 3A and B). Despite the inability of CR to reduce mTORC1 signaling, CR significantly reduced the proportion of fibers containing p62 aggregates in TSCmKO muscle (Figure 4B and C). Aggregates of p62, which are known to accumulate as a result of impaired autophagy (Bjorkoy et al, 2005), are observed in TSCmKO, but not in control muscle (Figure 4B and C). Western blot analysis confirmed the reduction in p62 in TSCmKO muscle after long-term CR (Figure 4D and E).

Interestingly, protein levels of PINK and Parkin were also reduced in TSCmKO mice after long-term CR (Figure 4D and E), suggesting a decreased need of the autophagic system. PINK and Parkin protein levels were previously reported to be increased (Chapter 1), due to impaired mitophagy. To assess whether or not changes in autophagic/mitophagic markers were related to changes in autophagic flux, I treated mice with colchicine on three consecutive days to block the degradation of material marked for autophagolysosomal degradation. In contrast to previously reported CR studies (Bagherniya et al, 2018; Makino et al, 2015; Yang et al, 2016), I found that colchicine similarly increased LC3II levels in *ad. libitum*-fed and CR conditions in 10.5-month-old control mice (Figure 4F and G). This suggests at least in healthy adult (10.5-month-old) B57CL/6JRj mice, that long-term CR does not promote induction of autophagy flux. Similarly, long-term CR did not induce autophagy in TSCmKO muscle, as shown by the lack of buildup in LC3II upon colchicine treatment in both *ad. libitum* and CR conditions (Figure 4G).

In order to visualize the involvement of upstream effectors, mRNA expression of genes encoding for proteins involved in the autophagolysosomal-mediated degradation of proteins and/or organelles was monitored. CR significantly downregulated relative *p62/Sqstm1* mRNA expression in TSCmKO mice (Figure 4H). The reduced *p62/Sqstm1* transcription levels could potentially be mediated through activating AKT/PKB-signaling and subsequently inhibiting FoxO. However, long-term CR did not change AKT-signaling in TSCmKO mice (Sup. Figure 3C). Together, these data indicate that CR reduces p62 accumulation in TSCmKO mice by reducing damage to organelles and proteins rather than reinitiating autophagy.

Long-term CR blunts cellular stress in TSCmKO mice and reduces ubiquitinated proteins

CR is known to increase cellular stress resistance (Sanz et al, 2004; Stankovic et al, 2013), by decreasing oxidative stress and increasing mitochondrial function (Hempenstall et al, 2012; Higami et al, 2004). Therefore, I wondered whether or not CR was sufficient to reverse oxidative stress in our TSCmKO mice. CR lowered the mRNA expression of markers of ER/cellular stress in TSCmKO muscle, including Tribbles Pseudokinase 3 (*Trib3*), Activating Transcription Factor 4 (*Atf4*), Glutathione S-Transferase Alpha 1 (*Gsta1*), and Glutathione Peroxidase 1 (*Gpx1*), which were all increased in TSCmKO *ad. libitum* fed mice compared to controls (Figure 5A). In addition, protein levels of GSS and ATF4, which are involved in the antioxidative stress response and ER stress, respectively, were also decreased in TSCmKO mice after CR (Figure 5B and C). The atrophy-related ubiquitin ligases — Atrogin1 (*Fbxo32*) and MuRF1 (*Trim63*) — also showed a tendency to be downregulated in TSCmKO mice after long-term CR (Figure 5D), thus suggesting a reduction in muscle breakdown through the ubiquitin-proteasome system. Furthermore, I observed a significant reduction in the accumulation of mono- and poly-ubiquitinated proteins in TSCmKO muscle after long-term CR (Figure 5E), which rather suggests a decreased accumulation of defective proteins.

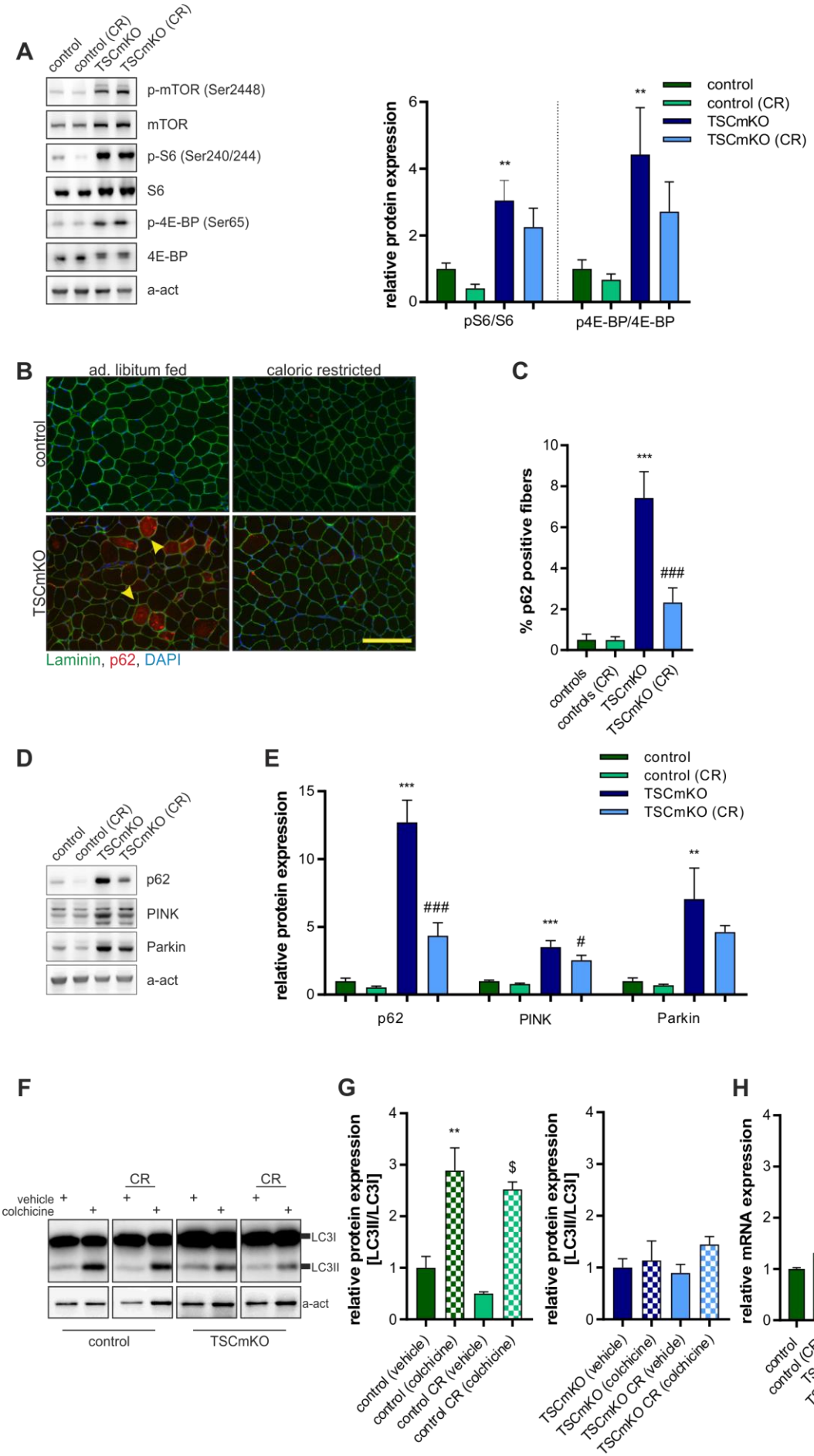
A
control
control (CR)
TSCmKO
TSCmKO (CR)
p-mTOR (Ser2448)
mTOR
p-S6 (Ser240/244)
S6
p-4E-BP (Ser65)
4E-BP
a-act
relative protein expression
control
control (CR)
TSCmKO
TSCmKO (CR)
pS6/S6
p4E-BP/4E-BP
B
ad. libitum fed
caloric restricted
control
TSCmKO
Laminin, p62, DAPI
C
% p62 positive fibers
controls
controls (CR)
TSCmKO
TSCmKO (CR)
D
p62
PINK
Parkin
a-act
E
relative protein expression
p62
PINK
Parkin
F
vehicle
colchicine
CR
LC3I
LC3II
a-act
control
TSCmKO
G
relative protein expression [LC3II/LC3I]
control (vehicle)
control (colchicine)
control CR (vehicle)
control CR (colchicine)
TSCmKO (vehicle)
TSCmKO (colchicine)
TSCmKO CR (vehicle)
TSCmKO CR (colchicine)
H
relative mRNA expression
control
control (CR)
TSCmKO
TSCmKO (CR)

Figure 4: Long-term CR decreases p62 accumulation independent of mTORC1 signaling and without reactivation of autophagy

(A) Immunoblots and quantification of control and TSCmKO littermates with and without long-term CR for the total- and phospho- (p-) proteins involved in mTORC1 signaling and subsequent quantification. p-sites indicated in brackets. Data normalized to α–actinin. Values represent mean ± SEM of data. $^{*}p < 0.05$, $^{**}p < 0.01$, $^{***}p < 0.001$, $^{\#}$ = statistical comparison to TSCmKO. $^{\#}p < 0.05$, $^{\#\#}p < 0.01$, $^{\#\#\#}p < 0.001$. n ≥ 6**. (B)** Immunostaining against p62 and laminin-γ1 on TA muscle cross-sections of TSCmKO mice and control littermates with and without long-term CR. Scale Bar=200 µm. **(C)** Quantification of p62 aggregated fibers. Values represent mean ± SEM. $^{*}p < 0.05$, $^{**}p < 0.01$, $^{***}p < 0.001$, $^{\#}$ = statistical comparison to TSCmKO. $^{\#}p < 0.05$, $^{\#\#}p < 0.01$, $^{\#\#\#}p < 0.001$. n=4. **(D)** Immunoblots for the indicated proteins in TA muscle total protein lysates of control and TSCmKO littermates with and without long-term CR. Data normalized to α–actinin. Values represent mean ± SEM of data. $^{*}p < 0.05$, $^{**}p < 0.01$, $^{***}p < 0.001$, $^{\#}$ = statistical comparison to TSCmKO. $^{\#}p < 0.05$, $^{\#\#}p < 0.01$, $^{\#\#\#}p < 0.001$. n ≥ 6. **(E)** Quantification of immunoblots (Figure 5D). Values represent mean ± SEM of data. $^{*}p < 0.05$, $^{**}p < 0.01$, $^{***}p < 0.001$, $^{\#}$ = statistical comparison to TSCmKO. $^{\#}p < 0.05$, $^{\#\#}p < 0.01$, $^{\#\#\#}p < 0.001$. n ≥ 6. **(F)** Relative gene expression of *Sqstm1*, encoding for p62, in TA from 10.5-month-old TSCmKO mice compared to control mice with and without CR. Values represent mean ± SEM of data normalized to *β-actin* levels. $^{*}p < 0.05$, $^{**}p < 0.01$, $^{***}p < 0.001$, $^{\#}$ = statistical comparison to TSCmKO. n ≥ 6. **(G)** Colchicine treatment (+) of control and TSCmKO mice with and without CR treatment. Data normalized to α–actinin. n ≥ 3. Only for CR controls n = 2. **(H)** Quantification of the LC3II/ LC3I ratio. Data normalized to α–actinin. Values represent mean ± SEM. $^{*}p < 0.05$, $^{**}p < 0.01$, $^{***}p < 0.001$, $^{\#}$ = statistical comparison to TSCmKO. $^{\#}p < 0.05$, $^{\#\#}p < 0.01$, $^{\#\#\#}p < 0.001$. n ≥ 3. Only for CR controls n = 2.

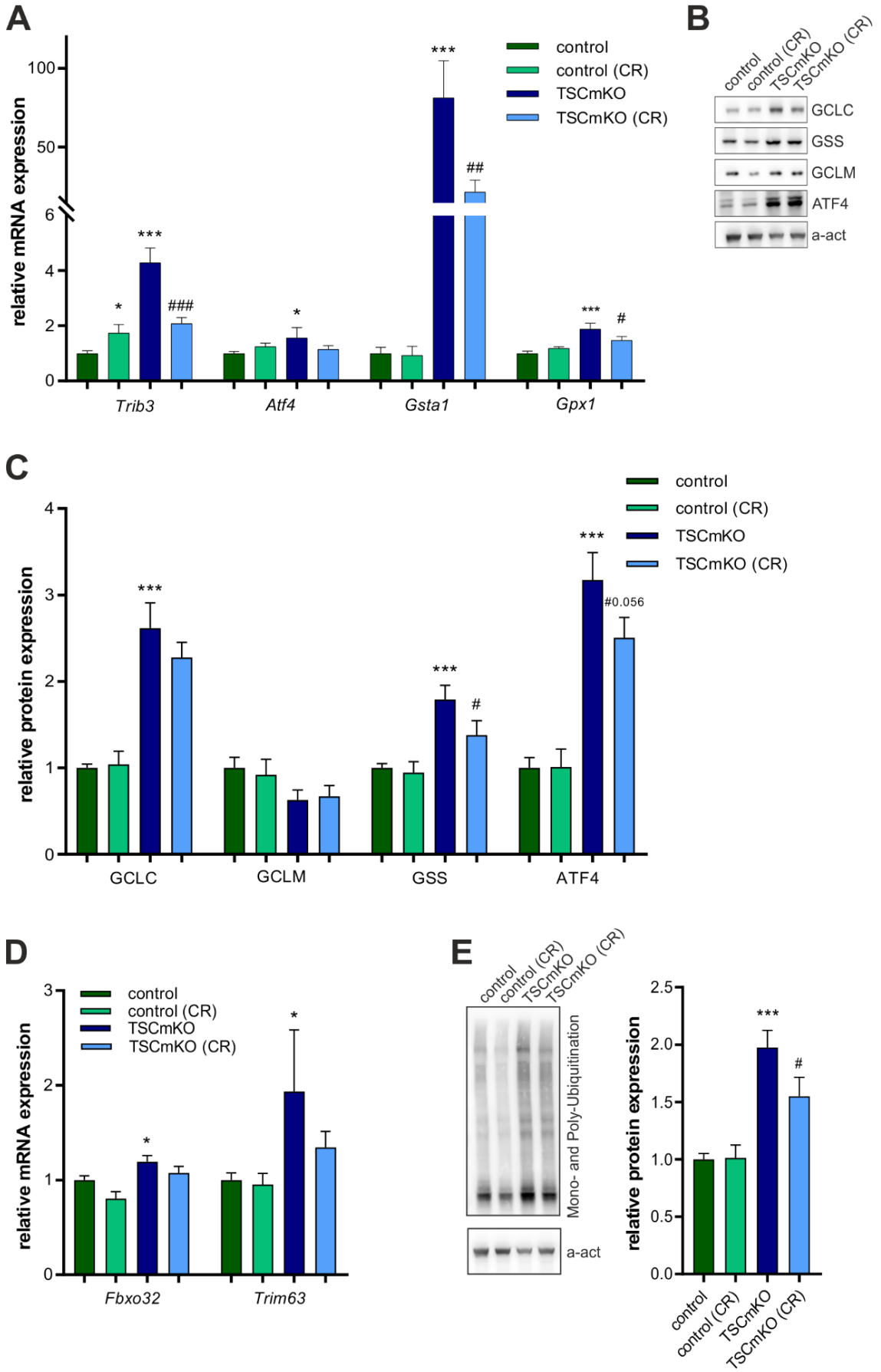
A
relative mRNA expression
100
50
6
4
2
0
control
control (CR)
TSCmKO
TSCmKO (CR)
***
*
***
###
*
##
***
#
Trib3
Atf4
Gsta1
Gpx1
B
control
control (CR)
TSCmKO
TSCmKO (CR)
GCLC
GSS
GCLM
ATF4
a-act
C
relative protein expression
4
3
2
1
0
control
control (CR)
TSCmKO
TSCmKO (CR)
***
***
***
#
***
#0.056
GCLC
GCLM
GSS
ATF4
D
relative mRNA expression
3
2
1
0
control
control (CR)
TSCmKO
TSCmKO (CR)
*
*
Fbxo32
Trim63
E
control
control (CR)
TSCmKO
TSCmKO (CR)
Mono- and Poly-Ubiquitination
a-act
relative protein expression
2.5
2.0
1.5
1.0
0.5
0.0
***
#
control
control (CR)
TSCmKO
TSCmKO (CR)

Figure 5: Long-term CR blunts cellular stress in TSCmKO mice

(A) Expression of genes encoding proteins involved in ER stress (*Trib3* and *Atf4*) and anti-oxidative stress response (*Gsta1* and *Gpx1*) in TSCmKO mice compared to control littermates with and without CR. Values are mean ± SEM of data normalized to ***β-actin*** levels. $^{*}p < 0.05$, $^{**}p < 0.01$, $^{***}p < 0.001$, $^{\#}$ = statistical comparison to TSCmKO. $^{\#}p < 0.05$, $^{\#\#}p < 0.01$, $^{\#\#\#}p < 0.001$. n ≥ 4. **(B)** Immunoblots of indicated proteins in TA muscle total protein lysates of proteins involved in glutathione synthesis. n = 4. **(C)** Quantification of immunoblots (Figure 6B). Data normalized to α–actinin. Values are mean ± SEM of data. $^{*}p < 0.05$, $^{**}p < 0.01$, $^{***}p < 0.001$, $^{\#}$ = statistical comparison to TSCmKO. $^{\#}p < 0.05$, $^{\#\#}p < 0.01$, $^{\#\#\#}p < 0.001$. n = 4. **(D)** mRNA expression levels of the E3 ubiquitin ligases *p62 and MAFbx/Atrogin-1* (*Fbox32*) in TA muscle. Values are mean ± SEM of data. $^{*}p < 0.05$, $^{**}p < 0.01$, $^{***}p < 0.001$, $^{\#}$ = statistical comparison to TSCmKO. n = 4. **(E)** Immunoblots of mono- and poly-ubiquitinylated proteins in TA whole muscle lysate and quantification in TSCmKO and in control mice with and without CR. Data normalized to α–actinin. Values are mean ± SEM of data. $^{*}p < 0.05$, $^{**}p < 0.01$, $^{***}p < 0.001$, $^{\#}$ = statistical comparison to TSCmKO. $^{\#}p < 0.05$, $^{\#\#}p < 0.01$, $^{\#\#\#}p < 0.001$. n ≥ 6.

Long-term CR decreases muscle damage in TSCmKO mice

Consistent with reduced signs of muscle damage and breakdown, I observed a visible amelioration of the pathology in TSCmKO CR cross sections of TA muscle H&E staining compared to TSCmKO *ad. libitum* fed littermates (Figure 6A). In line with the pathological amelioration, I observed decreased amounts of vacuolated fibers in TSCmKO mice after long-term CR compared to their *ad. libitum* fed littermates (Figure 6B). Besides the decrease in vacuolated fibers a significant decrease in the proportion of centro-nucleated fibers in TSCmKO muscle after CR was observed (Figure 5C). Furthermore, CR completely prevented the abnormally high levels of creatine kinase (CK), a common marker for determination of muscle damage (Brancaccio et al, 2010), detected in the blood of TSCmKO mice (Figure 5D). These results indicate that long-term CR reduces cellular stress in TSCmKO muscle, thus preventing muscle damage and the accumulation of p62-labeled proteins and organelles.

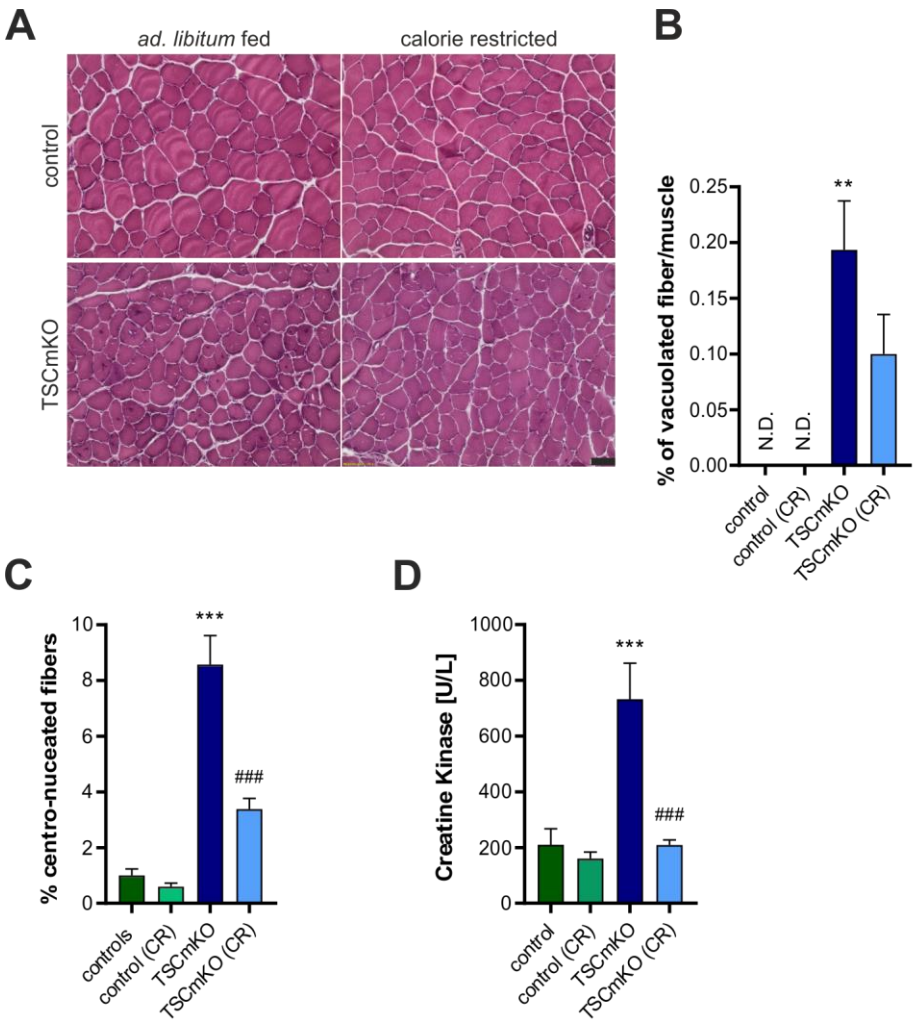

Figure 6: Long-term CR improves myopathy in TSCmKO mice

(A) Hematoxylin and Eosin staining of control and TSCmKO TA cross sections with and without CR. Scale Bar = 50µ. **(B)** Quantification of %-vacuolated fibers in TSCmKO mice and in control littermates with and without CR. N.D. = not detected. Values represent mean ± SEM. $^{*}p < 0.05$, $^{**}p < 0.01$, $^{***}p < 0.001$, $^{\#}$ = statistical comparison to in TSCmKO. $^{\#}p < 0.05$, $^{\#\#}p < 0.01$, $^{\#\#\#}p < 0.001$. n ≥ 6. **(C)** Quantification of %-centro-nucleated fibers in control and TSCmKO mice with and without long-term CR. Values represent mean ± SEM. $^{*}p < 0.05$, $^{**}p < 0.01$, $^{***}p < 0.001$, $^{\#}$ = statistical comparison to TSCmKO. $^{\#}p < 0.05$, $^{\#\#}p < 0.01$, $^{\#\#\#}p < 0.001$. n ≥ 6. **(D)** Creatine kinase levels measured from blood plasm by using COBAS in control and in TSCmKO mice with and without CR. Values are mean ± SEM of data. $^{*}p < 0.05$, $^{**}p < 0.01$, $^{***}p < 0.001$, $^{\#}$ = statistical comparison to TSCmKO. $^{\#}p < 0.05$, $^{\#\#}p < 0.01$, $^{\#\#\#}p < 0.001$. n ≥ 6.

7.4 Discussion

A growing body of evidence has shown that mild calorie restriction of 10-40% without malnutrition increases health and lifespan. A recent study in rhesus monkeys observed a decrease in age-related mortality rate with mild lifelong CR (Colman et al, 2014; Mattison et al, 2017). Additionally, CR in rodent animal models showed an extension in lifespan of up to 40% (Weindruch et al, 1986). Already in 1986, Weindruch and colleagues described that CR does not only extend lifespan but does this in a dose-dependent manner (Weindruch et al, 1986). Later studies showed that a 30-40% CR has beneficial health and life prolonging effects (Stankovic et al, 2013). mTORC1 is a well-recognized nutrient sensor, which is downregulated in response to starvation (Cheng et al, 2004; Kim et al, 2013; Peng et al, 2002). A recent study has discovered that, in the liver, TSC is required to mediate the beneficial effects of calorie restriction (Harputlugil et al, 2014). My experiments in TSCmKO mice now suggest that TSC1 is not entirely responsible for mediating the beneficial effects of CR in skeletal muscle. The results strongly indicate that mTORC1-independent pathways contribute to the amelioration of the myopathy observed in TSCmKO mice after long-term CR.

Calorie restriction decreases body mass in TSCmKO mice and alters their metabolism by decreasing metabolic rate

TSCmKO mice have been previously shown to exhibit a lean phenotype with a significant reduction in fat mass and decreased body weight (Castets et al, 2013). The reduced body weight and reduction in fat mass was also observed in the TSCmKO mice used for my CR study (Figure 1A and B). An explanation for the loss in fat mass might be the increase in FAO, which may result from the reported decreased ATP levels, and a subsequent metabolic shift towards slower energy supplies (Chapter 1, (Guridi et al, 2015)). These results indicate that TSCmKO mice, even without CR, are in a metabolic state similar to the one observed during fasting.

Following 6 months of CR, I observed a similar reduction in body weight (~15-20%) in TSCmKO mice and in wild type (littermate) control animals. However, when comparing the loss of body mass (in %) from TSCmKO *ad. libitum* fed mice and TSCmKO CR mice to the percentage weight loss of control *ad. libitum* fed mice and control CR mice, I found the weight decrease (in %) was smaller in TSCmKO mice than in wild-type controls (Sup. Figure 1B). I did not detect any significant changes in blood glucose between *ad. libitum* fed TSCmKO mice compared to *ad. libitum* fed controls (Figure 1J). However, unexpectedly, blood glucose was also not affected by CR. Metabolic adaptations to the long-term CR treatments might be caused by mice metabolism adapting to the CR state over a long period of time and to overcome the long-starvation phases. In particular, the insulin resistance developed in TSCmKO mice, as previously described in our group (Guridi et al, 2015), may be responsible for the adaptive glucose sparing. Glucose levels may therefore be high during and after their feeding period, and decrease only slightly during their fasting period.

Interestingly, ketone plasma levels are decreased in TSCmKO mice compared to control littermates (Figure 1K). Long-term CR also decreased blood ketones to an extend similar to that in TSCmKO *ad. libitum* fed littermates. Due to the increase in FAO, decreased ketone levels were rather surprising. However, ketone bodies are the major energy source for the brain during starvation and longer fasting periods upon glucose deprivation, which might explain the significant reduction of ketone bodies in both CR groups within the blood. Ketones also serve as an alternative energy source for skeletal muscle and the heart, which can also use other energy sources, whereas the brain cannot. CLAMS analysis revealed an increase in carbohydrate utilization during the fed period in TSCmKO mice, again, highlighting a predominant usage of fatty acids during their fasting period. Altogether, these results clearly indicate that the CR treatment successfully reduced body mass and basal metabolic rate in the TSCmKO mice.

Calorie restriction improves "mTORC1"- driven myopathy and features of sarcopenia without altering mTORC1 signaling

Sarcopenia, the age associated loss of muscle mass and strength, has been shown to share common signs with dystrophies (inherited myopathies) (Sakuma et al, 2014). By closer observation, TSCmKO mice suffer from a late-onset myopathy and show a range of sarcopenic characteristics. Common signs in sarcopenia and TSCmKO mice are: (I) an increase in fiber size variation; (II) atrophy; (III) an increase in centralized nuclei; (IV) impairment of autophagy/mitophagy; (V) defects in calcium homeostasis (Chapter 3); and (VI) an increase in oxidative stress (Chapter 1) (Castets et al, 2013). The involvement of the PI3K/Akt/mTOR signaling, however, remains debated. PI3K/Akt/mTOR signaling is thought to be decreased with age, whereas other publications report no alteration or even an increase, dependent on the model organism used or tissue examined (Baar et al, 2016; Johnson et al, 2013; Kapahi et al, 2004; Powers et al, 2006). In contrast, in TSCmKO mice, mTORC1 is always active in skeletal muscle tissue. Not surprisingly, mTORC1 signaling was still hyperactive in TSCmKO mice after long-term CR, due to the *Tsc1* genetic ablation (Figure 4A). In control mice undergoing the CR, mTORC1 signaling was downregulated, however not significantly. Inversely, Akt- signaling was only slightly increased in control CR mice compared to the *ad. libitum* fed controls (Sup. Figure 3A), which may also explain the normal expression levels of atrogenes.

As shown in chapter 1 and as previously described, TSCmKO mice display an increase in oxidative stress and ER stress, respectively (Guridi et al, 2015). The CR treatment significantly reduced mRNA as well as protein expression for a number of ER stress markers, and such involved in the antioxidative stress response in TA muscle of TSCmKO mice, thus indicating a reduced protein-folding stress in the ER (Figure 5A, B and C). The antioxidative stress response usually required to scavenge reactive oxygen species has been shown to be increased upon mild CR. In particular, the oxidative scavenger GSH (reduced glutathione) increases during long-term CR (Laganiere & Yu, 1989; Stankovic et al, 2013). Several

scientists explain this effect as “hormesis”. “Hormesis” is the favorable biological response to low levels of stress inducing adaptive mechanisms to increase cellular stress resistance (Le Bourg, 2009; Marques et al, 2009; Masoro, 1998; Radak et al, 2008). However, ER-stress and antioxidative stress response are downregulated in muscle from TSCmKO mice after long-term CR. The reduced expression of genes involved in the antioxidative stress response and the decrease of genes involved in the assembly of the reduced glutathione (GSH) suggests less accumulation of damage, rather than an adaptive increase of cellular stress resistance.

Long term CR limits the development of mTORC1-driven myopathy

CR has previously been reported to shift skeletal muscle towards a slower/more oxidative phenotype (De Andrade et al, 2015; Henriksson, 1990). This is thought to be an adaptive response of the muscle, as slow skeletal muscle has been shown to be more stress resistant and to be often spared by certain diseases (Gumerson et al, 2010; Rice & Blough, 2006; Selsby et al, 2012). Long term CR does indeed induce a shift towards a more oxidative muscle fiber phenotype, in control as well as in TSCmKO mice (Figure 2F and G). In line with the fiber-type switch, fatigue resistance, which was already increased in TSCmKO mice compared to wild-type controls, was even further increased after long term CR (Figure 2E). Investigation of skeletal muscle physiology revealed an increase in skeletal muscle endurance and motor coordination in control and in TSCmKO mice after long term CR (Figure 1G and H). This is in agreement with the observed fiber type switch in TA of both mouse groups towards more oxidative. Analyzing specific twitch and tetanic force confirmed the previously observed reduction of isometric force in the skeletal muscle of TSCmKO mice (Castets et al, 2013). Surprisingly, only TSCmKO mice show an increase in peak tetanic and twitch forces after CR, whereas the calorie deprivation did not have an effect on the force generation in control mice. This was rather unexpected, as studies have previously reported, at least in old sarcopenic mice, that CR increases isometric forces. As the control mice are rather young (10.5-month-

old), the effect of CR might be less significant compared to the old (24- to 32-months old) mice used in sarcopenia studies.

Interestingly, the effect of CR on the muscle physiology was much more profound in oxidative (SOL) muscle (Figure 3). Control and TSCmKO mice both show a significant increase in specific tetanic and twitch force compared to *ad. libitum*-fed mice of the same genotype. Surprisingly, however, CR did not significantly reduce the weight of the SOL muscle in TSCmKO mice, whereas this was indeed the case in wild-type mice (Figure 3A). It is known that CR can have different effects on slow compared to fast muscle. However, how this activation of different signaling pathways occurs is unknown. It would indeed be very interesting to identify the molecular mechanisms responsible for the SOL hypertrophy, for the resistance to CR, and for the significant amelioration in physiological performance. This may reveal new factors to counteract pathological features usually occurring in fast skeletal muscle due to particular pathologies. That said, the improvement in skeletal muscle physiology in TSCmKO in response to the CR treatment most likely has several underlying mechanisms: (I) a decrease in oxidative stress; (II) a decreased accumulation of defective proteins and organelles; (III) a decrease in muscle damage; or (IV) an interplay of all four.

TSCmKO mice display an impairment of autophagy (Castets et al, 2013) combined with an impairment of mitophagy (Chapter 1), leading to an increased density of skeletal muscle mitochondria. Impaired autophagy leads to an accumulation of defective proteins and organelles and can be detrimental for the cells function. CR significantly decreased the accumulation of the E3 ubiquitin binding protein p62 in TSCmKO mice. In addition, the amount of ubiquitinated proteins was significantly reduced by CR. CR has been previously described to increase autophagic flux (Makino et al, 2015). However, blocking autophagosomal degradation with colchicine *in vivo* failed to reveal that CR had a significant effect on autophagic flux in TSCmKO as well as in wild-type control mice (Figure 4F, G). As the mRNA for *p62/Sqstm1* was significantly downregulated in TSCmKO muscle in response to CR (Figure 4H), one can speculate that a lower input (transcription and protein synthesis) rather than an

increased autophagic flux accounts for the decrease in the accumulation of damaged material in TSCmKO mice after long-term CR. In support of this hypothesis, I found that long-term CR of TSCmKO mice significantly reduced various skeletal muscle parameters associated with muscle damage, such as the number of centralized nuclei and creatine kinase levels. Interestingly, recent findings uncovered an antioxidant response element within the *p62/Sqstm1* promoter, which is induced by the NF-E2-related factor 2 (NRF2) during oxidative stress (Jain et al, 2010). I previously showed the oxidative stress to be downregulated upon CR treatment in TSCmKO muscle. A decrease in oxidative stress with a subsequent decrease in NRF2 expression may therefore be responsible for the downregulation of *p62/Sqstm1* gene expression levels. The involvement of NRF2 in regulating *p62/Sqstm1* transcription in TSCmKO skeletal muscle still has to be elucidated.

In summary, my results clearly indicate a beneficial effect of CR on skeletal muscle metabolism, muscle pathology, and subsequent muscle physiology, thus ameliorating the skeletal muscle myopathy in TSCmKO mice. Myopathies are often multisystemic diseases, influencing various tissues and whole-body metabolism. As the physiological parameters only revealed minor, but significant amelioration, it may be of benefit to use combined therapies, such as CR and low intensity exercise to further boost skeletal muscle physiology in myopathies in the future. The beneficial effects of CR are also known to be mediated via SIRT1 or AMPK phosphorylation. It might be interesting to investigate these pathways in the context of the CR-mediated amelioration of the TSCmKO muscle phenotype. But one should bear in mind that CR acts in a multisystemic manner, influencing various tissues (Mitchell et al, 2015; Redman et al, 2008). Extrinsic factors might therefore contribute to the amelioration of the skeletal muscle myopathy. It would be interesting to observe the contribution of other organs — such as the liver, as an important metabolic organ — to the positive effects of CR on the well-being of the TSCmKO mice and the potential, extrinsically mediated effects on skeletal muscle metabolism, for example, by providing energy or proteins.

7.5 Appendix

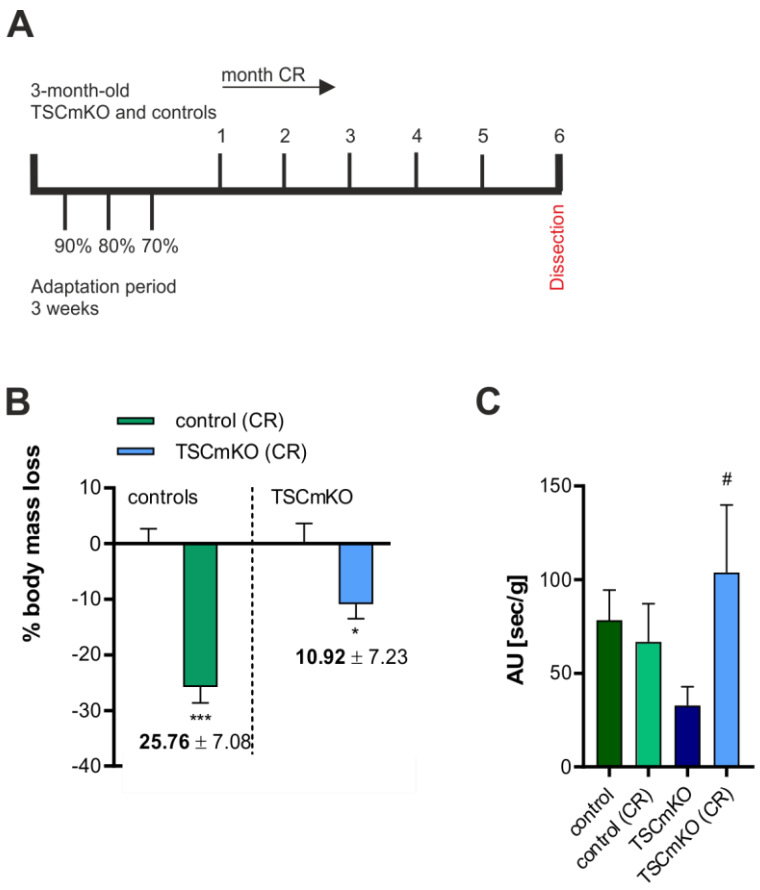

Supplemental Figure 1: Long-term calorie restriction decreases body mass and improves motor coordination in TSCmKO mice, Related to Figure 1.

(A) Schematic depiction of the long-term CR treatment. Mice were calorie restricted over a period of 6 months after a 3-week-long adaptation period with a reduction of food intake of 10% each week **(B)** Delta body mass loss in controls and in TSCmKO mice with and without CR. Weight as endpoint measurement, prior to dissection. Values represent mean ± SEM. $^{*}p < 0.05$, $^{**}p < 0.01$, $^{***}p < 0.001$. n ≥ 6. **(C)** Augmented value of inverted hangtime relative to body weight in controls CR and TSCmKO CR and in their control littermates. Values represent mean ± SEM. $^{*}p < 0.05$, $^{**}p < 0.01$, $^{***}p < 0.001$. $^{\#}$ = statistical comparison to TSCmKO. $^{\#}p < 0.05$, $^{\#\#}p < 0.01$, $^{\#\#\#}p < 0.001$. n ≥ 6.

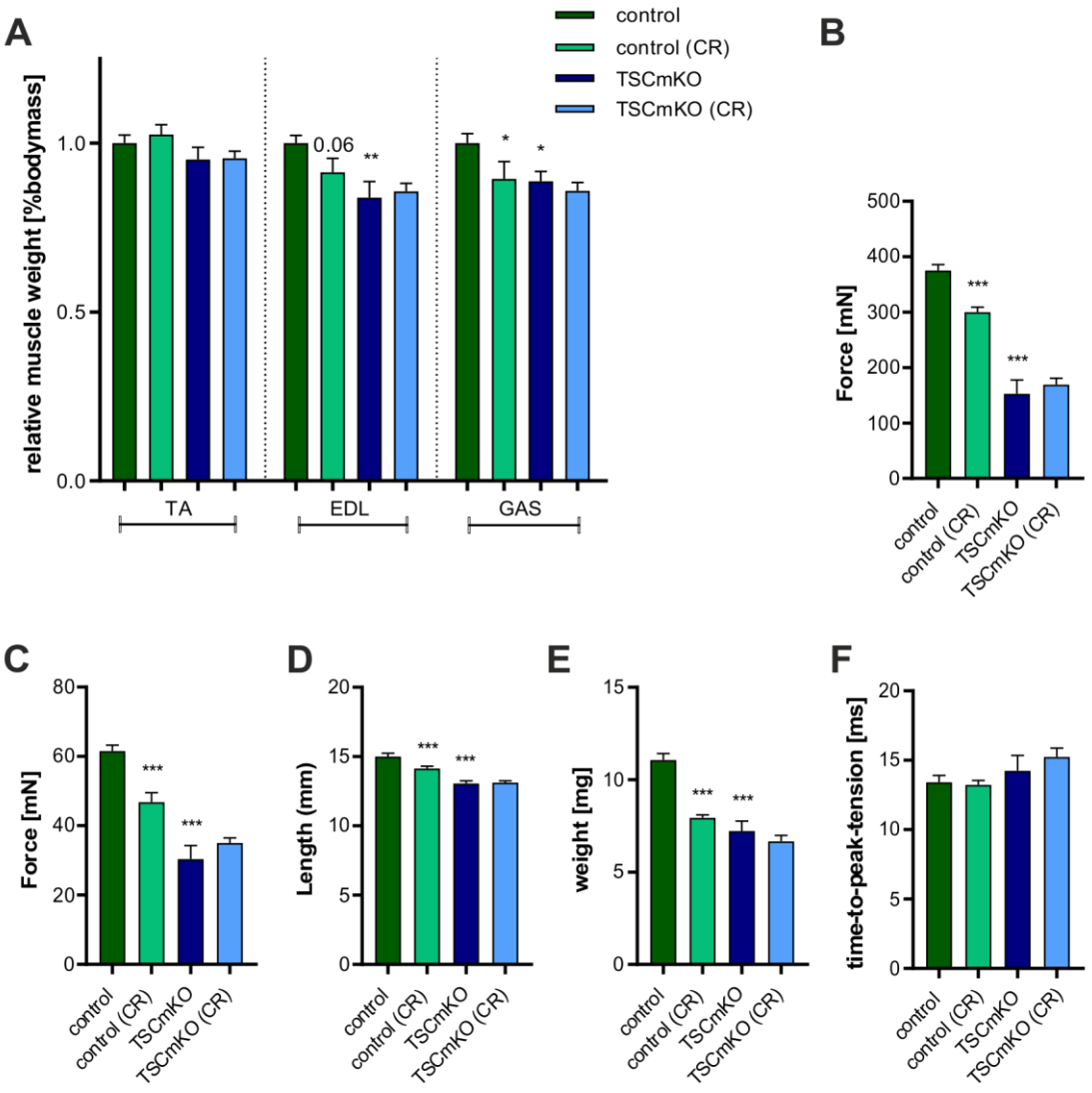

Supplemental Figure 2: Decrease of muscle mass an absolute isometric forces in TSCmKO mice, Related to Figure 2.

(A) Muscle weight relative to body weight of glycolytic hindlimb muscles in control and in TSCmKO mice with and without CR. Values represent mean ± SEM. $^{*}p < 0.05$, $^{**}p < 0.01$, $^{***}p < 0.001$. $^{\#}$ = statistical comparison to TSCmKO. $^{\#}p < 0.05$, $^{\#\#}p < 0.01$, $^{\#\#\#}p < 0.001$. n ≥ 6. **(B)** Absolut peak force measured in isolated EDL muscle *in vitro* in control and in TSCmKO mice with and without long-term CR. Values represent mean ± SEM. $^{*}p < 0.05$, $^{**}p < 0.01$, $^{***}p < 0.001$, $^{\#}$ = statistical comparison to TSCmKO. $^{\#}p < 0.05$, $^{\#\#}p < 0.01$, $^{\#\#\#}p < 0.001$. n ≥ 6. **(C)** Absolute twitch force measured in isolated EDL muscle *in vitro* in control and in TSCmKO mice with and without long-term CR. Values represent mean ± SEM. $^{*}p < 0.05$, $^{**}p < 0.01$, $^{***}p < 0.001$, $^{\#}$ = statistical comparison to TSCmKO. $^{\#}p < 0.05$, $^{\#\#}p < 0.01$, $^{\#\#\#}p < 0.001$. n ≥ 6. **(D)** Length of EDL recorded after force measurement in TSCmKO mice compared to control mice with and without CR. Values are mean ± SEM. $^{*}p < 0.05$, $^{**}p < 0.01$, $^{***}p < 0.001$, $^{\#}$ = statistical comparison to TSCmKO. $^{\#}p < 0.05$, $^{\#\#}p < 0.01$, $^{\#\#\#}p < 0.001$. n ≥ 6. **(E)** Weight of EDL muscle recorded after force measurement. Values of all four mice groups similar to muscle weight recorded during dissection (Figure 4A). Values are mean ± SEM. $^{*}p < 0.05$, $^{**}p < 0.01$, $^{***}p < 0.001$, $^{\#}$ = statistical comparison to TSCmKO. $^{\#}p < 0.05$, $^{\#\#}p < 0.01$, $^{\#\#\#}p < 0.001$. n ≥ 6. **(F)** Measurement of time-to-peak tension (TPT) on isolated EDL *in vitro* in TSCmKO mice compared to control mice with and without CR. Values are mean ± SEM. $^{*}p < 0.05$, $^{**}p < 0.01$, $^{***}p < 0.001$, $^{\#}$ = statistical comparison to TSCmKO. $^{\#}p < 0.05$, $^{\#\#}p < 0.01$, $^{\#\#\#}p < 0.001$. n ≥ 6.

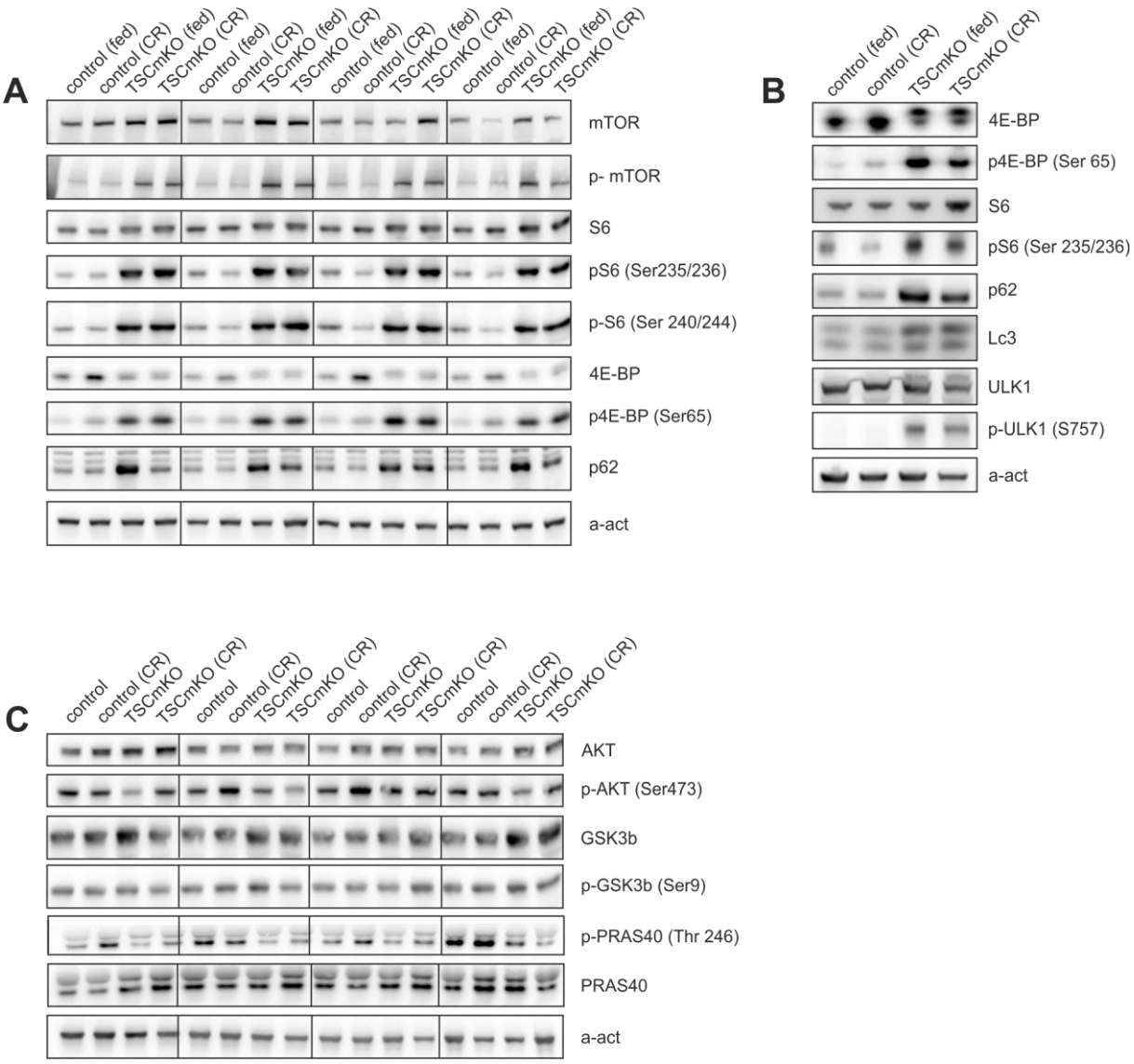

Supplemental Figure 3: Long-term CR is insufficient to decrease mTORC1 signaling in TSCmKO females and other glycolytic muscles and does not effect AKT/PKB/FoxO signaling, Related to Figure 4.

(A) Immunoblots for the indicated proteins in GAS muscle total protein lysates of control and TSCmKO littermates with and without long-term CR. Phospho-sites indicated in brackets. α–actinin used as a loading control. Values represent mean ± SEM of data. $^{*}p < 0.05$, $^{**}p < 0.01$, $^{***}p < 0.001$, $^{\#}$ = statistical comparison to TSCmKO. $^{\#}p < 0.05$, $^{\#\#}p < 0.01$, $^{\#\#\#}p < 0.001$. n = 4. **(B)** Immunoblots for the indicated proteins in TA muscle total protein lysates of control and TSCmKO female littermates with and without long-term CR. Phospho-sites indicated in brackets. α–actinin used as a loading control. Values represent mean ± SEM of data. $^{*}p < 0.05$, $^{**}p < 0.01$, $^{***}p < 0.001$, $^{\#}$ = statistical comparison to TSCmKO. $^{\#}p < 0.05$, $^{\#\#}p < 0.01$, $^{\#\#\#}p < 0.001$. n ≥ 4. **(C)** Immunoblots for the indicated proteins in TA muscle total protein lysates of control and TSCmKO littermates with and without long-term CR. Phospho-sites indicated in brackets. α–actinin used as a loading control. Values represent mean ± SEM of data. $^{*}p < 0.05$, $^{**}p < 0.01$, $^{***}p < 0.001$, $^{\#}$ = statistical comparison to TSCmKO. $^{\#}p < 0.05$, $^{\#\#}p < 0.01$, $^{\#\#\#}p < 0.001$. n = 4.

8 Chapter 3: Sustained activation of mTORC1 in skeletal muscle leads to disturbed calcium homeostasis and excitation-transcription coupling

8.1 Summary

TSCmKO mice exhibit a slower, more oxidative muscle phenotype. A detailed proteome and transcriptome analysis indicated that calcium signaling, and in particular the excitation-contraction (ECC) and transcription (ETC) coupling, are altered in TSCmKO muscle (data unpublished). Therefore, the sustained activation of mTORC1 appears to influence skeletal muscle contractile properties. Indeed, TSCmKO mice were shown to have reduced isometric skeletal muscle force as well as a contractile and metabolic shift from glycolytic to oxidative muscle fiber composition. This is reflected by the expression of myosin light chains, usually expressed in slow skeletal muscle, as well as by the upregulation of MYH7. In this chapter, I further analyzed the metabolic changes in TSCmKO skeletal muscle by using quantitative measurements of mRNA expression and Western blot analysis. The data confirm that TSCmKO muscle switched fiber types from fast (glycolytic) to slow (oxidative). The slowing of the contractile properties was additionally verified by the decrease of calcium storage proteins. In addition, I observed a reduction in the calcium ATPase SERCA1, with an increase in half-relaxation time and time-to-peak tension. Analyses of the CaN-NFAT signaling pathway points toward an increased activity of the slow fiber gene expression program.

8.2 Introduction

8.2.1 Skeletal muscle composition- Differentiation of fiber types

Skeletal muscle is a very plastic organ that has to adapt its composition and metabolism based on the energy demands. Muscle fibers differ from each other due to the composition and expression of different myosin heavy chains (MyHC), but also due to their metabolic properties, contractile properties, and the formation of the NMJs (Rakus et al, 2015; Schiaffino & Reggiani, 2011). Slow, oxidative muscles, with a high aerobic capacity, consist of high amounts of myoglobin, high amounts of mitochondria, low amounts of glycogen, and are fatigue resistant (Schiaffino & Reggiani, 2011). Slow fibers consists of up to 60% of the slow MyHC type I. Endurance activities and postures are usually generated through slow muscle; therefore, the rate of ATP breakdown by the ATPases is typically generated slower than in fast muscles. Moreover, slow muscles use oxidative phosphorylation as their major energy source (Westerblad et al, 2010). Pentose phosphate pathway elevation and subsequent increase in NADPH production in slow skeletal muscle is thought to be an adaptive mechanism to the predominant oxidative generation of energy (Summermatter et al, 2010).

Fast muscle can be subdivided into glycolytic type IIa fibers, and more glycolytic type IIx and IIb fibers, the latter being the “fastest” of the fast muscle fibers. Myoglobin content and mitochondrial number in fast fibers are lower than they are in slow fibers, explaining their lighter color. They show a low aerobic capacity and higher anaerobic capacity, due to the fast breakdown of ATP through the ATPases (Barany, 1967; Schiaffino & Reggiani, 2011). Their function ranges from endurance performance in endurance-trained muscles (mainly type IIa fibers) to rapid, intense movements and short-duration exercise (e.g. sprints). Skeletal muscle myosin consists of two MyHC and four myosin light-chains (Myl). Besides the indisputable role of MyHC in skeletal muscle type determination, a body of evidence acknowledges the important role of myosin light chains (Myl) within skeletal muscle. Myl are located in the head of the myosin and exist in two forms: the myosin regulatory light chain and the essential light chain. Myosin regulatory light-chains are phosphorylated (activated) by myosin light-chain kinases, Ca^{2+}/ Calmodulin (CaM)-dependent serine-threonine protein kinases, and

dephosphorylated (inactivated) by myosin light-chain phosphatases (Stull et al, 2011). Myl are located in the neck region of the myosin, building the junction between the myosin head, including the actin-binding site and the ATP biding site, and the C-terminus of the myosin containing the MyHC. Therefore, they play an important role in retaining the motor function of the skeletal muscle myosin.

However, fibers do not just differ in their MyHC composition and metabolism they also differ within the expression of components involved in skeletal muscle contraction mechanisms and calcium (Ca^{2+}) homeostasis associated proteins (Allen et al, 2008; Schiaffino & Reggiani, 2011). Different isoforms of the sarcoplasmic reticulum Ca^{2+} ATPase pump SERCA are found in skeletal muscle. Fast muscles predominantly express SERCA1, whereas slower muscle fibers primarily express the SERCA2 isoform. Parvalbumin, a very important calcium buffer within the cytosol and largely expressed in fast fibers, is nearly absent in slow muscle fibers. Another Ca^{2+} buffer is calsequestrin (CSQ). CSQ isoform 1 is expressed in fast, and in slow muscle but to a lower extent. Therefore, slow muscle does additionally express CSQ2 to compensate. Moreover, a proteomic approach showed that slow muscle expresses high levels of Myh1 and Myh7, whereas fast muscle predominantly expresses Myh4 (Rakus et al, 2015).

Fiber type switch is a common feature used by the muscle to adapt not only to exercise, but also other stimuli, such as CR for example (Chapter 2). Peroxisome proliferator-activated receptor gamma coactivator 1-alpha (PGC-1α), in the case of exercise, regulates the gene expression as a transcriptional coactivator. PGC-1α typically induces the expression of genes involved in the gene program of oxidative muscle fibers, playing an important role in fiber type determination. PGC-1α transgenic mice show an increase in mitochondrial biogenesis and function, as well as an increase in type I and type IIa fibers (Lin et al, 2002). This clearly shows a shift of fast muscle towards more oxidative and fatigue resistant in the PGC-1α transgenic mice. Calorie deprivation in mammals leads to an adaptive mechanism by increasing the efficiency to use available energy sources. In wild-type mice upon long-term CR, a decrease

in fat mass is usually associated with an increase in fatty acid oxidation (FAO), switching to slower fiber properties (Anderson & Weindruch, 2010; Bruss et al, 2010).

In slow and fast skeletal muscle, the expression of basic types of contractile proteins (e.g. troponins, actin) is very similar. However, slow muscle has also other characteristics. It is usually more resistant to external stimuli, more cellular stress resistant, and less susceptible to reactive oxygen species (ROS) (Schiaffino & Reggiani, 2011). Decreased amounts of slow fibers contribute to insulin resistance and increase obesity risk (Kwak, 2013). Furthermore, fast fibers were shown in Duchenne muscular dystrophy (DMD) patients to be more prone to degenerative changes (Webster et al, 1988).

8.2.2 Calcium signaling in skeletal muscle

Contraction of skeletal muscle is mediated through the excitation contraction coupling and highly dependent on calcium (Ca^{2+}) from intracellular calcium stores being released into the cytoplasm. The increase in intracellular free Ca^{2+} levels stimulates numerous calcium dependent pathways (Figure IV) (Bellinger et al, 2009; Berchtold et al, 2000; Kuo & Ehrlich, 2015; Schwaller et al, 1999).

The contractile apparatus of skeletal muscle consists of two major proteins: myosin and actin. As already mentioned in the general introduction, both proteins have a distinct arrangement within striated skeletal muscle. This distinct arrangement makes a Ca^{2+}-dependent muscle contraction possible in response to neuronal stimulation. The link between muscle excitation (the depolarization of the membrane during an action potential) to Ca^{2+} release from the sarcoplasmic reticulum is mediated by the excitation contraction coupling (ECC), a voltage- and calcium-dependent mechanism (Figure V) (Calderon et al, 2014; Rios & Brum, 1987; Sandow, 1952).

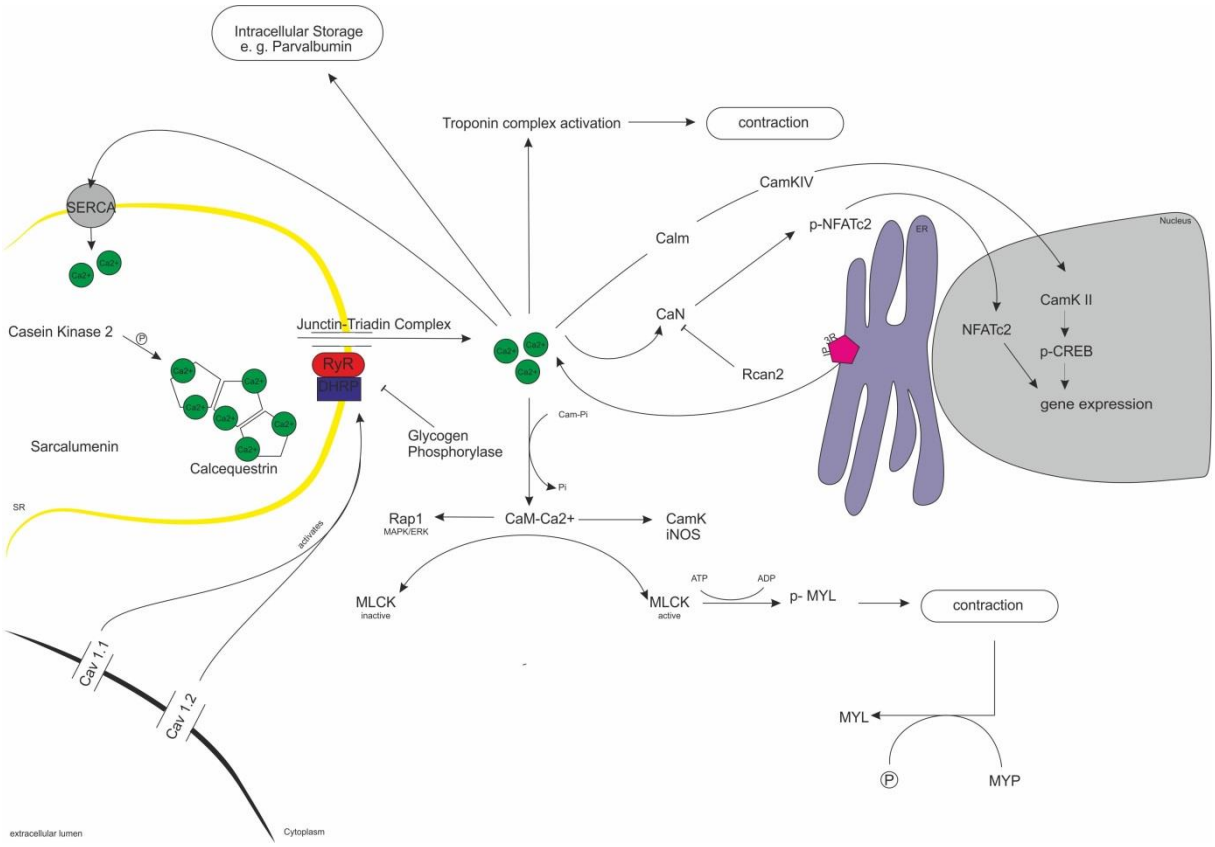

Figure IV: Simplified calcium signaling pathways in skeletal muscle

The NMJ forms the contact between motor neuron and a muscle fiber. The NMJ consists of three different parts, the presynaptic nerve terminal, the synaptic cleft, and the postsynaptic region located on the sarcolemma. The postsynaptic part of the muscle contains receptors for the neurotransmitter acetylcholine (ACh), which is released into the synaptic cleft upon an action potential (Kuo & Ehrlich, 2015). ACh diffuses across the cleft and binds to their receptors, the ligand-gated, nicotinic acetylcholine receptors (nAChRs) located at the postsynaptic membrane. This leads to a subsequent influx of sodium and

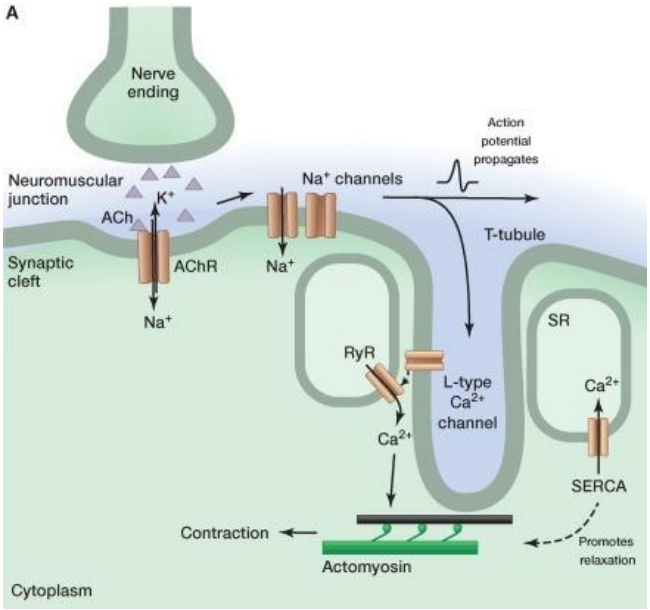

Figure V: Skeletal muscle action potential propagation and subsequent excitation contraction coupling
(Kuo & Ehrlich, 2015)

efflux of potassium, causing a depolarization of the muscle cell membrane (Kuo & Ehrlich, 2015). Through the depolarization, voltage-gated sodium channels are activated, provoking an action potential. This action potential is propagated over the sarcolemma to the t-tubules. T-tubules are infoldings of the membrane which increase surface area, but also allow voltage-gated sodium channels to be in close proximity to other voltage sensitive channels and proteins involved in the ECC. T-tubules also contain numerous of ion-channels.

Once the action potential reaches the t-tubules, it activates L-type voltage-gated calcium channels, $Ca_v1.1$, also known as dihydropyridine receptor (DHPR). A conformational change of DHPR upon activation enables the sarcoplasmic reticulum (SR) to release Ca^{2+} through the phosphorylation-dependent activation of the ryanodine receptor 1 (RyR1) (Calderon et al, 2014; Rios & Brum, 1987; Robin & Allard, 2012). Ca^{2+} diffuses into the cytosol, initiating a contraction (see general introduction). The sarcoendoplasmic reticulum calcium transport ATPase (SERCA) is responsible for the re-uptake of the calcium into the SR. Several cytoplasmic and SR proteins are associated with DHPR/RyR1 complex, such as: calsequestrin (CSQ), the major Ca^{2+} binding protein in the SR; FK506 binding protein for stabilizing RyR1; and calmodulin (CaM), a ubiquitous intracellular Ca^{2+} receptor, mainly activating downstream phosphatases (e.g. calcineurin) and kinases (e.g. Ca^{2+} /calmodulin-dependent protein kinase II) (Gaburjakova et al, 2001; Saucerman & Bers, 2008; Wei et al, 2006). Several other proteins are involved in the fine tuning of the SERCA pump such as phospholamban (PLN), inhibitor of SERCA2, and sarcolipin, a Ca^{2+} transporter (Asahi et al, 2003; Brittsan et al, 2000; Gustavsson et al, 2013).

Calcium signaling is also responsible for protein degradation and activity of calcium-dependent proteases and transcription factors (TF). Other Ca^{2+} stores, such as the endoplasmic reticulum, also play an important role within the calcium homeostasis regulation (Carreras-Sureda et al, 2018). Whereas SR is mainly involved in the ECC, calcium release from ER activates Ca^{2+} regulated transcriptional pathways. Calcium release from the ER is primarily mediated via the ubiquitous second messenger inositol 1, 4, 5,-trisphosphoate (IP3),

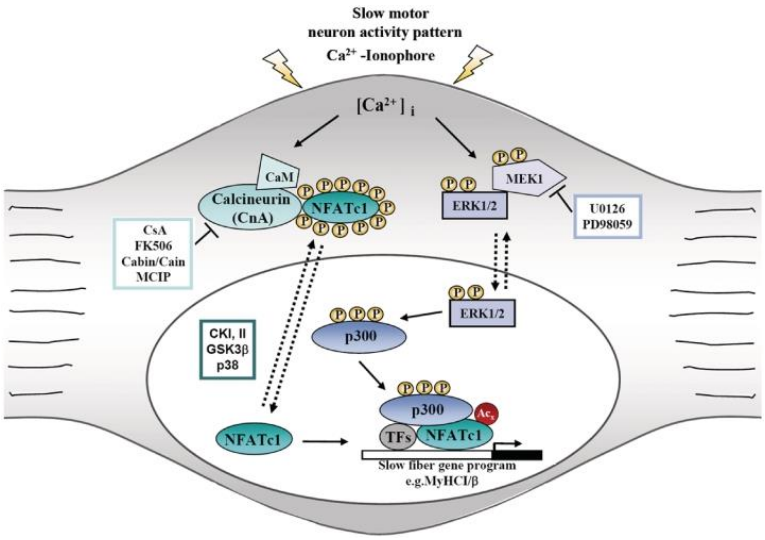

Figure VI: Schematic depiction of the excitation transcription coupling triggered by calcineurin/nucleic factor of activated T-cell signalling (Meissner et al, 2011)

located at the ER membrane (Carreras-Sureda et al, 2018). This excitation transcription coupling (ETC) alters the gene expression profile in skeletal muscle and has been proven, for example, to be switched on upon exercise.

One well-characterized ETC pathway is the calcineurin (CaN)/ nucleic factor of activated T-cell (NFAT) signaling pathway, wherein the main regulators are CaN, CaM and Ca^{2+} itself (Figure VI). CaN is a eukaryotic Ca^{2+} and a calmodulin-dependent serine/ threonine protein phosphatase that regulates various cellular processes, such as muscle remodeling and regeneration through upregulation of myogenin (*MyoG*), Myocyte Enhancer Factor 2A (*MEF2A*), and through the downregulation of myostatins (Long et al, 2007; Sakuma & Yamaguchi, 2010). CaN was also shown to control expression of Myogener Faktor 3 (*MyoD*) (Friday et al, 2003). In particular, CaN activates NFAT, which is responsible for a hypertrophic and slow fiber type gene program. CaN is even essential for the development of hypertrophy, as knockdown of CaN completely abolishes myofiber growth upon IGF-1 treatment *in vitro* (Semsarian et al, 1999). The pharmacological block of CaN by cyclosporine A (CyA) induces fiber atrophy, which is associated with the appearance of immature myotubes (Sakuma et al, 2003). Once NFAT is dephosphorylated, it translocates into the nucleus and assembles with various transcriptional co-activators to regulate target genes, including myosin heavy chain 7 (*Myh7*) (Chin et al, 1998). CaN is usually activated by calpain or CaM-Ca^{2+}, but can also be inhibited in a calcium- independent manner with exercise and high fat diet over the CaN inhibitor protein CAIN (Pfluger et al, 2015). More importantly, CaN was shown to regulate

muscle metabolism via changes in gene expression by dephosphorylating NFAT (Calabria et al, 2009; Hogan et al, 2003).

CaN itself is apparent in the cytosol in an inactive form consisting of two subunits: CaN A and CaN B. After a Ca^{2+}-influx, CaN binds CaM, changes its conformation to the active form, and dephosphorylates NFAT, which translocates into the nucleus (Figure VI). NFAT itself switches on a hypertrophic gene program, which has been shown to be the program responsible for the promotion of soleus hypertrophy (Parsons et al, 2003; Sakuma & Yamaguchi, 2010; Talmadge et al, 2004). CaN is widely regarded as being a major player in muscle fiber type determination; however, how this is caused is unknown. Inhibiting CaN by CyA was shown to induce inflammation, leads to fiber atrophy, and cause accumulation of immature myotubes and calcification in the regenerating muscle, whereas transgenic CaN induction promotes regeneration after muscle damage (Sakuma et al, 2003; Sakuma & Yamaguchi, 2010).

The role of NFAT signaling and its involvement in fiber type specification is still very controversial. Transcription of slow or fast muscle fiber specific myosin was shown to be dependent on the combination of different NFATs. Whereas myosin heavy chain (MyHC-) I required the expression of all four NFATs (1-4), MyHC IIb only requires NFATc4 (Calabria et al, 2009). Schiaffinos group reported that the constitutive active NFATc1 mutant stimulates the expression of MyHC I and inhibits MyHC IIb expression (McCullagh et al, 2004). However, through various studies *in vivo*, including the observation that NFATc2 and NFATc3 knockout mice develop an atrophy without altering muscle fiber composition, which indicates that CaN can stimulate fiber type composition through other, rather unknown mechanisms (Calabria et al, 2009; Chin et al, 1998; Long et al, 2007; McCullagh et al, 2004). By inducing NFATc1 activity in mice, and additionally by blocking CaN dependent NFAT activity with a specific inhibitory peptide, McCullagh et al. were able to show that NFAT acts rather as a nerve activity sensor controlling activity-dependent fiber type composition in slow skeletal muscle (McCullagh et al, 2004). Mice lacking NFATc1 show a fiber type shift to more MyHC IIx and MyHC IIb in soleus muscle, whereas its constitutively active form expresses predominantly

MyHC-slow fibers. Interestingly, NFATc1-induced MyHC-slow expression is only occurring in regenerating SOL and EDL muscle, but not in adult EDL muscle (McCullagh et al, 2004). This is explained by the greater plasticity of regenerating muscle. However, it was also indicated that muscle fiber type switch, at least in rats, only occurs within a small adaptive range (Schiaffino & Reggiani, 2011).

8.2.3 Calcium signaling in disease and aging

Several diseases are associated with a malfunctioning Ca^{2+} signaling system, in particular with hyper- or hypo-stimulation of the Ca^{2+} release from the SR. Malignant hypothermia is one of the most well-known Ca^{2+} release disorders and it is caused by a mutation in the RyR1 and in the integrity of proteins involved in the t-tubule/SR connection (Rosenberg et al, 2015). Mutations in SERCA1 have been shown to cause Brody's Disease, a rare inherited muscle disorder, characterized by the impairment of reuptake of Ca^{2+} into the SR (Odermatt et al, 1996). Patients with Brody's Disease are unable to relax their muscles, leading to increased muscle stiffness. Those muscle diseases, myotonias, are usually associated with other pathological muscle alterations. In the case of Brody's Disease, atrophy in type IIb fibers and an increase in central-nucleated fibers was observed.

The most frequent amongst the rare dystrophinopathies is Duchenne Muscle Dystrophy (DMD). It is a hereditary disease characterized by progressive muscle wasting and weakness resulting from a dystrophin deficiency. Patients do not underlay direct changes in the calcium signaling, but show a disturbance of calcium handling of the muscle. *Mdx* mice, an established mouse model used in DMD research, show an increase in resting cellular Ca^{2+} (Bellinger et al, 2009). This increase was mainly caused by the increased S-nitosylation of the RyR1, which depleted calstabin-1 (FKBP12), thus resulting in a leaky RyR1. Leaky RyR1 is thought to contribute to the observed muscle weakness within DMD patients (Bellinger et al, 2009).

The involvement of mTORC1 in Ca^{2+} signaling has also been acknowledged during the last few years. In 2015, for example, it was shown that *Rptor* ablation in skeletal muscle, switches muscle kinetics towards a slower phenotype (Bentzinger et al, 2008). It additionally decreases

the expression of Cav1.1 and affects ECC function by altering elementary calcium release events (ECRE) (Lopez et al, 2015). Furthermore, mTORC1 is activated during exercise, promoting skeletal muscle hypertrophy, activated in turn by the increase in intracellular Ca^{2+} signaling through the $P2Y_2$ receptor/inositol 1,4,5-trisphosphate receptor pathway, *in vitro* (Ito et al, 2018). More interestingly, this gene program is exclusively switched on in *soleus*, but not in fast/glycolytic muscle (*plantaris*). Much evidence is therefore strongly suggesting mTORC1 plays a role in the maintenance of Ca^{2+} homeostasis. As TSCmKO transcriptome and proteome indicated changes within the calcium signaling (unpublished data), I was wondering how those changes appear on a molecular level upon a sustained activation of mTORC1 in skeletal muscle. Additionally, I wanted to know how possible alterations within the ECC and ETC might be contributing to the physiological changes, in particular the lowering of muscle force within the TSCmKO mice.

8.3 Results

Expression of skeletal muscle contractile subunits is altered in TSCmKO mice

Myosin light chain kinases (MYLK) are Calcium/Calmodulin-dependent serine-threonine kinases phosphorylating regulatory myosin light chains (RLC), which were shown to be involved in the generation of peak isometric twitch tension. Deficient expression of MYLK can lead to muscle weakness through insufficient muscle contraction (Zhi et al, 2005). Twitch force and tetanic force are significantly downregulated in 3- and 9-month-old TSCmKO mice (Chapter 2; (Castets et al, 2013)). However, in line with our transcriptomics data (unpublished data), an increase in *Mylk2* and *Mylk4* gene expression was observed in TA muscle of 3-month-old TSCmKO mice compared to control littermates (Figure 1A), indicating alterations within the contraction profile of TSCmKO skeletal muscle. An upregulation of Mylk2 in the TA of TSCmKO mice was also observed on the protein level (Figure 2B). In skeletal muscle, MYL function was reported to be important for the translation of energy (ATP) into movement. The presence of mutations in MYL genes decreases myosin cross bridging, thus resulting in lower muscle contraction and loss of muscle force. Therefore, I quantified MYL gene expression in TA whole muscle lysates. *Myl2*, predominantly expressed in slow skeletal muscle, was significantly upregulated in TA muscle of TSCmKO mice (Figure 1A). This is in line with a shift of fast/glycolytic muscle towards a slower phenotype, as shown in chapters 1 and 2. However, *Myl3*, another isoform predominantly expressed in slow muscle was significantly downregulated (Figure 1A). *Myl4*, which is mainly expressed in embryonic muscle during muscle development, was also upregulated in the TA of TSCmKO mice (Figure 1A). While TSCmKO mice do show an increase in damaged muscle fibers (Chapter 2; (Castets et al, 2013)), no increase in muscle regeneration or repair as such is seen. The upregulation of embryonic myosin, however, suggests the recruitment of compensatory mechanisms in the diseased muscle.

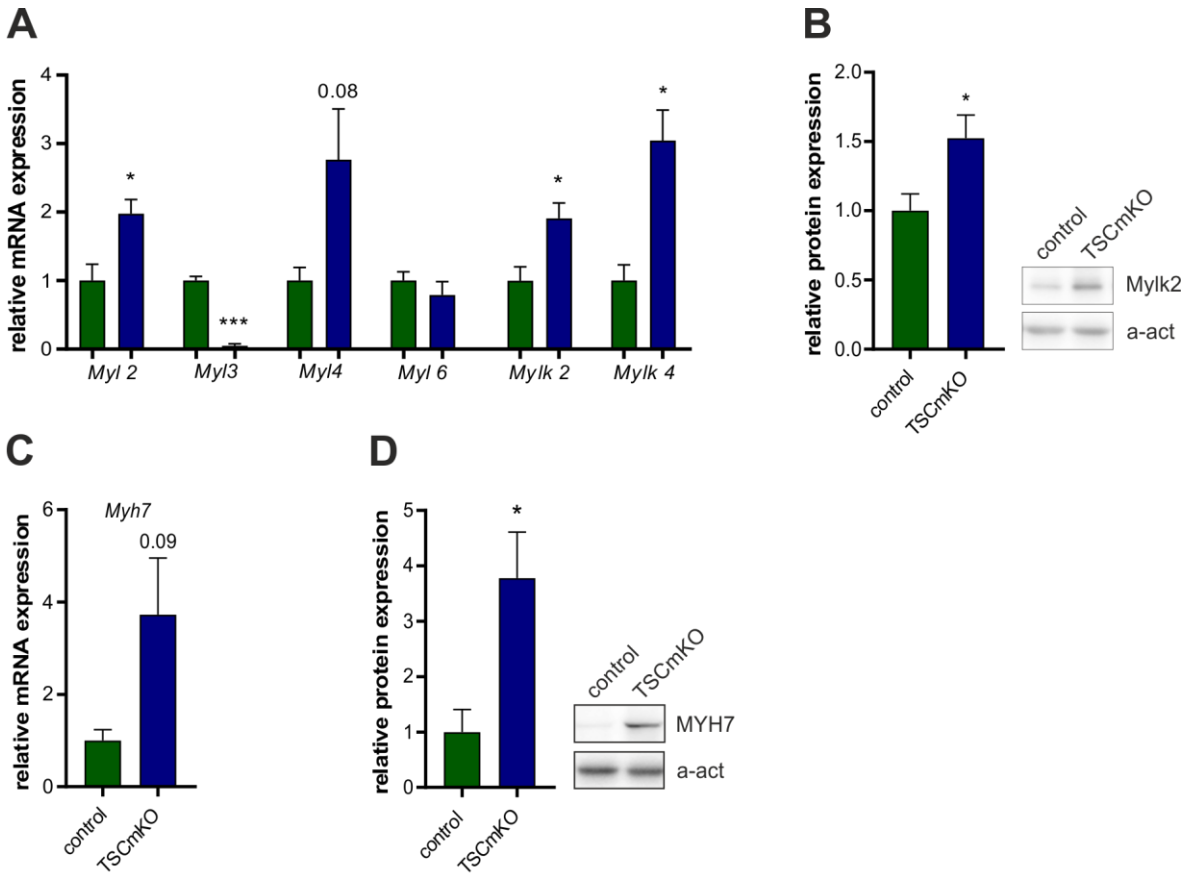

Figure 1: Expression of skeletal muscle contractile subunits is altered in TSCmKO mice

(A) Relative gene expression of *Myl* indicated, and *Mylk*, respectively, in TA muscle from 3-month-old TSCmKO mice compared to control mice. Values represent mean ± SEM. Data normalized to *β-actin* levels. $^{*}p < 0.05$, $^{**}p < 0.01$, $^{***}p < 0.001$. n =3. **(B)** Immunoblots for MYLK2 and subsequent quantification in TA muscle total protein lysates of control and TSCmKO littermates. Data normalized to α–actinin. Values represent mean ± SEM of data. $^{*}p < 0.05$, $^{**}p < 0.01$, $^{***}p < 0.001$, n = 4. **(C)** Relative gene expression of *Myh7* in TA from 3-month-old TSCmKO mice compared to control mice. Values represent mean ± SEM. Data normalized to *β-actin* levels. $^{*}p < 0.05$, $^{**}p < 0.01$, $^{***}p < 0.001$. n =3. **(D)** Immunoblots for MYH7 and subsequent quantification in TA muscle total protein lysates of control and TSCmKO littermates. Data normalized to α–actinin. Values represent mean ± SEM of data. $^{*}p < 0.05$, $^{**}p < 0.01$, $^{***}p < 0.001$, n = 4.

To further substantiate my finding that fast/glycolytic skeletal muscles in TSCmKO mice are shifted towards a slower/oxidative phenotype, I analyzed expression of myosin heavy chain 7 (MYH7), which is predominantly expressed in slow muscles. While MYH7 was significantly upregulated in TA muscle of TSCmKO mice at the protein level (Figure 1D), the upregulation was not significant on the transcriptional level (Figure 1C). Together with the observed changes in the expression of different myosin light chain isoforms and myosin light chain kinases, increased expression of MYH7 indicates that TSCmKO skeletal muscle physiology is shifted

towards a slow muscle phenotype and corroborates alterations within the contractile apparatus.

Glycolytic TSCmKO muscle contractile profile is switched towards more slow/oxidative muscle

Most of the cellular calcium is buffered by specific proteins within the cytosol, or calcium storage units, such as the sarco- or endoplasmic reticulum and mitochondria. In *mdx* mice, the decrease of calcium buffers in fast skeletal muscle is thought to be associated with abnormal calcium handling, subsequently leading to chronic fiber necrosis (Pertille et al, 2010). Using immunoblot analysis of TA muscle lysate, I observed a downregulation of parvalbumin (PV), an important cytosolic calcium buffer in TSCmKO muscle (Figure 2A). Interestingly, short rapamycin treatment in 3-month-old control and TSCmKO mice increased PV protein expression to a similar extent (Figure 2B). This suggests that PV expression is negatively regulated by mTORC1. Sarcalumenin (SRL), another important calcium buffer/glycoprotein that works in close correlation with SERCA in the SR, is also downregulated (Figure 2A). However, CSQ1 protein expression in total TA muscle lysates appears to be upregulated in TSCmKO mice compared to their control littermates (Figure 2A). Disruption in calcium buffering was shown to cause impairment within the calcium transient (Schwaller et al, 1999; Yoshida et al, 2005). Therefore, I measured resting calcium levels in FDB single isolated fibers by using fura-2-AM, an acetoxymethyl ester. Resting Ca^{2+} in isolated FDB fibers of TSCmKO mice was increased by 11.89%, but the effect was not significant (Figure 2C). SERCA1, the isoform predominantly expressed in fast skeletal muscle, was significantly decreased in TA whole muscle protein lysates of TSCmKO mice (Figure 2D). DHPR protein levels, however, were unchanged (Figure 2D). Those results are in accordance with the previously obtained delay in calcium re-uptake and the increase in HRT and TPT described in chapter 2. By screening the proteomics data, I found a 0.746-fold decrease in SERCA1 expression in TSCmKO skeletal muscle compared to controls. In contrast, a 5.143-fold increase was

observed for the slow isoform SERCA2 (data unpublished). Altogether, these results suggest physiological changes in skeletal muscle of TSCmKO mice that are supported by the previously observed fiber type switch towards a slower phenotype (Chapter 1).

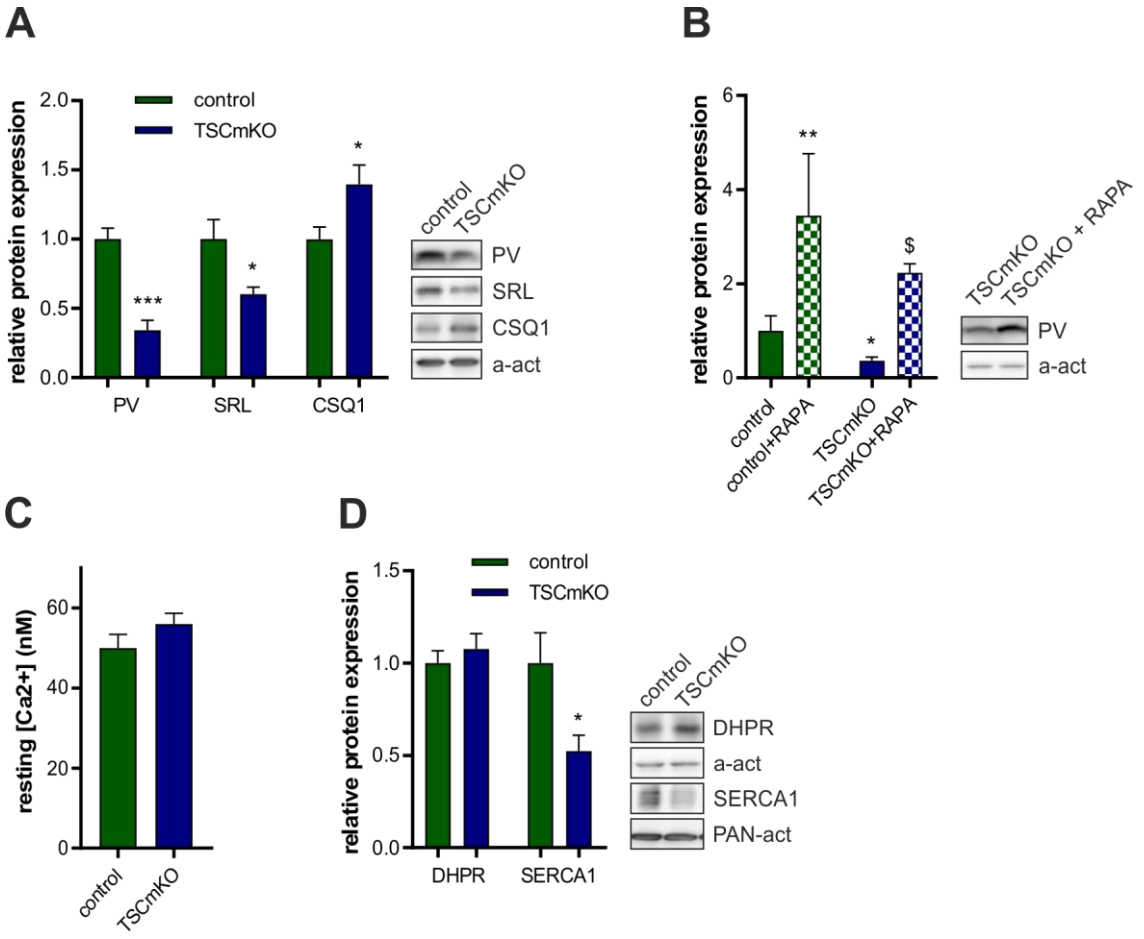

Figure 2: Contractile profile of glycolytic muscle of TSCmKO mice is shifted towards more slow/oxidative fibers

(A) Immunoblots for indicated proteins and subsequent quantification in TA muscle total protein lysates of controls and TSCmKO littermates. Data normalized to α–actinin. Values represent mean ± SEM of data. $^{*}p < 0.05$, $^{**}p < 0.01$, $^{***}p < 0.001$, n ≥ 5. **(B)** Immunoblot for PV and subsequent quantification in TA muscle total protein lysates of control and TSCmKO vehicle and rapamycin (RAPA) treated mice. Data normalized to α–actinin. Values represent mean ± SEM of data. $^{*}p < 0.05$, $^{**}p < 0.01$, $^{***}p < 0.001$, n ≥ 3. **(C)** Determination of resting calcium levels in 3-month-old TSCmKO single isolated FDB fibers compared to single isolated FDB fibers of control littermates. $^{*}p < 0.05$, $^{**}p < 0.01$, $^{***}p < 0.001$, n = 3 with a biological replicate of n ≥ 15. **(D)** Immunoblots for SERCA1 (slow) and DHPR and subsequent quantification in TA muscle total protein lysates of control and TSCmKO mice. Data normalized to PAN–actin. Values represent mean ± SEM of data. $^{*}p < 0.05$, $^{**}p < 0.01$, $^{***}p < 0.001$, n ≥ 6.

Alterations in cellular calcium signaling upregulate the excitation-transcription coupling in TSCmKO mice

A decrease in cytosolic calcium buffers may lead to alterations within the calcium transient and subsequently alter the ECC and ETC (Prins & Michalak, 2011; Schwaller, 2010; Schwaller et al, 1999; Yoshida et al, 2005). I have previously observed a switch of fast/glycolytic muscle fiber of TSCmKO mice towards slower muscle fibers and was wondering, whether or not the CaN-NFAT-axis may be responsible for the fiber type switch or partially involved in it. The CaN-NFAT signaling, an ETC pathway, is involved in the determination of muscle fiber type specification (Calabria et al, 2009).

CaN was significantly upregulated in TSCmKO mice compared to their control littermates (Figure 3A). Dephosphorylation of NFAT by CaN is initiated via CaM-Ca^{2+} binging. However, the increased CaN availability does not reveal the activity of the protein. Therefore, I analyzed the expression and activation profile of upstream regulators and downstream targets of CaN. I did not observe any significant changes in CaM protein expression in TSCmKO mice compared to their control littermates (Figure 3B). Due to the lack of p-NFAT antibodies, I first quantified overall NFAT mRNA and protein expression. Whereas *Nfatc2* and *Nfatc4* mRNA expression was upregulated in TSCmKO mice, I did not observe any changes in *Nfatc3* expression (Figure 3C). No differences, however, were observed in NFATc3 and NFATc4 protein expression (Figure 3D). Unfortunately, NFATc1 and NFATc2 protein levels could not be quantified, due to the presence of multiple unspecific bands in the Western blot. NFAT activity can be determined by analyzing the mRNA expression of *Myh7*, a NFAT regulated gene, which was previously reported to be slightly increased in TSCmKO mice (Figure 1C).

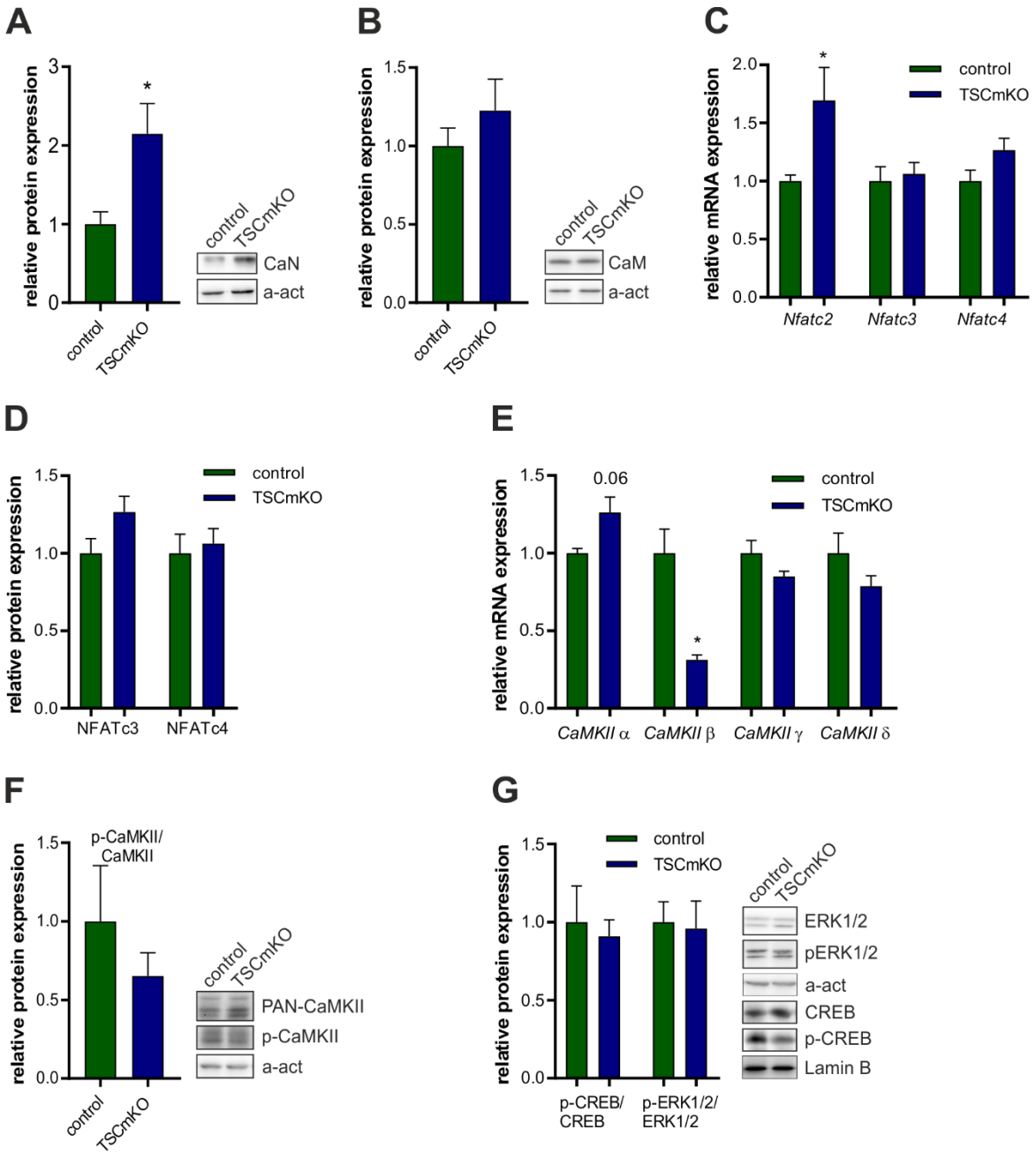

Figure 3: Sustained activation of mTORC1 is skeletal muscle alters calcium signaling and subsequently ETC

(A) Immunoblot of CaN and subsequent quantification in TA muscle total protein lysates of control and TSCmKO mice. Data normalized to α–actinin. Values represent mean ± SEM of data. $^{*}p < 0.05$, $^{**}p < 0.01$, $^{***}p < 0.001$, n ≥ 5. **(B)** Immunoblot for CaM and subsequent quantification in TA muscle total protein lysates of control mice and TSCmKO littermates. Data normalized to α–actinin. Values represent mean ± SEM of data. $^{*}p < 0.05$, $^{**}p < 0.01$, $^{***}p < 0.001$, n ≥ 6. **(C)** Relative gene expression of *Nfatc2, c3* and *c4* in TA from 3-month-old TSCmKO mice compared to control mice. Values represent mean ± SEM of data normalized to *β-actin* levels. $^{*}p < 0.05$, $^{**}p < 0.01$, $^{***}p < 0.001$. n = 5. **(D)** Quantification of NFATc3 and NFATc4 protein levels in TA muscle total protein lysates of control mice and TSCmKO littermates. Data normalized to α–actinin. Values represent mean ± SEM of data. $^{*}p < 0.05$, $^{**}p < 0.01$, $^{***}p < 0.001$, n = 5. **(E)** Relative gene expression of *CaMKII* isoforms as indicated in TA from 3-month-old TSCmKO mice compared to control mice. Values represent mean ± SEM of data normalized to *β-actin* levels. $^{*}p < 0.05$, $^{**}p < 0.01$, $^{***}p < 0.001$. n = 5. **(F)** Immunoblot for total-CaMKII (CaMKII) and p-CaMKII (T286) and

subsequent quantification in TA muscle total protein lysates of control mice and TSCmKO littermates. Data normalized to α–actinin. Values represent mean ± SEM of data. $^{*}p < 0.05$, $^{**}p < 0.01$, $^{***}p < 0.001$, $n \geq 6$. **(G)** Immunoblot for total-CREB (CREB) and p-CREB (S133) protein in TA muscle nucleic fractions. total-p44/42 MAPK (ERK1/2) and p-p44/42 MAPK (p-ERK1/2) (Thr202/Tyr204) in TA muscle total protein lysates of control mice and TSCmKO littermates. p-p44/42 MAPK data normalized to α–actinin. p-CREB/CREB data normalized to Lamin B. Values represent mean ± SEM of data. $^{*}p < 0.05$, $^{**}p < 0.01$, $^{***}p < 0.001$, $n \geq 3$.

Another ETC pathway is the CaMKII-CREB signaling pathway, which activates a large number of gene programs, predominantly in the heart (Wheeler et al, 2008). However, CaMKIIβ gene expression in TSCmKO mice was significantly downregulated, whereas the other CaMKII isoforms (α, γ, δ) remained unchanged (Figure 3E). The activity of CaMKII can be assessed by immunoblot analysis of the phosphorylation status. The p-CaMKII/CaMKII ratio in total TA muscle lysates was similar in TSCmKO mice and in controls, thus indicating that CaMKII activity is not changed (Figure 3F). In line with a normal CaMKII activity, no differences in nuclear p-CREB/CREB levels were observed (Figure 3G). The phosphorylation status of CREB and its subsequent translocation into the nucleus is also regulated in a calcium-independent manner by ERK1/2. However, I did not observe any changes in p-ERK1/2/ ERK1/2 protein expression levels (Figure 3G). Although, I did not observe dramatic changes in the CaN-NFAT or CaMKII-CREB signaling pathway, my results provide evidence for the ETC alterations in TSCmKO mice, but this requires further analysis. For example, analyzing cytosolic and nucleic fractions or immunostainings could give a clearer indication regarding translocation of an active transcription factor involved in the ETC.

In summary, my findings suggest that alterations in calcium signaling in TSCmKO skeletal muscle affect ECC and ETC. I observed a shift of ECC components towards a slower muscle phenotype, whereas the CaN-NFAT-axis is clearly involved in driving the slow fiber type transcriptional program. This reveals that mTORC1 is important for the maintenance of muscle calcium homeostasis, and therefore in muscle force generation.

8.4 Discussion

Depletion of TSC1 in skeletal muscle perturbs calcium signaling and calcium homeostasis

As described in chapter 1, I found that the glycolytic muscles of TSCmKO mice undergo a shift towards a more slow/oxidative status. This metabolic shift had a severe effect on the progression of pathology and revealed a mitochondrial myopathy like phenotype. Disruptions in calcium homeostasis and signaling can even have detrimental consequences within skeletal muscle, as seen in malignant hyperthermia or the calcium mishandling in DMD, leading to irreversible membrane damage (Pertille et al, 2010; Vallejo-Illarramendi et al, 2014). Contraction is primarily regulated via excitation-contraction coupling and it involves the interplay of various organelles. Phosphorylating Myl the calcium/CaM/myosin light-chain kinase (Mylk)-axis plays a subordinate role within the skeletal muscle contraction, and only becomes important under submaximal saturating calcium conditions (Stull et al, 2011). Earlier, it had been shown by Lowey and colleagues that myosin light chains are not essential for the enzymatic activity of the ATPase (Lowey et al, 1993). However, Myl were shown to play an important role in the translation of an action potential into movement, through and by the reduction of actin filament velocity upon Myl removal (Lowey et al, 1993). Slow Myl expression in TSCmKO fast skeletal muscle increased (Figure 1). These results are in line with the previously observed metabolic fiber type switch (Chapter 1), and they indicate that the contractile apparatus in TSCmKO glycolytic skeletal muscle adapts to a slower/oxidative phenotype.

Releasing calcium from the sarcoplasmic reticulum results in the Ca^{2+}/troponin-dependent force generation, which is triggered by Mylk-mediated phosphorylating the regulatory light chains (RLC). In TSCmKO muscle, I observed an increase in *Mylk2* mRNA, as well as in protein expression in fast skeletal muscle. This seems rather surprising, as previously I observed a fiber-type switch towards a more oxidative phenotype in the transgenic mice. However, the phosphorylation of RLC can increase myosin motor function; therefore, it serves

as a biochemical memory to enhance and facilitate muscle mechanical function during prolonged or repetitive activity (Perrie et al, 1973; Stull et al, 2011). Additionally, it has been shown that the absence of the RLC phosphorylation is associated with elevated fatigability (Gittings et al, 2011; Stull et al, 2011). On the other hand, phosphorylation of RLC has been shown to slow the rate of relaxation in skeletal muscle fibers (Patel et al, 1998). Taking these distinct functions of RLC phosphorylation into consideration, it seems that the increase in Ca^{2+}/troponin-dependent force generation might be responsible for the increase in fatigue resistance and HRT in TSCmKO glycolytic skeletal muscle (Chapter 2, Figure 2D and E), and it could also serve as a mechanism that compensates for the loss of isometric forces. Moreover, these results strongly indicate perturbations in the calcium homeostasis of the TSCmKO glycolytic skeletal muscle.

Perturbations in calcium homeostasis in TSCmKO skeletal muscle alters excitation-contraction coupling

Perturbations in calcium signaling and/or homeostasis in skeletal muscle have been shown in various types of diseases. One is the myotonic dystrophy type 1 (DM1). It is known that the expansion of CUG repeats in DMPK (dystrophin myotonia protein kinase) leads to alternative splicing of several mRNAs of proteins involved in the ECC, such as SERCA1, DHPR, and CSQ. In a recent study, Ravel-Chapuis *et al.* have found that the defective regulation of calcium handling proteins promotes hyperactivation of CaN, thus resulting in increased activation of CaN/NFATc1-signaling in the skeletal muscle of DM1 patients (Ravel-Chapuis et al, 2017). CaN overexpression in *mdx* mice, a mouse model for DMD, ameliorated the dystrophic phenotype of those mice (Chakkalakal et al, 2003; Stupka et al, 2006; Stupka et al, 2008). In TSCmKO glycolytic skeletal hindlimb muscle, I also observe an upregulation of CaN protein levels. CaN is associated with inducing a slow fiber gene program over the CaN/NFAT-axis. However, it is also involved in the transcriptional regulation of muscle fiber hypertrophy. TSCmKO mice, however, suffer from skeletal muscle atrophy (Castets et al, 2013), which is

mainly explained by the impairment in autophagy. CaN/NFATc1-signaling, therefore, is either not upregulated, or insufficient to induce a compensatory hypertrophy program.

It was shown that NFAT acts as a nerve activity sensor in skeletal muscle. NFAT controls the activity-dependent myosin switch (McCullagh et al, 2004), and later studies identified the translational specification of the different isoforms. All NFAT isoforms must be present in the nucleus (dephosphorylated) to mediate the transcriptional effect of slow-Myh, whereas only NFATc4 is required to be present for the expression of Myh type IIb (Calabria et al, 2009). In my study, I did not observe any changes in NFAT isoform protein expression levels in TSCmKO mice (Figure 3D), which suggests that the fiber type switch is additionally regulated via other pathways. NFATc1, c2 and c3 also play an important role in lymphocytes (Chuvpilo et al, 1999; Luo et al, 1996; Macian, 2005; Shaw et al, 1988). Upon subtle inflammation, NFATs are upregulated. Inflammatory herds in skeletal muscle of TSCmKO mice have been observed in the intermyofibrillar tissue. As total muscle TA lysate contain non-muscle nuclei from intermyofibrillar tissue, minor changes of NFAT protein levels could be difficult to observe. In order to determine the activity of the CaN/NFAT-signaling, immunostaining of different NFATs and their nucleic translocalization might be a better approach.

The activity of the CaN/NFAT-signaling axis can also be assessed by analyzing transcripts regulated by the ETC pathway. I observed a 2.7-fold increase in the expression of *Myh7* mRNA levels in the TA muscle of TSCmKO mice. However, the effect was not statistically significant. This might be explained by the high variability between samples, but again it also indicates that the fiber type switch is not exclusively regulated by the CaN/NFAT-axis. The upregulation of *Myh7* in fast TSCmKO skeletal muscle is not only an indication for an increase in the CaN/NFAT-signaling, it is also another indication for a shift of the transgenic mouse muscle towards a slow contractile profile.

The excitation-contraction coupling and the calcium buffering capacity is disrupted in TSCmKO skeletal muscle

Recently, a study reported that *Rptor* ablation in skeletal muscle leads to a decrease in Cav1.1 expression and affects the ECC supramolecular complex (Lopez et al, 2015). Additionally, mutations in the RYR1 and DHPRα1 subunit, both core components of ECC, have been shown to be related to core myopathies (Treves et al, 2008). TSCmKO mice are characterized by a late-onset myopathy and already show a decrease in isometric forces at young age (3-month-old) (Castets et al, 2013). Interestingly, TSCmKO mice display a slight increase, although not significant, in resting calcium levels (Figure 2C). By analyzing the transcriptome, I found the calcium ATPase SERCA1 to be downregulated in glycolytic skeletal muscle of TSCmKO mice, which was confirmed by Western blot analysis (Figure 2D). Furthermore, the protein expression of important cytosolic (PV) and sarcoplasmic (SRL) calcium buffers were downregulated, whereas others (CSQ1) were found to be upregulated. These results would be in accordance with studies performed in PV-KO mice. In PV knockout mice, HRT increases in fast skeletal muscles and they show a prolonged calcium decay (Schwaller et al, 1999); features, which were also observed in TSCmKO mice. A drastic reduction in SRL protein levels were shown in *mdx* mice, and the same study revealed a tight interaction between SERCA1 and SRL (Dowling et al, 2004). Calcium re-uptake has been reported to be enhanced by SRL, through its interaction with SERCA and CSQ. The concomitant reduction in both SERCA1 and SRL protein levels in TSCmKO fast muscle may, therefore, have a direct influence on the ECC, and be involved in impairing calcium buffering.

CSQ is regarded as an organellular calcium buffer (SR), but it also serves as a luminal regulator of RyR activity by inhibiting calcium release (which requires the presence of junctin and triadin). By calcium demand from the SR, CSQ1 changes its confirmation and dissociates from the junction. This activates RyR and releases calcium into the cytosol. Just by analyzing the CSQ1 total protein levels, no statement can be made regarding the function of the calcium release from the SR. However, TPT in the skeletal muscle of TSCmKO mice was not

significantly changed, which diminishes the possibility of a defect in calcium release. However, further experiments are needed to address whether RyR1 function is normal in TSCmKO skeletal muscle. Interestingly, rapamycin treatment for seven days in young TSCmKO and in control mice increased the expression of PV in skeletal muscle (Figure 2B). This provides evidence that mTOR is involved in the maintenance and/or regulation of calcium homeostasis. However, whether or not PV is transcriptionally regulated by mTORC1 requires further investigation. In a study analyzing the role of calcium-binding proteins in skeletal muscle of *mdx* mice, Pertille *et al.* found a significant downregulation of CaM and CSQ in the most affected dystrophic muscles, strongly suggesting that the fiber-type composition explains the different behavior of metabolically opposing skeletal muscles to molecular changes (Pertille et al, 2010). In the TSCmKO mice, slow and fast muscles reveal different phenotypes, but similar changes regarding their contractile properties. As CaN/NFAT signaling is not only involved in fiber-type determination but is also involved in hypertrophy sensing in skeletal muscle, it might be interesting to further analyze the CaN/NFAT-axis in the hypertrophic SOL of the TSCmKO mice. This may reveal pathways involved in the opposing behavior of slow and fast muscle upon sustained mTORC1 activation. The TSCmKO mouse model might be beneficial in revealing how slow skeletal muscle “escapes” certain disease states or molecular changes.

Our results clearly suggest a shift towards a slower, oxidative contractile muscle in TSCmKO mice. Those results are in line with the previously observed metabolic shift of TSCmKO muscle towards a slow phenotype (Chapter 1 and 2). Slow muscle is more resistant to cellular stressors and might therefore, be a compensatory mechanism of the muscle fiber to react to the developing skeletal muscle myopathy. Rapamycin treatment in TSCmKO mice was shown to increases muscle force and induces autophagic flux. It would be interesting to know whether the regulation of calcium buffers, the developing fatigue resistance, and the slower contractile properties in TSCmKO skeletal muscle would also be reversed by rapamycin treatment. A first indication is provided by the downregulation of PV protein levels in TSCmKO skeletal muscle after rapamycin treatment (Figure 2B).

Due to the alteration in calcium-handling proteins, the slight increase in resting calcium levels, and the increased HRT (Chapter 2), it is expected that calcium transients are significantly changed in skeletal muscle of TSCmKO mice. This could be confirmed by measurement of calcium transients in single isolated muscle fibers. In conclusion, the results of this study strongly highlight the important signaling role mTORC1 plays in the maintenance of calcium homeostasis and in the generation of isometric forces.

9 Material and Methods

Animal Experiments

Generation of transgenic TSCmKO mice was described previously (Castets et al, 2013). Briefly, Tsc1-floxed-mice were crossed with mice containing the Cre- recombinase under the control of the human skeletal actin (HAS) promoter. Mice were kept single caged in a conventional facility under fixed 12h day-night-cycle conditions. Mice were either fed CR standardized food (OpenSource Diet- D10012M) or normal chow diet maintenance food (KLIBA NAFAG- 3432) for 6.5 months starting at the age of 12 weeks. Food intake was measured 3 weeks prior to the food reduction and constantly monitored on a weekly basis. Inverted hangtest was performed once, two weeks prior to dissection. Mice were euthanized between 8 am and 12 pm. All animal experiments were performed in accordance with the Swiss regulations for animal experimentations and approved by the veterinary commission of the Basel-Stadt canton.

Body Composition Analysis

MRI was performed on mice by using the EchoMRI-100H and by immobilizing mice in an MRI tube. Weight was monitored prior to the MRI measurement.

Animal Monitoring

To analyze metabolic status of mice before and after long-term CR, mice were put in a CLAMS (Comprehensive Lab Animal Monitoring System) for 3 days, of which day 1 was used for acclimatization. Parameters were measured under single caged conditions, recorded, and analyzed by using the Oxymax software.

Blood Analysis

Blood was taken from tail veins of living mice by restraining them. 80µl of blood was taken weekly within the 3-week adaptation period, and then monthly within the 3-6 months of CR. Terminal blood collection was performed by taking the blood from the *inf. vena cava* after mice have been anesthetized. Food was removed from *ad. libitum* fed mice at 7 am in the morning, and mice were transferred into clean cages. Prior to dissection glucose levels and ketone

bodies were determined in blood taken from tail vain with the Accu-Check Aviva and appropriate test strips (Roche) for glucose measurements, and with the FreeStyle Precision and appropriate test strips (Abbott Laboratories) for ketone bodies determination.

Mitochondrial respiration

Mitochondrial respiration was measured by using the Seahorse bioscience XF24 Analyzer. Mitochondria were isolated from fresh skeletal muscle according to the manufacturer's protocol (Seahorse Bioscience). Basal measurements were performed every ten minutes, 30 minutes prior to adding ADP. Proton leak is the difference in OCR after the FCCP injection. ATP linked respiration is the difference within OCR before and after oligomycin treatment and antimycin A. The maximal respiration is the OCR value after the FCCP injection. The reserve capacity is the difference between the basal and the maximal OCR.

Glycogen determination

Glycogen content of skeletal muscle was measured by using the Glucose (HK) Assay Kit (Sigma Aldrich; GAHK-20) according to the manufacturer's protocol. Briefly, frozen muscles were weighed and digested in 1 mol/L NaOH (1:9 wt/vol) at 85°C for 10 min. After a cool-down to RT, digested muscle was neutralized by using 1 mol/L HCl (1:9 wt/vol). 5 mol/L HCl were added and lysates were incubated again at 85°C for 2h before being neutralized with 5 mol/L NaOH. The concentration of hydrolyzed glucose residues was measured enzymatically with the hexokinase glucose assay reagent (Sigma). Glycogen content was expressed as micromoles of glucose units per gram (wet weight) of muscle. Samples were diluted 1:100 and measured against a glucose standard curve.

Functional *in vitro* analysis of skeletal muscle

EDL and SOL muscle force measurements were carried out as previously described (Bentzinger et al, 2008). Muscle fatigue was measured by repeated stimulation (number of contractions) at 200Hz every 8s and then recorded by using the Aurora Scientific Inc. Model 610A Dynamic Muscle Control Software. Graph displays maximal peak force of each contraction.

Physiological muscle measurements

For muscle endurance performance, inverted hangtest was performed by determining the time the mouse can hang on an inverted metal grit on 3 consecutive days. Cut off was placed after the first day of measurement to 120 minutes. Grip strength of fore- and hindlimb muscles was performed by using the Grip Strength Meter (Columbus Instruments). Measurements were taken three times in a row, with a 15min break in between measurements. Rota Rod was performed to determine muscle endurance and motor coordination by using the Rota Rod (Ugo Basile), on 3 consecutive days. Cut-off was set to 600 seconds, with an acceleration from 7 to 50, constantly increasing every 5s.

FDB fiber isolation and resting calcium measurements

FDB fibers were isolated by collagenase digestion (1.66mg/ml), incubated for 55min at 37°C with delicate shaking, and finally separated. Fibers were placed in modified Tyrode's buffer (137mM NaCl, 5.4mM KCl, 0.5mM $MgCl_2$, 1.8mM $CaCl_2$, 11.8mM HEPES-NaOH, 0.1% Glucose, 2%BSA, 1:100 Pen/Strep) and recovered at 37°C for approximately 2h. A glass bottom dish (Matek, #P35G-10-14-C) was coated with 5µl of laminin (Invitrogen cat. 23017-015), covered with a drop of water, and incubated for 1h at 37°C. After removing the water, 1ml of fiber solution was added onto the glass bottom dish after removal of the water and then 1ml of modified Tyrode's buffer is added. For the fibers to attach, they were incubated for 1-3h at 37°C. 7.5µl of FURA-2AM were added and incubated for 15min at 37°C. Sample was washed with Krebs buffer. Resting calcium was recorded by using the Axiovert S100 TV Camera (Zeiss) and the VisiView software. Exposure was set to 100ms. Wavelength was adjusted to 1:380nm MD1. EMCCD gain was set to 1,513 and pictures captured at 340nm and 380nm.

GSH/GSSG ratio detection

GSH/GSSG ratio detection was performed by using the GSH/GSSG ratio detection assay kit II (Fluorometric-Green) according to manufacturer's protocol (Abcam). After muscle tissue was

lysed and depolarized, total muscle lysates were used to determine reduced or oxidized amount of Glutathione within the sample.

Histology and Electron Microscopy

TA muscle was embedded in Tissue-Tek (Sakure Finetek), frozen in nitrogen-cooled isopentane, and then cut into 10µm thick consecutive sections. Sections were stained with hematoxylin (Merck: 1.09249.0500) and with eosin (Merck 1.09844.1000), followed by sequential dehydration with 75%, 90% and 100% ethanol, and final fixation by 100% xylene.

Periodic Acid Schiffs' (PAS) staining was performed by using the 395B-1KT Kit (Sigma Aldrich). Sections were fixed with Carnoy's solution, immersed in periodic acid solution (3951, Sigma Aldrich), and lastly incubated with Schiffs' solution (3952, Sigma Aldrich). Hematoxylin was added and sections mounted with xylol containing mounting Medium.

COX and SDH staining was performed by the Pathology Department, University of Basel, according to standard operation procedure described previously (Bancroft & Cook, 1984). Slides were mounted with touluol containing mounting medium.

Transmission electron microscopy was performed (Cinzia TIBERI, BioEM lab, Biozentrum) for thin sectioning and TEM. Briefly, mice were perfused via the heart with 4% paraformaldehyde (PFA) in 0.1M PIPES buffer pH 7.3 and 2mM $CaCl_2$. Small pieces of TA muscle were cut and transferred into a Petri dish with 2.5% glutaraldehyde (GA) and 2% PFA solution in 0.1M PIPES buffer with pH 7.3 and 2mM $CaCl_2$ for 1h. Afterwards, samples were washed once in PIPES buffer, pre-fixed in 1% reduced osmium tetroxide (containing 1.5% potassium ferricyanide) for 40min, and subsequently fixed in 1% osmium tetroxide for an additional 40min. After being washed in water, fixed samples were dehydrated with ethanol, embedded in Epon resin and processed for TEM as previously described (Winey et al, 2014). EM micrographs were recorded on Veleta CCD camera (EMSIS, Germany) by using a T12 Spirit transmission electron microscope (FEI, The Netherlands) operating at an acceleration voltage of 80 kV.

Immunostainings

10um thick section of TA muscle were thawn at RT for 10min and fixed in 4% PFA for 6min. Sections were washed twice for 15min at RT in 0.1M Glycine (pH7.4) for neutralization, and blocked afterwards at RT for 1.5h with blocking solution containing 3%BSA (IgG free), 1%Fab anti-mouse, and 0.25% Triton-X. The primary antibody incubation (dilutions listed below) was carried out overnight at 4°C. Slides were washed with PBS, and secondary antibody was incubated for 1.5h at RT. Afterwards, sections were washed twice in PBS and mounted by using Vectashield DAPI (vector Laboratories).

Dihydroethidium staining was performed as described previously (Menazza et al, 2010). In short, skeletal muscle cryosections (10-12µm thick) were incubated with 5uM DHE (Sigma D7008 Sigma-Aldrich; Dihydroethidium ≥95%) in 1xPBS at 37°C in a humid chamber for 30min. Sections were washed 4 times for 5min with 1x PBS in a glass chamber and then mounted with Vectashield (without DAPI).

For fiber ferret and fiber type determination, immunostaining was performed by using a different protocol. In short, slides were thawn at RT for 5min and rehydrated in PBS. Blocking was performed for 30min by using blocking solution containing PBS, 4% Triton X-100, and 4% Goat Serum (Biological Industries, Cat# 04-009-1A). Afterwards, sections were washed 3X for 5min, and primary antibody was incubated at RT for 1h. Prior to secondary antibody incubation, sections were washed in PBS, and secondary antibody was incubated for 1h at RT in the dark. Slides were washed again and sections were mounted by using the “ProLong Gold Antifade Mountant” (Life Technologies, P36930). Primary antibodies and corresponding dilution used are listed below.

Primary antibodies and corresponding dilution factors: anti-p62 (GP62-C, 1:300), anti-Laminin (ab11575, Abcam, 1:160- 1:300), anti- Myosin Heavy Chain I (BA-D5, DSHB, 1:50), anti-Myosin Heavy Chain IIa (SC-71, 1:200), anti- Myosin Heavy Chain IIb (BF-F3, DSHB, 1:100).

Images

Mitochondrial size and density was determined and calculated according to methods described previously (Arnold et al, 2014). It was also digitally converted and analyzed in Adobe Illustrator Photoshop. Electron micrographs were analyzed by using Adobe Illustrator Photoshop. Immunostaining images were analyzed by using the Imaris Software. Quantification of fiber types and fiber ferret were performed by using Fiji and Python Jupyter.

Quantitative real-time PCR

Total RNA from TSCmKO and control mice was isolated by using the RNeasy Mini Kit (Qiagen). Procedures were carried out as described in detail in the manufacturers protocol. Equal amounts of RNA were translated into cDNA by the iScript cDNA Synthesis Kit (BioRad) containing oligoDTs and random hexamer primers.

Genomic DNA (gDNA) isolation was performed as previously described (Guo et al, 2009). In short, homogenized muscle tissue was incubated over night at 55°C in lysis buffer (10mM Tris-HCl (pH8.0), 1mM EDTA, 0.1%SDS and 5% Proteinase K). Sample were vortexed and centrifuged for 15min at RT. Supernatant was incubated with RNase A (20mg/ml) for 30min at 37°C and inactivated at 95°C for 5min. Phenol/Chloroform/Isoamylalcohol (25:24:1) was added. After 15min centrifugation, aqueous phase was transferred and incubated with chloroform. Supernatant again was incubated with 10% of 3M NaAc and 1:1 with isopropanol. gDNA precipitates were kept at -20°C for minimum 30min. Samples were centrifuged and supernatant discarded. Pellet was washed twice in ice-cold Ethanol (75%) and afterwards resuspended in 15µl ddH_2O.

Genes of interest were amplified and detected by using the SYBR green, and quantitative expression was determined by the LightCycler® 480 (Roche). Relative expression of the genes was analyzed by using the ΔΔCq calculation method and normalized to the housekeeping gene encoding for β-*actin*, the expression of which is not affected by the conditional knockout of TSC1, specifically in skeletal muscle. Samples were pipetted in duplicates. The primers used are listed in the table below.

Gene of interest	Forward primer (3'-5')	Reverse primer (3'-5')
ATF4	AGCAAAACAAGACAGCAGCC	ACTCTCTTCTTCCCCCTTGC
ATP6	AGTATGAGCTGGAGCCGTAATTACA	TGGAAGGAAGTGGGCAAGTG
β-actin	CAGCTTCTTTGCAGCTCCTT	GCAGCGATATCGTCATCCA
β-Globulin	GGAGCAGCGATTCTGAGTAGA	GAAGCGATTCTAGGGAGCAG
CaMK IIα	TGACAGAGCAGCTGATCGAA	AGGTGGATGTGAGGGTTCAG
CaMK IIβ	TGAAGACATCGTGGCAAGAG	AGGCTTGAGGTCTCTGTGGA
CaMK IIγ	GGTCCGGAGGTGTGTAAAGA	TCATGGAGACGCACAATGTT
CaMK IIδ	TTGGGCAACTTAGTGGAAGG	ACGTGTGGGTTGAGGATGAT
Cox4i1	TACTTCGGTGTGCCTTCGA	TGACATGGGCCACATCAG
Cox5	CTTCAGGCACCAAGGAAGAC	TTCACAGATGCAGCCCACTA
CS	CCCAGGATACGGTCATGCA	GCAAACTCTCGCTGACAGGAA
CytC	AAATCTCCACGGTCTGTTCG	TATCCTCTCCCCAGGTGATG
D-loop	GGTTCTTACTTCAGGGCCATCA	GATTAGACCCGTTACCATCGAGAT
Drp1	GTTCCACGCCAACAGAATAC	CCTAACCCCCTGAATGAAGT
Fis1	AAGTATGTGCGAGGGCTGT	TGCCTACCAGTCCATCTTTC
Fbxo32	CTCTGTACCATGCCGTTCCT	GGCTGCTGAACAGATTCTCC
Gpx1	GTCTCTCTGAGGCACGATCCG	TTCCGCAGGAAGGTAAACAGC
Gsta1	CCAGAGCCATTCTCAACTA	TGCCCAATCATTTCAGTCAG
Map1lc3a	GTTGGATGTGTTCTGTCTCGTCAC	CTACGTGATTATTTCCGTGTTGCT
Mfn2	GGTCAGGGGTATCAGCGAAG	TTGTCCCAGAGCATGGCATT
Myl2	GCACCAAAGAAAGCCAGAAG	ATTGGACCTGGAGCCTCTTT
Myl3	AATCCTACCCAGGCAGAGGT	TGCCAGTGTCCTTGTTCTTG
Myl4	CCCAAGCCTGAAGAGATGAG	AGACAACAGCTGCTCCACCT
Myl6	GCTGGACTTTGAGCACTTCC	AGGACATGACGGATTTCAGC
Mylk2	AGGACCGGAAATGTCAACAG	TTTCCTTGTCCTTGGGTGTC
Mylk4	CTTGACAGAGCTGGACACCA	TCTGGGGTTCCAAAGTCCAC
Myh7	TCTGAGAAGGAGAGGCTGGA	GACACGATCTTGGCCTTGA
ND1	TCTGCCAGCCTGACCCATA	GGGCCCGGTTTGTTTCTG
Ndufv1	CCAAAACCCAGTGATCCAGC	CTTCCCCACTGGCCTCAAG
Nfatc2	ACAGGATCACTGGGAAAACG	TGGTGGCTCTCATGTTGTTC
Nfatc3	TACAGCAACAAGCGGGTGTC	CGGAGAGATGAGTCTGGTAGGG
Nfatc4	CTGTGCAAACCCCACCTC	GCCCAGAAATCGGTGAAC
OPA1	CGCTCTCCAGTGAAGGTGAC	GCAAGATCTTCCTCCTTGGTGA
Parkin	AAACCGGATGAGTGGTGAGT	AGCTACCGACGTGTCCTTGT

Gene of interest	Forward primer (3'-5')	Reverse primer (3'-5')
PYGM-1	CAC TTA CCA GCT GGG CTT GGA CAT	AAA GCA AGC TGC CAG GCG TC
PGM	CCCAAAATGTGTGGCAAGTT	TGTCAGGCTGGCTATCATCA
Ptgs1	TGCTAGCCGCAGGCATTACT	GCGGGATCAAAGAAAGTTGTG
SDHc	AGTTCAAACCGTCCTCTGTCTC	CCTCCACTCAAGGCTATTCCAG
SDHd	TTCTCTTAAAGCTGGGCGTTCT	GAAATGCTGACACATAAGCGGG
Sqstm1	TACTCGAACGACACAAGGGA	GACTCAGCTGTAGGGCAAGG
Trim63	ACCTGCTGGTGGAAAACA	AGGAGCAAGTAGGCACCTCA
Trib3	GGACAAGATGCGAGCCACAT	CCACAGCAGGTGACAAGTCT

Immunoblotting

TA and GAS muscles were frozen in liquid nitrogen and grinded in frozen condition. RIPA buffer (10 % glycerol, 150mM NaCl, 1 % NP-40, 0.1 % SDS, 0.5 % sodium deoxycholate, 1 % Triton X-100, 50mM Tris-HCl pH8, in ddH_2O) was supplemented with Protease and Phosphatase inhibitor cocktail tablets (Roche). Samples were incubated for 2h at 4°C and underwent two cycles of sonication, before lysates were centrifuged at 16,000g for 30min at 4°C. Total protein was determined with the Pierce BCA Protein Assay Kit (Thermo Fisher Scientific). Proteins were separated on 17-well 4-12% NuPage Bis-Tris Proteins Gels (NuPage Novex, Thermo Fisher Scientific) and transferred onto a nitrocellulose membrane of 0.45µm thickness (Whatman). Membrane was blocked for 1h at RT by using 3% BSA in TBS containing 0.1% of Tween-20. Primary antibody was incubated at 4°C overnight. After washing, secondary antibody, conjugated with the horseradish peroxidates, was incubated for 1.5h at RT. Signal was captured on Fusion Signal with the Fusion Capt Advance Software, in which grey values are automatically corrected for background. All expression levels were normalized to the loading control α-actinin/PAN-actin. Phosphorylation of proteins and total-protein levels were analyzed separately and ratio calculated after normalization. Primary antibodies and their dilution factors:

anti-α-Actinin (A7732, Sigma, 1:5,000), anti-PAN-actin (#4968S, CST, 1:1,000); anti-ATF4 (sc-200, Santa Cruz, 1:500), anti-ATP2a1/SERCA1 (4274S, CST, 1:1,000), anti-CaM (4830S,

CST, 1:1,000), anti-PAN-CamKII (3362S, CST, 1:1,000), anti-phospho-CamKII (T286) (3361S, CST, 1:1,000), anti-CaN (2614S, CST, 1:1,000), anti-CREB (9197S, CST, 1:1,000), anti-phospho-CREB (9198S, CST, 1:1,000), anti-CSQ1 (ab3516, Abcam, 1:1,000), anti-DHPR/Cav1.1 (#MA3-920, Invitrogen, 1:1,000), anti-DRP1 (BD61112, BD Biosciences, 1:1,000), anti-phospho-4E-BP1 (Ser65) (9451S, CST, 1:1,000), anti-phospho-4E-BP1 (9452S, CST, 1:1,000), anti-Fis1 (Alx-210-907, Enzo Life Sciences, 1:1,000), anti-GCLC (ab190685, Abcam, 1:,'000), anti-GCLM (ab153967, Abcam, 1:1,000), anti-GP (NBP1-32799, Novus biomedical, 1: 1,000), anti-GS (3893S, CST, 1: 1,000), anti-phospho GS (Ser641) (3891S, CST, 1: 1,000), anti-GSS (ab91591, Abcam, 1:500), anti-LC3b (2775S, CST, 1:1,000), anti-p44/42 MAPK (ERK1/2) (4695S, CST, 1:1,000), anti-phospho-p44/42 MAPK (ERK1/2) (Thr202/tyr204) (8544S, CST, 1:1,000), anti-MFN1 (sc-50330, Santa Cruz, 1:1,000), anti-MFN2 (sc-515647, Santa Cruz, 1:1,000), anti-mTORC1(2972S, CST, 1:1,000), anti-phospho-mTORC1 (Ser2448) (2971S, CST, 1:1,000), anti-MYLK2 (sc-9456, Santa Cruz, 1:1,000), anti-myosin heavy chain slow (Myh7) (A4.840, DSHB, 1.500), anti-NFATc3 (sc-8405, Santa Cruz, 1:1,000), anti-NFATc4 (sc-271597, Santa Cruz, 1:1,000), anti-OPA1 (BD612607, BD Biosciences, 1:1,000), OXPHOS (ab110413, Abcam, 1:1,000), anti-Parkin (ab15954, Abcam, 1:1,000), anti-PINK (ab23707, Abcam, 1:1,000), anti-PV (ab11427, Abcam, 1:1,000), anti-p62 (GP62-C, Pro-Gene, 1:1,000), anti-sarcalumenin (MA3-932, Thermo Scientific, 1:1,000), anti-S6 ribosomal protein (2217S, CST, 1:1,000), anti-phospho-S6 ribosomal protein (Ser235/236) (2211S, CST, 1:1,000), anti-phospho-S6 ribosomal protein (Ser240/244) (5364S, CST, 1:1,000), anti-mono and poly-ubiquitin (BML-PW8810-0100, Enzo Life Sciences, 1:1,000).

Statistical analysis

Compiled data is expressed in mean value ± standard error of the mean (SEM). All experiments were performed in independent biological samples of minimum 3. Statistical comparison of conditions was performed by using the one-way ANOVA with Fisher's LSD to determine statistical significance between two independent groups. Linear regression was employed to analyze significance in time dependent measurements. $P_{value} \leq 0.05$ is considered statistically significant.

10 Appendix

The Journal of Clinical Investigation RESEARCH ARTICLE

Targeting deregulated AMPK/mTORC1 pathways improves muscle function in myotonic dystrophy type I

Marielle Brockhoff,[1] Nathalie Rion,[2] Kathrin Chojnowska,[2] Tatiana Wiktorowicz,[1] Christopher Eickhorst,[2] Beat Erne,[1] Stephan Frank,[3] Corrado Angelini,[4] Denis Furling,[5] Markus A. Rüegg,[2] Michael Sinnreich,[1] and Perrine Castets[1,2]

[1]Neuromuscular Research Group, Departments of Neurology and Biomedicine, University of Basel, University Hospital Basel, Basel, Switzerland. [2]Biozentrum, University of Basel, Basel, Switzerland. [3]Institute of Pathology, Division of Neuropathology, University of Basel, University Hospital Basel, Basel, Switzerland. [4]Fondazione San Camillo Hospital IRCCS, Venice Lido, Italy. [5]Sorbonne Universités, University Pierre and Marie Curie (UPMC) Paris 06, Inserm, CNRS, Centre de Recherche en Myologie, Institut de Myologie, GH Pitié-Salpêtrière, Paris, France.

Myotonic dystrophy type I (DM1) is a disabling multisystemic disease that predominantly affects skeletal muscle. It is caused by expanded CTG repeats in the 3′-UTR of the dystrophia myotonica protein kinase (*DMPK*) gene. RNA hairpins formed by elongated *DMPK* transcripts sequester RNA-binding proteins, leading to mis-splicing of numerous pre-mRNAs. Here, we have investigated whether DM1-associated muscle pathology is related to deregulation of central metabolic pathways, which may identify potential therapeutic targets for the disease. In a well-characterized mouse model for DM1 (HSA^{LR} mice), activation of AMPK signaling in muscle was impaired under starved conditions, while mTORC1 signaling remained active. In parallel, autophagic flux was perturbed in HSA^{LR} muscle and in cultured human DM1 myotubes. Pharmacological approaches targeting AMPK/mTORC1 signaling greatly ameliorated muscle function in HSA^{LR} mice. AICAR, an AMPK activator, led to a strong reduction of myotonia, which was accompanied by partial correction of misregulated alternative splicing. Rapamycin, an mTORC1 inhibitor, improved muscle relaxation and increased muscle force in HSA^{LR} mice without affecting splicing. These findings highlight the involvement of AMPK/mTORC1 deregulation in DM1 muscle pathophysiology and may open potential avenues for the treatment of this disease.

Introduction

Myotonic dystrophy type I (DM1; OMIM #160900) is a multisystemic neuromuscular disorder, which represents the most common form of muscular dystrophy in adults (1). In particular, DM1 patients suffer from muscle wasting, weakness, and myotonia. DM1 is an autosomal dominant disease caused by an expansion of unstable CTG repeats located within the 3′-UTR of the dystrophia myotonica protein kinase (*DMPK*) gene. Toxic expanded transcripts containing RNA hairpins formed by the triplet repeats accumulate as RNA foci in the nuclei of affected cells (2, 3). These mutant transcripts are thought to sequester RNA-binding proteins, such as muscleblind-like 1 (MBNL1), and to increase CUG triplet repeat RNA-binding protein 1 (CUGBP1) levels. The resulting splicing defects are considered the primary cause of DM1 symptoms (4–6). HSA^{LR} mice, which carry a CTG repeat expansion in the human skeletal actin (*HSA*) gene, constitute a well-characterized mouse model for DM1 (5). These mice express (CUG)n-expanded transcripts specifically in skeletal muscle and reiterate the dystrophic phenotype and myotonic discharges observed in muscle of patients. HSA^{LR} mice also recapitulate DM1 molecular characteristics such as foci accumulation, MBNL1 sequestration, and splicing abnormalities (5, 7, 8). Therapeutic strategies have mainly focused on targeting DM1-associated mis-splicing and mRNA toxicity (9–11), although a more complete understanding of pathogenic pathways would clearly be of interest for the development of alternative or additional therapeutic options.

Recently, deregulation of cellular processes and signaling pathways important for maintaining proper muscle homeostasis has been reported in DM1. This includes abnormal activation of the ubiquitin-proteasome system and increased autophagic flux, which were both related to muscle atrophy and weakness in DM1 (12–14). In parallel, perturbation in the PKB/Akt pathway may arise from altered expression of the insulin receptor, which correlates with glucose intolerance in DM1 patients (15). Although PKB/Akt deregulation has been reported in *Dmpk*-deficient mice (16), in DM1 flies (13), and in DM1 human neural stem cells (17), contradictory results have been obtained in human muscle cells (18, 19).

To obtain further insight into the pathomechanisms associated with the disease, we investigated whether deregulated metabolic pathways may be involved in muscle alterations in DM1. We uncovered that muscles from HSA^{LR} mice do not efficiently respond to fasting by displaying impaired activation of AMPK and delayed inhibition of the mTOR complex 1 (mTORC1) pathway. Moreover, we observed mild perturbations of the autophagic flux in both HSA^{LR} muscle and myotubes from DM1 patients, which may arise from AMPK/mTORC1 deregulation. Importantly, we established that treatments normalizing these pathways improved

Conflict of interest: M. Sinnreich owns shares of Novartis and is coinventor on a patent application for drug discovery in DM1 (EP 16/166212.7). M. Sinnreich's institution (University Hospital Basel) has received research support from CSL Behring and Roche, not in relation to this study. C. Angelini is part of the European Board of Genzyme-Sanofi.
Submitted: July 19, 2016; **Accepted:** November 17, 2016.
Reference information: *J Clin Invest*. 2017;127(2):549–563.
https://doi.org/10.1172/JCI89616.

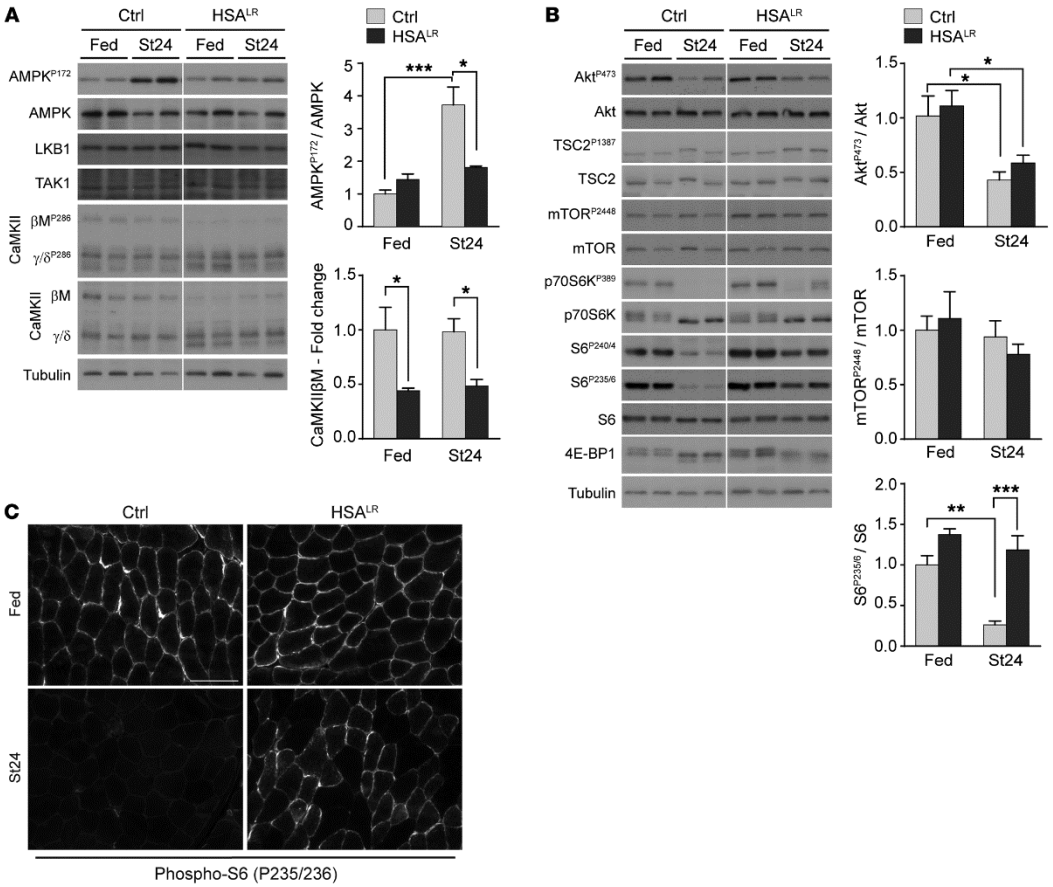

Figure 1. AMPK and mTORC1 pathways do not respond to starvation in HSA^{LR} muscle. (**A** and **B**) Two-month-old HSA^{LR} and control (Ctrl) mice were examined in fed conditions and after 24 hours of starvation (St24). Immunoblots for phospho- (P) and total proteins of the AMPK (**A**) and mTORC1 (**B**) pathways reveal reduced AMPK activation and increased phosphorylation of some mTORC1 targets upon starvation in mutant muscle. Samples were run on the same gel but were noncontiguous. Protein quantification is given for AMPK^{P172} (n = 4 Ctrl and 3 HSA^{LR}), CaMKIIβM, Akt^{P473}, mTOR^{P2448} (Fed, n = 3; St24, n = 4), and S6$^{P235/6}$ (Fed, n = 3; St24, n = 7 Ctrl and 6 HSA^{LR}). Data are relative to fed control mice and are mean ± SEM. $^*P < 0.05$, $^{**}P < 0.01$, $^{***}P < 0.001$, 2-way ANOVA with Tukey's multiple comparisons test correction. (**C**) Immunostaining on muscle cross sections from fed and starved (St24) HSA^{LR} and control (Ctrl) mice shows high levels of phospho-S6 in mutant muscle upon starvation. Scale bar: 100 μm.

skeletal muscle strength and strongly reduced the myotonia in HSA^{LR} mice. Our data provide evidence for the pathological role of metabolic pathways in DM1 and may open interesting avenues for alternative therapeutic strategies for the disease.

Results

AMPK and mTORC1 pathways are deregulated in HSA^{LR} muscle. To identify pathomechanisms involved in DM1-related muscle alterations, we examined the potential deregulation of metabolic pathways in HSA^{LR} mice (Supplemental Figure 1A; supplemental material available online with this article; doi:10.1172/JCI89616DS1). To this purpose, the activation state of key proteins was compared in muscle from 2-month-old mice analyzed in fed conditions or subjected to a physiological stimulus like fasting (20). No major difference was observed in the activation state of AMPK, PKB/Akt, and mTORC1 pathways in muscle from fed mutant and control mice, as reflected by the similar phosphorylation levels of AMPK (AMPK^{P172}), PKB/Akt (Akt^{P473}), and the mTORC1 targets ribosomal protein S6 kinase (p70S6K^{P389}) and S6 ribosomal protein (S6$^{P235/6}$ and S6$^{P240/4}$) (Figure 1, A and B). After 24 hours of starvation, HSA^{LR} mice showed impaired activation of the AMPK pathway, as revealed by the reduced levels of AMPK^{P172} in tibialis anterior (TA) mutant muscle (Figure 1A). Regardless of the nutritional status, protein expression of the known AMPK regulatory kinases

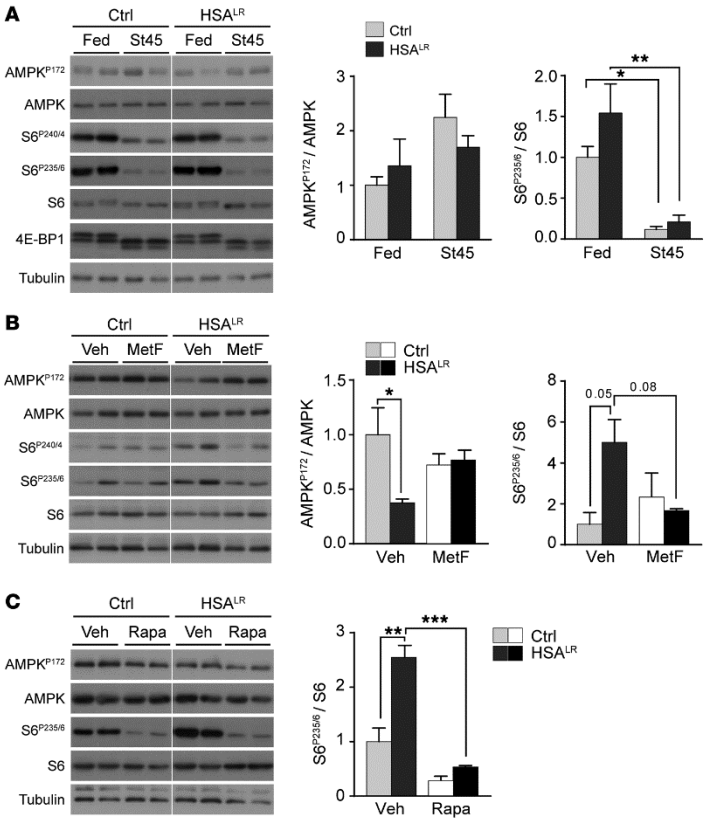

Figure 2. AMPK and mTORC1 pathways can be modulated by caloric and pharmacological treatments in HSA^{LR} muscle. Immunoblots for phospho- (P) and total AMPK and S6 proteins reveal efficient inhibition of mTORC1 signaling upon 45 hours of starvation (St45, **A**) and with metformin (MetF, **B**) or rapamycin (Rapa, **C**) treatment in muscle from HSA^{LR} mice. AMPK activation shows a trend toward increase in mutant muscle with metformin treatment (**B**). Samples were run on the same gel but were noncontiguous. Protein quantification is shown for AMPK$^{P1/2}$ and S6$^{P235/6}$ (Fed, n = 3; St45, n = 4 Ctrl and 3 HSA^{LR}; Veh [**B**], n = 3; MetF, n = 4; Veh [**C**], n = 4 Ctrl and 3 HSA^{LR}; Rapa, n = 3 per genotype). Data are relative to fed (**A**) or vehicle-treated (**B** and **C**) control mice and are mean ± SEM. $^*P < 0.05$, $^{**}P < 0.01$, $^{***}P < 0.001$, 2-way ANOVA with Tukey's multiple comparisons test correction.

liver kinase B1 (LKB1) and TGF-β–activated kinase 1 (TAK1) was unchanged in HSA^{LR} muscle compared with control (Figure 1A). In contrast, mutant muscle displayed an altered expression profile for Ca^{2+}-calmodulin–dependent kinase II (CaMKII) isoforms, with marked reduction in levels of the CaMKIIβM muscle-specific form and of its phosphorylated, active form (Figure 1A). Such deregulation was consistent with splicing defects in the *Camk2* genes previously described in tissues from DM1 patients and mouse models (11, 21–23). We confirmed by quantitative PCR that splicing of *Camk2b* was altered in muscle from HSA^{LR} mice (exon 13 exclusion; Supplemental Figure 1B), while overall expression of *Camk2* transcripts was unchanged in comparison with controls (Supplemental Figure 1C). As CaMKII regulates AMPK (24–26), these results suggest that impaired AMPK activation in HSA^{LR} muscle may rely on mis-splicing–dependent CaMKII deficiency.

In parallel, higher phosphorylation of p70S6K and S6 was detected upon starvation in HSA^{LR} muscle compared with control muscle (Figure 1B). Accumulation of phosphorylated S6 in muscle from starved mutant mice was further confirmed by immunostaining (Figure 1C), suggesting an abnormal activation of the mTORC1 signaling in HSA^{LR} mice. The specificity of the staining was confirmed by use of the S6$^{P235/6}$ blocking peptide and by immunostaining of sections from muscles with a constant activation (TSCmKO; ref. 27) or depletion (RAmKO; ref. 28) of mTORC1 (Supplemental Figure 1D). Notably, no major change in the phosphorylation of mTOR was observed in mutant and control muscles from fed versus starved mice (Figure 1B). Moreover, upon starvation, changes in 4E-BP1 levels were similar between HSA^{LR} and control muscles (Figure 1B), consistent with previous reports indicating differential regulation of mTORC1 targets (29). Interestingly, mTORC1 deregulation was not related to abnormal activity of PKB/Akt, since levels of the active phosphorylated form of PKB/Akt were efficiently decreased upon starvation in mutant mice (Figure 1B). Accordingly, we did not detect any changes in the splicing (exon 11, mis-spliced in DM1 patients) or expression of the gene encoding insulin receptor (*Insr*) in TA muscle from 2-month-old HSA^{LR} mice (Supplemental Figure 1E). Moreover, mTORC1 and AMPK activation state in nonmuscle tissue, such as liver, was similar in control and mutant mice (Supplemental Figure 1F), indicating that deregulation of these pathways is confined to skeletal muscles, which specifically express (CUG)n-expanded transcripts.

In an attempt to normalize mTORC1/AMPK pathways, control and HSA^{LR} mice were subjected to starvation for 45 hours. Mutant mice lost less weight than controls after prolonged starvation (Supplemental Figure 2). Moreover, upon 45 hours of star-

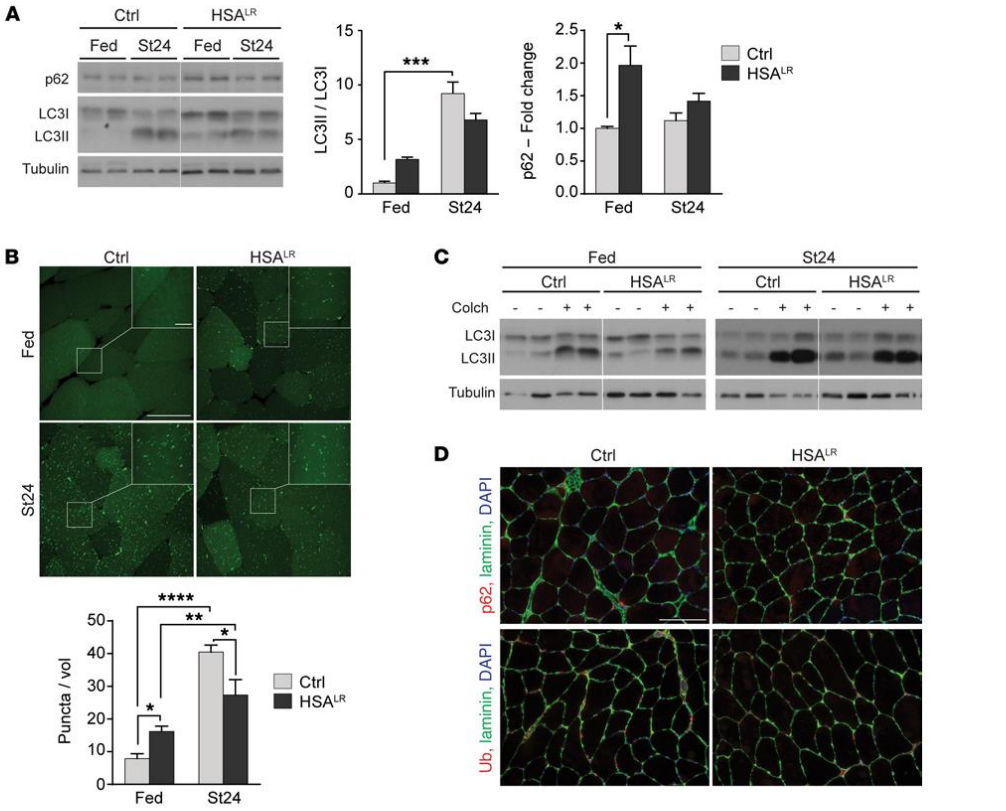

Figure 3. HSA^{LR} muscles show mild deregulation of the autophagic flux. (**A**) Immunoblots for autophagy-related proteins show accumulation of autophagic substrates in HSA^{LR} TA muscle in fed conditions. A reduced LC3I-to-LC3II switch is observed in mutant muscle upon 24 hours of starvation (St24), compared with control (Ctrl). Samples were run on the same gel but were noncontiguous. (Fed, $n = 3$; St24, $n = 7$ Ctrl and 6 HSA^{LR} for LC3 ratio, $n = 4$ for p62.) For LC3I and LC3II levels, see Supplemental Figure 3A. (**B**) HSA^{LR} mice expressing GFP-LC3 display increased number of GFP-positive puncta in TA muscle compared with control (Ctrl) in fed conditions ($n = 3$ Ctrl and 4 HSA^{LR}), but reduced accumulation after 24 hours of starvation (St24, $n = 3$). Scale bar: 50 μm; 10 μm for insets. A volume unit (vol) corresponds to 2.8×10^3 μm^3. (**C**) Treatment with colchicine (Colch) leads to milder changes in LC3II levels in TA muscle from fed and starved HSA^{LR} mice, compared with control (Ctrl) mice. For LC3II/LC3I quantification, see Supplemental Figure 3C. (**D**) Immunostaining of muscle sections from starved control (Ctrl) and HSA^{LR} mice reveals no major accumulation of p62 or ubiquitinated proteins in mutant muscle. Scale bar: 100 μm. Data are relative to control fed mice and represent mean ± SEM. *$P < 0.05$, **$P < 0.01$, ***$P < 0.001$, ****$P < 0.0001$, 2-way ANOVA with Tukey's multiple comparisons test correction.

vation, 4E-BP1 and phospho-S6 levels were similar in mutant and control muscles, while AMPK phosphorylation showed only a trend toward increase in HSA^{LR} muscle (Figure 2A). We next addressed whether pharmacological treatments would be sufficient to modulate AMPK/mTORC1 pathways in HSA^{LR} mice. Control and mutant mice were treated for 5 days with metformin, a drug known to induce AMPK signaling. The treatment slightly activated AMPK in muscle from starved HSA^{LR} mice, which was accompanied by a decrease in phospho-S6 levels (Figure 2B). Conversely, a single injection of rapamycin, a canonical inhibitor of mTORC1, strongly reduced S6$^{P235/6}$ levels in muscle from HSA^{LR} mice, to levels similar to those in controls. This further confirmed that S6 deregulation is dependent on mTORC1/p70S6K and does not involve ERK/p90S6K, which can also phosphorylate S6 at Ser235/6 (30). Levels of AMPK^{P172} remained unchanged in rapamycin-treated mice (Figure 2C). Although no obvious change was detected in AMPK-dependent phosphorylation of TSC2 (TSC2^{P1387}), an upstream inhibitor of mTORC1 (Figure 1B), these results suggest that AMPK deregulation may primarily be responsible for the defective response to starvation and for mTORC1 signaling perturbation in HSA^{LR} muscle.

Autophagic flux is perturbed in HSA^{LR} muscle. It is well established that mTORC1 and AMPK are key regulators of autophagy and that perturbation of their activities can lead to severe tissue alterations, especially in skeletal muscle (31–33). To determine whether the expression of the CUG repeats impairs the autophagy process, we

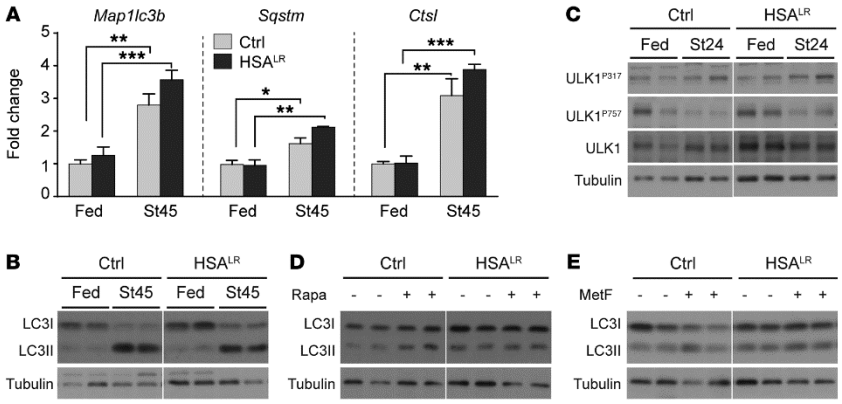

Figure 4. HSA^{LR} muscles display perturbed response of autophagy to caloric and pharmacological treatments. (**A**) Expression of autophagy-related genes is efficiently upregulated after 45 hours of starvation (St45) in HSA^{LR} TA muscle. Data are normalized to *Actn2* levels (Fed, $n = 4$; St45, $n = 4$ Ctrl and 3 HSA^{LR}). Data are relative to control fed mice and represent mean ± SEM. $^{*}P < 0.05$, $^{**}P < 0.01$, $^{***}P < 0.001$, 2-way ANOVA with Tukey's multiple comparisons test correction. (**B**) Immunoblots reveal limited switch from LC3I to LC3II in HSA^{LR} muscle upon 45 hours of starvation (St45) compared with controls (Ctrl). Samples were run on the same gel but were noncontiguous. For LC3II/LC3I quantification, see Supplemental Figure 4B. (**C**) Levels of the inhibited phosphorylated form of ULK1 (Ser^{P757}) remain slightly higher upon starvation in HSA^{LR} muscle, compared with control (Ctrl) muscle. For quantification, see Supplemental Figure 4C. (**D** and **E**) Immunoblots for LC3 show blunted induction of LC3II upon rapamycin (Rapa, **D**) or metformin (MetF, **E**) treatments, compared with controls (Ctrl). For LC3II/LC3I quantification, see Supplemental Figure 4, D and E. Samples were run on the same gel but were noncontiguous.

assessed the ability of HSA^{LR} muscle to induce autophagy when the mice were subjected to starvation. First, we evaluated levels of the soluble (LC3I) and autophagosome-associated (LC3II) forms of the widely used LC3B (MAP1LC3 for microtubule-associated protein light chain 3) autophagy marker. The amount of LC3II correlates with the intracellular accumulation of autophagic vesicles (34). Under fed conditions, LC3II levels were increased, although not significantly, in mutant muscle, which reflects either a slight increase in autophagy induction or a mild defect in the degradation steps (Figure 3A and Supplemental Figure 3A). After 24 hours of starvation, a clear switch from LC3I to LC3II occurred in control muscle, while HSA^{LR} muscle displayed reduced changes in LC3 levels and LC3II/LC3I ratio (Figure 3A and Supplemental Figure 3A). To confirm these results, we starved HSA^{LR} and control mice expressing the GFP-LC3 fusion protein for 24 hours. In control muscle, a striking increase in the number of GFP-LC3–positive puncta, representing autophagic vesicles, was observed upon starvation (Figure 3B and Supplemental Figure 3B). In HSA^{LR} mice, the number of puncta was higher under fed conditions, but was significantly less increased upon starvation as compared with control muscle (Figure 3B and Supplemental Figure 3B). These results confirmed that autophagy is perturbed in HSA^{LR} muscle, which may rely on impaired induction and/or degradation steps.

To assess the status of the autophagic flux, mice were treated for 2 days with colchicine, a drug preventing degradation of the autophagic content. Under both fed and starved conditions, colchicine induced a major switch from LC3I to LC3II in control muscle (Figure 3C). Comparing colchicine-treated and untreated mice, we observed that the fold change in the LC3II/LC3I ratio was less in HSA^{LR} muscle compared with controls, in both fed and starved conditions (Figure 3C and Supplemental Figure 3C). This result ruled out that elevated LC3II levels in fed conditions were due to increased autophagy induction in HSA^{LR} muscle; accumulation of autophagic vesicles was therefore likely related to restricted degradation. Consistently, levels of the autophagosome cargo protein p62 were higher in muscle from fed mutant mice than in controls (Figure 3A). However, we detected neither p62 aggregates nor accumulation of ubiquitinated proteins in muscle from fed and starved HSA^{LR} mice (Figure 3D), indicating that autophagy is only mildly affected. Similarly, distribution of lysosomal vesicles, visualized by LAMP1 immunostaining, was unchanged between 2-month-old mutant and control mice (Supplemental Figure 3D). Together, these results suggest that autophagy is slightly deregulated in DM1 muscle, which results from reduced degradation in combination with attenuated autophagy induction upon starvation.

Under fed conditions, increased amounts of p62 and LC3II were not due to abnormal transcript expression in HSA^{LR} muscle (Figure 4A). Moreover, expression of the *Map1lc3b*, *Sqstm* (encoding p62), and *Ctsl* (encoding cathepsin L) genes was unchanged after 24 hours of fasting, but we observed an efficient induction of the genes upon 45 hours of starvation in both mutant and control muscles (Figure 4A and Supplemental Figure 4A). It should be noted that following prolonged starvation, autophagy induction remained weaker in mutant muscle compared with control muscle (Figure 4B and Supplemental Figure 4B). To gain further insight into autophagy deregulation, we assessed the phosphorylation state of Unc-51–like kinase 1 (ULK1), as mTORC1 and AMPK phosphorylate and thereby inhibit or activate ULK1, respectively (31). Upon starvation, levels of the inactive form of ULK1 (ULK1^{P757}) remained slightly higher in mutant muscle as compared with control muscle, while no major difference was observed for its active form (ULK1^{P317}; Figure 4C and Supplemental Figure 4C). Interestingly, rapamycin and metformin treatments were both sufficient

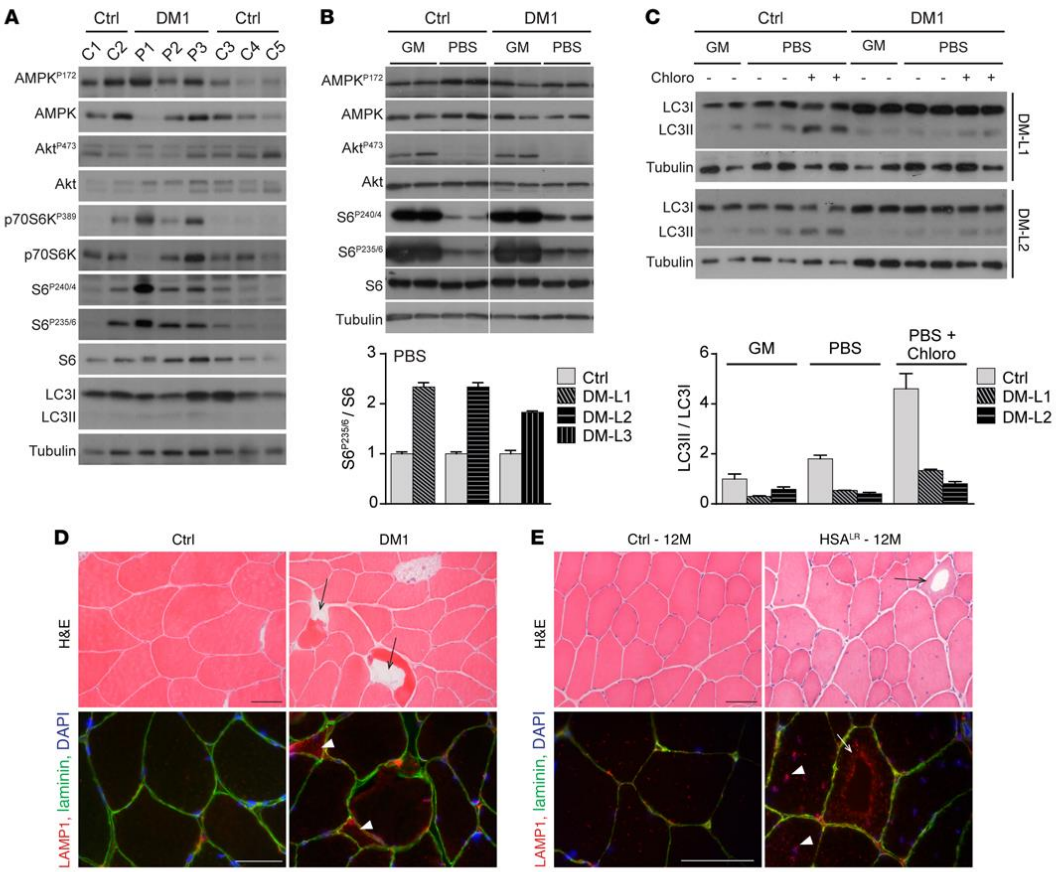

Figure 5. Autophagy perturbation contributes to muscle alterations in DM1. (**A**) Protein lysates from muscle biopsies of control individuals (C1–5) and DM1 patients (P1–3) were analyzed for phospho- (P) and total proteins of the AMPK and PKB/Akt–mTORC1 pathways. (**B**) MyoD-transduced fibroblasts from controls (Ctrl) and DM1 patients were differentiated to myotubes and subjected to growth medium (GM) or deprived conditions (PBS) for 3 hours. Immunoblots for phospho- (P) and total proteins reveal increased phospho-S6 levels upon deprivation in the 3 cell lines of DM1 patients (DM-L1–3), compared with controls. Samples were run on the same gel but were noncontiguous. Quantification is given for deprived conditions; values are mean ± SEM of technical replicates. (**C**) Immunoblots for LC3 marker show defective accumulation of LC3II in DM1 myotubes upon energy and amino acid deprivation (PBS) as well as with deprived conditions and chloroquine treatment (Chloro), compared with control cells (Ctrl). Quantification of LC3II/LC3I ratio is shown for 2 DM1 cell lines (DM-L1/2) in enriched (GM) and deprived conditions; values are mean ± SEM of technical replicates. (**D**) H&E stain reveals the presence of vacuolated fibers (arrows) in muscle biopsy from 1 DM1 patient, together with lysosomal accumulation (arrowheads) observed by immunostaining in some affected muscle fibers (red, bottom panel). Scale bars: 50 μm. (**E**) Vacuoles (arrows) are observed in muscle from aging HSA^{LR} mice; the periphery of the vacuoles is strongly reactive with anti-LAMP1 antibodies (red, bottom panel), indicating accumulation of lysosomal structures in these regions. High density of lysosomes is also observed in nonvacuolated muscle fibers from 12-month-old (12M) mutant mice (arrowheads), compared with muscle from age-matched control mice (Ctrl). Scale bars: 50 μm.

to increase LC3II levels in control muscle, but did not induce autophagy in HSA^{LR} muscle (Figure 4, D and E, and Supplemental Figure 4, D and E). Hence, mTORC1/AMPK deregulation in conjunction with mTORC1/AMPK-independent mechanisms likely contributes to autophagy perturbation in HSA^{LR} muscle.

Lastly, upon starvation, expression of the atrogenes *Trim63* and *Fbxo32* was similarly induced in HSA^{LR} and control muscles (Supplemental Figure 4F). However, caspase- and trypsin-like activities associated with the proteasome system were increased in muscle from fed and starved mutant mice, compared with control animals (Supplemental Figure 4G). This is consistent with a previous report showing higher proteasome activity in muscle from a DM1 mouse model expressing 550 CTG triplets (12).

Involvement of AMPK/mTORC1 deregulation in DM1 pathology. To ascertain the relevance of the changes observed in HSA^{LR} mice for DM1 pathology, we evaluated the activation state of AMPK/

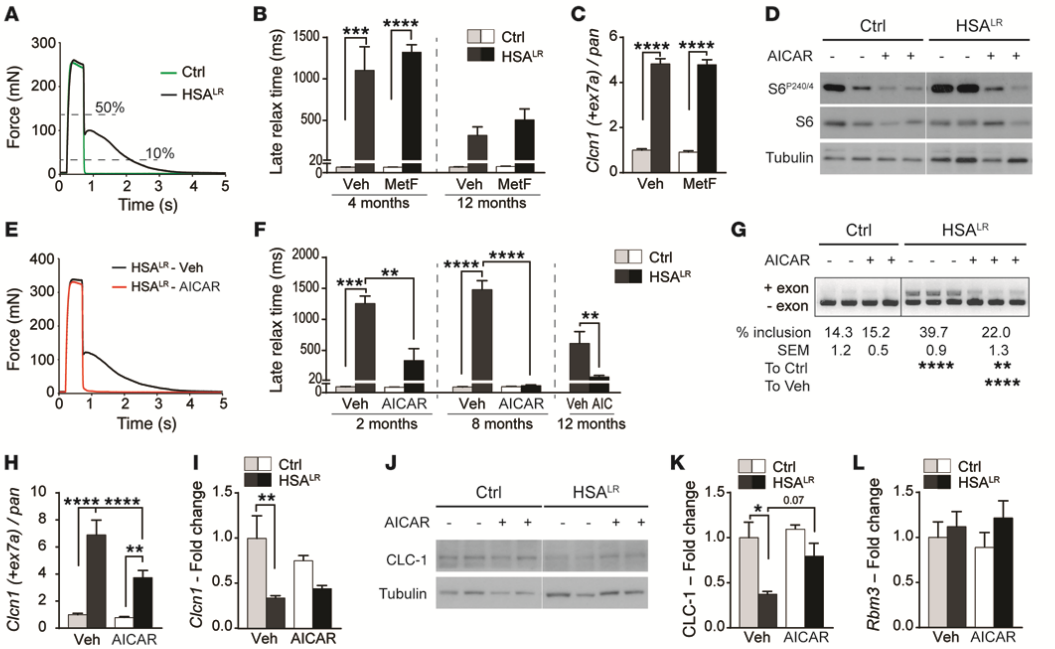

Figure 6. AICAR markedly decreases myotonia in HSA^{LR} mice and reduces mis-splicing in mutant muscle. (**A**) In vitro tetanic stimulation of EDL muscle reveals strongly increased relaxation time in HSA^{LR} muscle. (**B**) Metformin (MetF) treatment does not reduce muscle late relaxation time in 4-month-old (Ctrl, n = 5; HSA^{LR}, n = 6 Veh and 8 MetF) and 12-month-old (Ctrl, n = 3; HSA^{LR}, n = 7 Veh and 8 MetF) HSA^{LR} mice, as compared with vehicle-treated mutant mice. (**C**) Inclusion of exon 7a of the *Clcn1* gene is not changed in muscle from metformin-treated (MetF) HSA^{LR} mice, compared with vehicle-treated mice (n = 3). (**D**) Immunoblots for phospho- and total S6 protein reveal efficient inhibition of indirect AMPK target in muscle from control (Ctrl) and mutant mice treated with AICAR. Samples were run on the same gel but were noncontiguous. (**E**) AICAR treatment normalizes the time to relax of HSA^{LR} muscle upon tetanic stimulation, compared with muscle from vehicle-treated (Veh) mutant mice. (**F**) Late relaxation time is significantly reduced in EDL muscle from 2-month-old (n = 3 Ctrl and 4 HSA^{LR}), 8-month-old (Ctrl, n = 3; HSA^{LR}, n = 6 Veh and 7 AICAR), and 12-month-old (n = 4 Veh and 5 AICAR) HSA^{LR} mice that were treated with AICAR, as compared with age-matched vehicle-treated (Veh) mutant mice. (**G**–**K**) End-point PCR (**G**) and quantitative PCR (**H** and **I**) reveal strong reduction in exon 7a inclusion of the *Clcn1* gene in muscle from HSA^{LR} mice treated with AICAR, compared with vehicle-treated (Veh) mutant mice (Ctrl, n = 3; HSA^{LR}, n = 5 Veh and 4 AICAR [**G**], n = 5 [**I**]). Protein levels of CLC-1 are also increased in mutant muscle from AICAR-treated mice (**J** and **K**, n = 3 Ctrl and 4 HSA^{LR}). (**L**) Quantitative PCR shows similar transcript levels of *Rbm3* in muscle from AICAR-treated and untreated mice (n = 3 Ctrl and 4 HSA^{LR}). Data represent mean ± SEM. *P < 0.05, **P < 0.01, ***P < 0.001, ****P < 0.0001, 2-way ANOVA with Tukey's multiple comparisons test correction (except 12M AICAR, unpaired 2-tailed Student's t test).

mTORC1 signaling in muscle biopsies from 3 DM1 patients (P1–3) of 33, 34, and 49 years of age. There was no major difference in total and phosphorylated levels of PKB/Akt and AMPK proteins in muscle from DM1 patients compared with age-matched control individuals (C1/2 and C3–5 aged 30 and 50 years, respectively) (Figure 5A). Notwithstanding, we noticed that levels of the active phosphorylated forms of p70S6K and S6 were increased in muscle biopsies from DM1 patients compared with control individuals (Figure 5A). However, the nutritive status of the patients at the time of the biopsy could not be ascertained and may have influenced the results. For this reason, we next tested the ability of DM1 human muscle cells to modulate mTORC1/AMPK signaling in response to energy and nutrient deprivation. Fibroblasts of 3 DM1 patients (DM-L1–3) were transduced with MyoD and differentiated for 10 days into myotubes, before being subjected to growth medium or to amino acid– and glucose-deprived conditions (i.e., PBS) for 3 hours. Upon deprivation, levels of the active phosphorylated forms of PKB/Akt and S6 were strongly reduced in control muscle cells; there was no major activation of AMPK in comparison with enriched conditions (Figure 5B). A similar response was observed in DM1 muscle cells, although they retained higher phosphorylation of S6 in deprived conditions compared with control cells (Figure 5B). In parallel, a major switch from LC3I to LC3II occurred in control muscle cells upon deprivation. LC3II levels were further increased in control cells treated with chloroquine, consistent with high autophagy induction in deprived cells (Figure 5C). In contrast, LC3II levels were only slightly changed when DM1 myotubes were subjected to deprivation, even in the presence of chloroquine, indicating that the autophagic flux is blocked at the induction steps (Figure 5C). Together, these data indicate that DM1 human muscle cells do not efficiently respond to nutrient/energy deprivation and display deregulation of the autophagy process.

Table 1. Changes in muscle cross-sectional area and tetanic forces upon treatments in HSA^{LR} and control mice

	Ctrl		HSA^{LR}	
	Vehicle	**AICAR**	**Vehicle**	**AICAR**
CSA EDL (mm^2)				
2M	1.38 ± 0.02	1.31 ± 0.03	1.65 ± 0.05^{C}	1.62 ± 0.01^{C}
8M	1.52 ± 0.00	1.70 ± 0.2	1.86 ± 0.07	1.70 ± 0.04
12M	–	–	2.46 ± 0.07	2.32 ± 0.02
Po (mN)				
2M	185.20 ± 9.01	255.79 ± 9.09^{D}	197.91 ± 13.96	279.97 ± 17.25^{E}
8M	285.37 ± 33.67	273.71 ± 36.71	288.31 ± 15.15	274.39 ± 12.27
12M	–	–	260.90 ± 26.53	339.42 ± 24.22$^{0.07}$
sPo (mN/mm^2)				
2M	134.58 ± 4.84	194.73 ± 2.67^{D}	121.23 ± 12.16	173.60 ± 11.05^{D}
8M	187.58 ± 22.01	168.80 ± 34.37	156.89 ± 11.95	161.94 ± 7.34
12M	–	–	107.33 ± 13.02	146.46 ± 10.51$^{0.06}$
	Vehicle	**Rapamycin**	**Vehicle**	**Rapamycin**
CSA EDL (mm^2)				
4M	1.69 ± 0.12	1.61 ± 0.07	2.04 ± 0.07^{B}	1.96 ± 0.02^{B}
12M	1.67 ± 0.09	1.50 ± 0.10	1.90 ± 0.06	1.77 ± 0.09
Po (mN)				
4M	180.94 ± 26.37	170.07 ± 3.91	193.80 ± 13.01	274.48 ± 16.11^{B,E}
12M	226.14 ± 28.30	245.67 ± 16.07	209.59 ± 30.94	240.28 ± 18.95
sPo (mN/mm^2)				
4M	114.98 ± 21.53	111.32 ± 8.79	99.41 ± 7.64	144.37 ± 8.32^{E}
12M	137.66 ± 23.49	168.87 ± 20.50	109.78 ± 15.01	137.12 ± 12.41
	Vehicle	**AZD8055**	**Vehicle**	**AZD8055**
CSA EDL (mm^2)	1.24 ± 0.42	1.67 ± 0.03	2.09 ± 0.09^{A}	2.06 ± 0.04
Po (mN)	185.19 ± 76.17	241.13 ± 80.46	257.96 ± 28.02	353.06 ± 8.90
sPo (mN/mm^2)	190.13 ± 23.13	192.38 ± 6.94	124.30 ± 13.88^{A}	171.96 ± 5.22^{D}

CSA, cross-sectional area; M, month; Po, tetanic muscle force; sPo, specific tetanic muscle force. CSA = weight/(1.06 * length * 0.44), where 1.06 corresponds to the density of the muscle and 0.44 the correction factor for EDL muscle. AICAR, 2-month-old (n = 3 Ctrl and 4 HSALR), 8-month-old (Ctrl, n = 3; HSALR, n = 6 Veh and 7 AICAR), 12-month-old (HSALR, n = 4 Veh and 5 AICAR) mice; rapamycin, 4-month-old (Ctrl, n = 4; HSALR, n = 8 Veh and 10 Rapa), 12-month-old (Ctrl, n = 3; HSALR, n = 5 Veh and 6 Rapa) mice; AZD8055, 8-month-old (Ctrl, n = 3; HSALR, n = 5 Veh and 8 AZD) mice. Values are mean ± SEM. $^{A}P < 0.05$, $^{B}P < 0.01$, $^{C}P < 0.001$ compared with control mice with same treatment; $^{D}P < 0.05$, $^{E}P < 0.01$, compared with same genotype treated with vehicle; 2-way ANOVA with Tukey's multiple comparisons test correction; for 12-month-old AICAR-treated mice, unpaired 2-tailed Student's t test.

To test the relevance of autophagy changes in DM1, we looked for muscle alterations related to autophagy defects in muscle biopsies from DM1 patients and in muscle from aged HSA^{LR} mice. As previously reported (14, 35–37), vacuolated fibers were observed in muscle biopsy of 1 DM1 patient, out of the 3 examined (Figure 5D). Lysosome accumulation was also detected in affected fibers from DM1 muscle (Figure 5D). However, in contrast to biopsies from an inclusion body myositis (IBM) patient, there was no accumulation of LC3, ubiquitinated proteins, or p62 in DM1 patient muscles (Supplemental Figure 5A). Consistently, LC3 levels detected by Western blot were similar in DM1 and control biopsies (Figure 5A). Interestingly, we observed some intracellular vacuoles in muscle from 12-month-old HSA^{LR} mice, as well as accumulation of the lysosomal marker LAMP1 near the vacuolar structures and myonuclei (Figure 5E). Secondary antibodies alone did not react with the vacuoles, and we did not observe such features in muscle from age-matched control mice (Figure 5E and Supplemental Figure 5B). Electron microscopy confirmed the presence of vacuoles in mutant mouse muscle: they were surrounded by dense, disorganized areas of contractile elements and usually limited by a single, discontinuous membrane (Supplemental Figure 5C). Together with the lysosome staining, these features argue for the presence of autophagic vacuoles in muscle from older HSA^{LR} mice. These results suggest that autophagy perturbation may contribute to the alteration of muscle tissue in DM1, but is unlikely to be a predominant feature of the disease.

AICAR, an AMPK agonist, abrogates myotonia in HSA^{LR} mice. In light of the deregulation of AMPK signaling in HSA^{LR} muscle, we investigated whether AMPK normalization would have a beneficial effect on muscle function in mutant mice. As readout of the disease, we evaluated myotonia by measuring the late relaxation time of skeletal muscle (i.e., time to reduce the maximal force from 50% to 10%) after ex vivo tetanic stimulation (8). As reported previously, we observed no change in the late relaxation time of soleus muscle from HSA^{LR} mice compared with controls (Supplemental Figure 6A), whereas this parameter was strongly increased in extensor digitorum longus (EDL) mutant muscle (Figure 6A). Since AMPK activation by metformin has recently been shown to correct mis-splicing in human DM1 cells in vitro (38), 4- and 12-month-old control and HSA^{LR} mice were treated with metformin for 10 days. Despite using high doses of metformin, we observed only a limited and nonreproducible effect of the treatment on AMPK/S6 activation state in these groups of mice analyzed under basal nutritive conditions (Supplemental Figure 6B). Besides, the treatment failed to reduce the late relaxation time of EDL muscle in mutant mice (Figure 6B), and it did not modify the expression and splicing of genes affected in DM1, including *Clcn1* (encoding CLC-1, chloride channel protein 1; inclusion of exon 7a) and *Atp2a1* (encoding sarcoplasmic/endoplasmic reticulum Ca^{2+}-ATPase 1; exclusion of exon 22) (Figure 6C and Supplemental Figure 6C).

As we did not detect any effect of metformin on HSA^{LR} muscle, we tested whether 5-aminoimidazole-4-carboxamide ribonucleotide (AICAR), an agonist of AMPK, may constitute an alternative strategy to target AMPK activation in muscle. Following a 7-day treatment with AICAR, control and mutant muscles showed a clear reduction in phospho-S6 levels (Figure 6D). We further confirmed that AICAR increased phosphorylated levels of AMPK and those of its direct target acetyl-CoA carboxylase shortly after the last injection (30 minutes), while inhibition of the indirect AMPK target S6 was detected only after 2 hours in control muscle (Supplemental Figure 6D). Importantly, following tetanic stimuli, a strong and significant reduction in the late

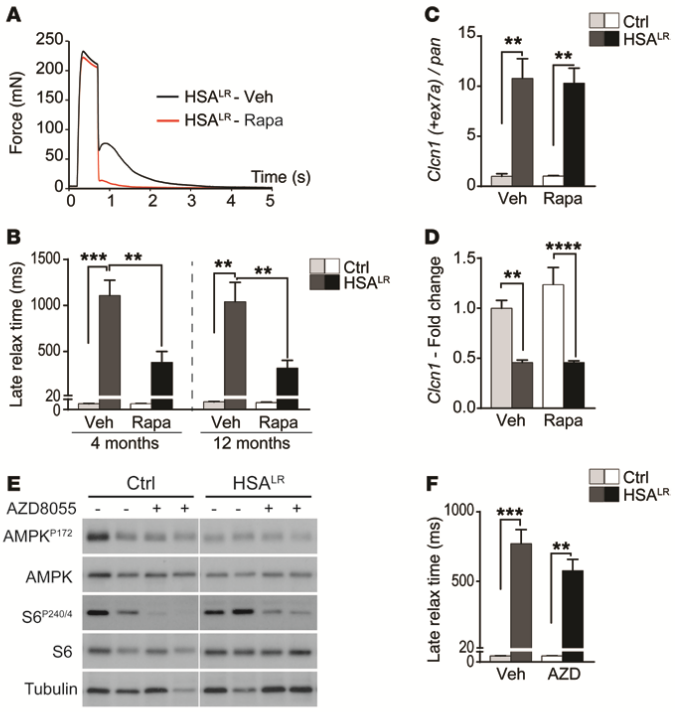

Figure 7. Rapamycin improves muscle function in HSA^{LR} mice via splicing-independent mechanisms. (**A**) Rapamycin treatment strongly reduces the time to relax of HSA^{LR} muscle upon tetanic stimulation, compared with muscle from vehicle-treated (Veh) mutant mice. (**B**) Rapamycin (Rapa) treatment significantly reduces late relaxation time of muscle from 4-month-old (Ctrl, $n = 4$; HSA^{LR}, $n = 8$ Veh and 10 Rapa) and 12-month-old (Ctrl, $n = 3$; HSA^{LR}, $n = 5$ Veh and 6 Rapa) HSA^{LR} mice, as compared with age-matched, vehicle-treated mutant mice. (**C** and **D**) Splicing (**C**) and overall transcript expression (**D**) of the *Clcn1* gene are not modified in muscle from rapamycin-treated (Rapa) HSA^{LR} mice, compared with vehicle-treated (Veh) mutant mice. Values are relative to vehicle-treated control mice ($n = 3$ Ctrl and 4 Veh-treated and 5 Rapa-treated HSA^{LR}). (**E**) Treatment with AZD8055 for 10 days efficiently reduces phosphorylation of mTORC1 target, S6, in control (Ctrl) and HSA^{LR} muscle, but does not change AMPK activation. Samples were run on the same gel but were noncontiguous. (**F**) AZD8055 (AZD) does not reduce late relaxation time of EDL mutant muscle, compared with vehicle-treated (Veh) mutant mice. ($n = 3$ Ctrl and 5 Veh and 8 AZD HSA^{LR} mice.) Data represent mean ± SEM. $^{**}P < 0.01$, $^{***}P < 0.001$, $^{****}P < 0.0001$, 2-way ANOVA with Tukey's multiple comparisons test correction.

relaxation time of EDL muscle was detected in 2- and 12-month-old AICAR-treated mutant mice, and myotonia was completely abrogated with AICAR in the group of 8-month-old HSA^{LR} mice (Figure 6, E and F). Normalization of the half-relaxation time (i.e., time to reduce the maximal force from 100% to 50%) of mutant muscle was also observed upon treatment (Supplemental Figure 6E). As mis-splicing of the *Clcn1* gene is thought to be the primary cause of myotonia in DM1 (7, 39–41), we investigated whether the effect of AICAR was related to changes in *Clcn1* splicing. By end-point PCR, a significant improvement of the misregulated *Clcn1* splicing was detected upon AICAR treatment (Figure 6G). We confirmed by quantitative PCR that the expression of the mis-spliced *Clcn1* transcript (containing exon 7a) was strongly reduced in muscle from AICAR-treated HSA^{LR} mice, while overall transcript levels of *Clcn1* were unchanged compared with those in untreated mutant mice (Figure 6, H and I). Furthermore, AICAR led to a slight increase in CLC-1 protein levels in mutant muscle (Figure 6, J and K). It is worth noting that AICAR did not change splicing of the *Atp2a1* and *Camk2b* genes in HSA^{LR} muscle (Supplemental Figure 6, F and G). Moreover, we did not detect any reduction in transcript levels of *Rbm3*, encoding RNA-binding protein 3 (Figure 6L), previously suggested to mediate the effect of AMPK activation on splicing (38).

Besides its effect on myotonia, we wondered whether AICAR treatment would change muscle force in mutant mice. As initially reported (5), we detected neither muscle wasting nor reduction in total twitch (Pt) and tetanic (Po) muscle forces in HSA^{LR} mice compared with controls (Table 1 and Supplemental Table 1). Nonetheless, as cross-sectional area [CSA: mass/(density * length * correction factor)] of EDL muscle was increased in mutant mice, specific muscle forces (sPt and sPo), representative of the contractile capacity of the myofibers, were reduced in HSA^{LR} mice compared with control animals (Table 1 and Supplemental Table 1). Upon AICAR treatment, we observed that both total and specific forces of EDL muscle were increased in 2-month-old HSA^{LR} and control mice, but not in older mice (Table 1 and Supplemental Table 1). Altogether, these results indicate that targeting AMPK activation by AICAR improves muscle function in HSA^{LR} mice by reducing myotonia and potentially increasing muscle force, at least in part, through splicing correction.

Rapamycin treatment improves muscle function in HSA^{LR} mice. Based on the abnormal activation of mTORC1 signaling detected in HSA^{LR} muscle, we wondered whether indirect mTORC1 inhibition was part of the effect of AICAR and whether direct mTORC1 inhibition would improve muscle function in mutant mice. To this purpose, we subjected 4- and 12-month-old mice to rapamycin treatment for 7 and 10 days, respectively. Rapamycin treatment efficiently inhibited mTORC1 signaling, as shown by reduced phospho-S6 levels in muscle from control and HSA^{LR} mice (Supplemental Figure 7A). Rapamycin did not affect muscle half-relaxation time (Supplemental Figure 7B), but significantly reduced the late relaxation time of EDL muscle from 4- and 12-month-old HSA^{LR} mice (Figure 7, A and

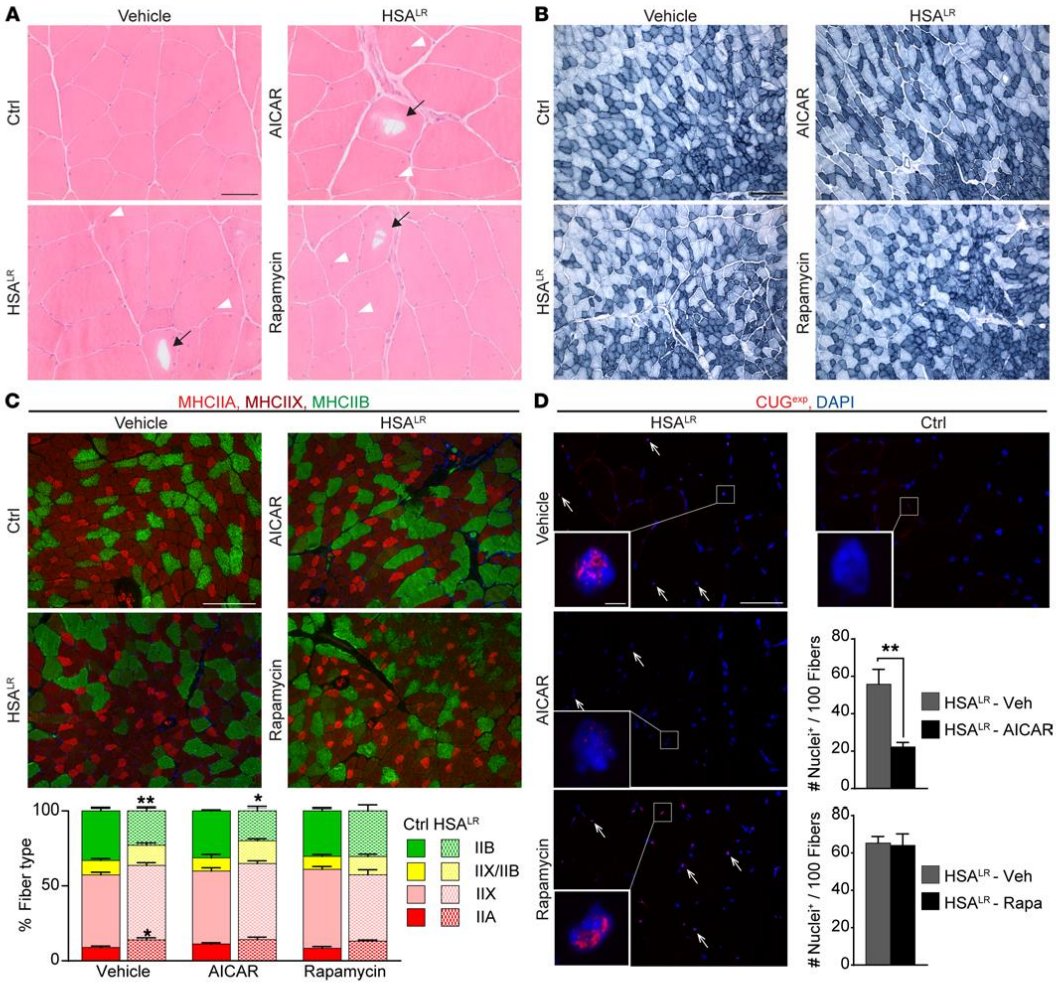

Figure 8. AMPK activation by AICAR leads to nuclear foci dispersion in HSA^{LR} muscle. (**A** and **B**) H&E (**A**) and NADH (**B**) stains reveal no major change in muscle histopathology and oxidative capacity upon AICAR or rapamycin treatment in HSA^{LR} mice. Arrowheads and arrows show internalized nuclei and vacuoles, respectively. Scale bars: 50 μm (**A**), 200 μm (**B**). (**C**) Immunostaining for type IIA (bright red), IIX (dark red), and IIB (green) myosin heavy chains (MHC) reveals no significant change in the respective proportion of fiber types in TA mutant muscle upon AICAR (n = 3 Ctrl and 4 HSA^{LR}) or rapamycin (n = 4) treatment, compared with vehicle-treated HSA^{LR} mice (n = 6 Ctrl and 7 HSA^{LR}). Scale bar: 200 μm. (**D**) FISH on TA muscle sections with a Cy3-CAG$_{10}$ DNA probe shows accumulation of nuclear foci in HSA^{LR} muscle (arrows). The number of stained nuclei is significantly decreased upon AICAR treatment (n = 4), but not with rapamycin (Rapa, n = 3), compared with vehicle-treated (Veh) mutant mice. Foci are not detected in control (Ctrl) muscle. Scale bar: 50 μm; 2 μm for insets. Data in **C** and **D** represent mean ± SEM. *P < 0.05, **P < 0.01, 2-way ANOVA with Tukey's multiple comparisons test correction.

B). Moreover, we detected a significant increase in total and specific muscle forces in young rapamycin-treated mutant mice compared with vehicle-treated animals. Forces remained unchanged upon treatment in older mice (Table 1 and Supplemental Table 1).

To test whether the effect of rapamycin on muscle function relied on splicing improvement, we assessed *Clcn1* mis-splicing (i.e., exon 7a inclusion) by quantitative PCR. Interestingly, rapamycin affected neither *Clcn1* splicing (Figure 7C) nor the overall transcript expression of the gene (Figure 7D) in mutant muscle. Consistently, splicing of the *Atp2a1* gene was also not restored in rapamycin-treated HSA^{LR} mice (Supplemental Figure 7C). Together, these data suggest that mTORC1 inhibition by rapamycin is sufficient to improve muscle function in HSA^{LR} mice likely through splicing-independent mechanisms.

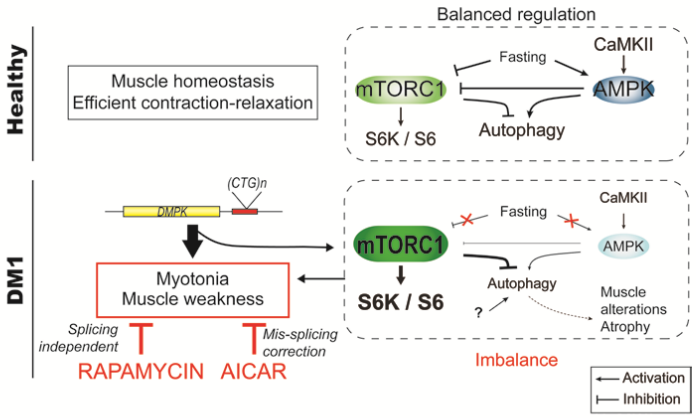

Figure 9. Scheme depicting the deregulation of AMPK/mTORC1 signaling pathways in DM1 muscle. In healthy muscle, the pathways are tightly regulated depending on external and internal stimuli (e.g., growth factors, energy, nutrients). Upon fasting, mTORC1 is inhibited, while AMPK is activated, leading to the induction of autophagy. In DM1, skeletal muscle does not respond to fasting conditions. Deregulation of the AMPK/mTORC1 signaling likely contributes to muscle dysfunction: rapamycin, an inhibitor of mTORC1, and AICAR, an AMPK agonist, both lead to marked reduction of myotonia and normalize muscle weakness in DM1 mice. The underlying mechanisms include RNA splicing–dependent and –independent mechanisms.

Since rapamycin has been shown to impact on channel function (e.g., ryanodine receptor 1, RyR1) via its binding to FKBP12, we wondered whether mTORC1 inhibition or the drug itself mediated the effect of the treatment on myotonia. Hence, control and HSA^{LR} mice were treated for 10 days with AZD8055, an ATP-competitive inhibitor of mTORC1. We confirmed that AZD8055 strongly decreased phospho-S6 levels in control and mutant muscle, while the activation state of AMPK remained unchanged (Figure 7E). In contrast to rapamycin, AZD8055 had no effect on late relaxation time of mutant muscle (Figure 7F). Nonetheless, total and specific forces of EDL muscle were increased in AZD8055-treated mutant mice, as observed with rapamycin (Table 1 and Supplemental Table 1). Together, these results indicate that mTORC1 inhibition may ameliorate the contractile capacity of muscle in HSA^{LR} mice and suggest that improvement of muscle relaxation upon rapamycin and AICAR treatments may be independent of mTORC1.

AICAR, but not rapamycin, leads to nuclear foci dispersion in HSA^{LR} muscle. To further understand the beneficial effect of AICAR and rapamycin in HSA^{LR} mice, we investigated whether the treatments improved muscle function by affecting the properties of the diseased muscle. First, we did not observe major changes in the histopathology of HSA^{LR} muscle upon 7-day AICAR or 10-day rapamycin treatment, compared with untreated conditions (Figure 8A). Notably, vacuoles remained present in muscle fibers from 12-month-old AICAR- or rapamycin-treated HSA^{LR} mice (Figure 8A), indicating that the treatments were not sufficient to reverse muscle alterations related to impaired autophagy in aging mice. As no myotonia was detected in the slow, soleus muscle of HSA^{LR} mice and as AICAR and rapamycin were previously shown to alter muscle fiber types (42, 43), we tested whether changes in muscle function upon treatments were related to modification of muscle metabolic and contractile capacities. By reduced nicotinamide adenine dinucleotide (NADH) staining, we first observed that the overall oxidative property of TA muscle was unchanged in AICAR- and rapamycin-treated mutant mice, compared with untreated animals (Figure 8B). Immunostaining against type I, IIA/X, and IIB myosin heavy chains (MHCs) was then conducted in TA muscle from HSA^{LR} and control mice to identify changes in muscle contractile properties upon treatment. Few type I fibers were present in all the muscles analyzed (data not shown). Mutant muscle displayed a switch to slower fibers (i.e., increased and reduced proportion of IIA and IIB fibers, respectively) compared with control muscle (Figure 8C). However, upon AICAR or rapamycin, there was no significant change in the proportion of the different fiber types in comparison with vehicle-treated mice (Figure 8C).

Since aggregation of (CUG)n-expanded RNA in nuclear foci is a histological hallmark in DM1 diseased muscle, we next wondered whether the treatments affected their accumulation in HSA^{LR} muscle. To this purpose, we performed FISH using a CAG_{10} DNA probe on TA muscle sections from mutant untreated and treated mice. Numerous foci were observed in HSA^{LR} muscle, while none were detected in control muscle (Figure 8D). Interestingly, the number of nuclei showing foci was significantly decreased in muscle from AICAR-treated mutant mice, while no change was observed with rapamycin (Figure 8D). Moreover, foci appeared more diffuse in positive nuclei from mutant muscle upon AICAR treatment, compared with untreated conditions (Figure 8D). Altogether, these results indicate that changes in muscle metabolic and contractile properties do not account for the beneficial effect of the short treatments applied to HSA^{LR} mice, while reduced muscle pathology upon AICAR-mediated acute AMPK activation likely involves nuclear foci dispersion in the mutant muscle.

Discussion

The pathogenic mechanisms underlying DM1 disease are still not well understood, and most investigations so far have focused on splicing defects caused by mRNA toxicity. In this study, we uncovered that in DM1, the AMPK and the mTORC1 pathways are deregulated and that the autophagic flux is perturbed in skeletal muscle. Most importantly, we established that AICAR and rapamycin, which interfere with AMPK/mTORC1 signaling, ameliorate DM1 muscle function (Figure 9).

AMPK signaling and PKB/Akt–mTORC1 signaling are central metabolic pathways in muscle cells, and their deregulation has been related to muscle alterations and disease (27, 32, 44).

We found that DM1 muscle shows an altered response to energy/nutrient-deprived conditions, with impaired AMPK activation and abnormal activation of mTORC1 signaling. Although we have not studied the upstream mechanisms involved in this deregulation, mis-splicing–dependent CaMKII deficiency could well account for the limited AMPK activation in DM1 muscle (21, 23–26). Interestingly, Jones et al. recently reported increased GSK3β levels and activity in HSA^{LR} muscle (45), which may also contribute to the perturbation of AMPK in DM1 muscle (46). In parallel, AMPK constitutes an upstream regulator of mTORC1 (47), and its deregulation could thus be responsible for abnormal mTORC1 activation in DM1 muscle cells. Nonetheless, as we did not detect changes in 4E-BP1 levels or mTOR phosphorylation in mutant muscle, evidence that the state of mTORC1 is modified in DM1 muscle and not only the activation of its downstream axis p70S6K/S6 is missing. Previous reports suggested that mTORC1 is inhibited in DM1 human neural and muscle cells (14, 17), although results were only obtained in vitro and the underlying mechanisms have not been investigated. On the basis of the abnormal splicing and protein trafficking of the insulin receptor in metabolic tissues in DM1 (15, 16), it has also been hypothesized that PKB/Akt–mTORC1 may be less responsive to insulin. However, results regarding the activation state of PKB/Akt signaling in DM1 human muscle biopsies or cells are conflicting (18, 19). In our experiments, we did not detect changes in PKB/Akt activation or in the expression of *Insr* in HSA^{LR} muscle, suggesting that AMPK/mTORC1 deregulation is independent of insulin receptor deficiency.

Autophagy as a major catabolic process essential for proteostasis has also been suggested to contribute to muscle alterations in DM1 (48). The involvement of autophagy in DM1 was largely deduced from the presence of autophagic vesicles and/or accumulation of autophagic markers in DM1 cells, but usually without dynamic measurement of the autophagic flux (13, 14, 17, 19, 36, 37, 49). In our study, we combined several methods to establish that mild changes in autophagic markers in muscle from HSA^{LR} mice are caused by autophagic flux limitation during the degradation steps. Further, we showed that even prolonged starvation did not fully induce autophagy in mutant muscle. We hypothesize that AMPK- and mTORC1-independent mechanisms contribute to autophagy perturbation, as rapamycin and metformin were not sufficient to normalize the flux in HSA^{LR} mice. Although this autophagy deregulation may contribute to muscle atrophy in DM1, it is unlikely to be the main pathogenic event, as autophagic features were scarce in DM1 muscle biopsies, compared with diseases primarily related to autophagy defects, such as vacuolar myopathies.

Importantly, we identified that AMPK/mTORC1 deregulation likely contributes to alteration of muscle function in DM1. Myotonia, which is due to membrane hyperexcitability, is thought to be caused primarily by mis-splicing and thereby deficiency in the CLC-1 (5, 7, 39, 41). In contrast to a recent report studying cultured human DM1 cells (38), we did not find any effect of metformin on the mis-splicing of DM1-affected genes or on the severe myotonia observed in HSA^{LR} mice. While we cannot rule out that changes in dosage and administration may lead to different results, much higher concentrations may be required to efficiently stimulate AMPK in rodent muscle tissue. Although metformin is commonly used to treat diabetes, clinical evaluation of its effect on muscle function in DM1 patients is lacking. In contrast to metformin, we found a profound effect of AICAR, a more potent AMPK agonist. AICAR led to a strong reduction of myotonia in HSA^{LR} mice, which correlated with improved splicing of the *Clcn1* gene and increased protein levels of the channel. While AMPK activation was related to repression of the RNA-binding protein *Rbm3* in vitro, *Rbm3* expression was unchanged in HSA^{LR} muscle upon AICAR treatment. As we observed dispersion of the nuclear foci formed by the (CUG)n-expanded RNA aggregation after AICAR treatment, the effect of AMPK activation on splicing may be mediated by its interaction with other RNA-binding proteins, such as hnRNP H, which were implicated in foci stability in DM1 (50, 51). Hence, one may argue that AMPK deregulation likely contributes to pathogenesis in DM1 muscle by perturbing RNA-binding proteins and thereby accentuating foci stability and mis-splicing events (52–54). Notably, we cannot rule out that amelioration of muscle relaxation also relies on splicing-independent mechanisms. In particular, changes in sodium- and calcium-activated potassium channels or in Ca^{2+} homeostasis, which have also been suggested to contribute to myotonia in DM1 (55–60), may mediate some of the observed effect. Consistently, AMPK has been shown to modulate chloride and potassium channels in several cell types, including cardiomyocytes (61, 62). Such mechanisms may also contribute to the beneficial effect of rapamycin, as it occurs in the absence of splicing changes. Rapamycin could influence intracellular calcium mobilization by dissociating FKBPs (FK506-binding protein) from RyR1, thereby modifying channel activity (63–65). Although AZD8055-dependent mTORC1 inhibition did not improve muscle relaxation, further investigations are required to rule out the involvement of mTORC1 signaling in myotonia reduction, given the complexity of the signaling.

While muscle weakness is observed in DM1 patients, it was initially not reported in HSA^{LR} mice (5). Consistently, in our study, total muscle force was not affected in mutant mice but we observed reduced specific strength of EDL muscle in HSA^{LR} mice. Both specific and total muscle forces were increased upon AICAR, rapamycin, and AZD8055 treatments in young mutant mice, which may be mediated by mTORC1 inhibition as the signaling was shown to modulate Ca^{2+} homeostasis and excitation-contraction coupling in skeletal muscle (66). Myotonia reduction and increase in muscle force were not caused by modified metabolic and contractile properties of the mutant muscle upon the applied short-term treatments. However, one can hypothesize that the changes expected upon long-term administration of these drugs (i.e., switch toward slower fibers) may further positively affect DM1 muscle function.

In conclusion, we identified that deregulation of AMPK/mTORC1 signaling, together with mild autophagy perturbation, contributes to DM1-associated muscle alterations. We showed that treatments targeting the AMPK/mTORC1 imbalance are beneficial for muscle function, though to varying degrees. Whether alternative AMPK/mTORC1–targeting compounds, as well as changes in the dosage, administration mode, or treatment duration, may further improve muscle function remains to be investigated. As the drugs used in our study can target the pathways body-wide, they may also be beneficial in other tissues and thus may represent new treatment options for DM1.

Methods

Mice. Homozygous mice of the mouse line LR20b carrying about 250 (CTG) repeats within the *HSA* transgene (HSA^{LR}) were obtained from Thornton and colleagues (University of Rochester Medical Center, Rochester, New York, USA) (5). Mice of the corresponding background strain (FVB/N) were used as control. GFP-LC3 HSA^{LR} and GFP-LC3 FVB/N mice were obtained by crossing of GFP-LC3–expressing mice (20) with HSA^{LR} or FVB/N mice. Mice were genotyped for HSA^{LR} transgenes by quantification of *ACTA1* levels normalized to endogenous actin (mouse *Acta1*) in genomic DNA. Mice were maintained in a conventional specific-pathogen–free facility with a fixed light cycle (23°C, 12-hour dark-light cycle). Mice were injected i.p. with colchicine (Sigma-Aldrich; 0.4 mg/kg) for 2 days, rapamycin (LC Laboratories) for 1 day (4 mg/kg) or 7 or 10 days (2 mg/kg), AICAR (Toronto Research Chemicals; 500 mg/kg) for 7 days, or AZD8055 (LC Laboratories; 10 mg/kg) for 10 days. Mice were treated with metformin (Sigma-Aldrich; 300 mg/kg) by gavage for 5 or 10 days. For starvation experiments, mice were sacrificed after 12 hours of food deprivation followed by 4 hours of free access to food (fed), or after 24 or 45 hours of food deprivation but free access to water (starved). In vitro force measurement of EDL and soleus muscles was conducted as previously described (32). Half- and late relaxation times were calculated according to Moyer et al. (8).

Human muscle cells and biopsy samples. Muscle biopsies frozen in nitrogen-cooled isopentane from 3 DM1 patients, aged 33, 34, and 49 years, and from an IBM patient were analyzed and compared with 5 control muscle samples from age-matched individuals showing no clinical signs of DM1 and normal muscle histology. MyoD-transduced fibroblasts from control individuals and patients were cultured in growth medium (DMEM, 10% FBS, 50 μg/ml gentamicin) at 37°C under 5% CO_2. At confluence, transduction into myoblasts was induced by differentiation medium (DMEM, 50 μg/ml gentamicin, 3 μg/ml doxycycline hyclate, 10 μg/ml human recombinant insulin) (67). Myotubes obtained after 10 days were incubated for 3 hours in growth medium (refed), PBS (starved), or PBS supplemented with chloroquine (100 μM).

Western blotting. Cell pellets and muscles powdered in liquid nitrogen were lysed in cold RIPA+ buffer (50 mM Tris-HCl pH 8, 150 mM NaCl, 1% NP-40, 0.5% sodium deoxycholate, 0.1% SDS, 1% Triton X, 10% glycerol, phosphatase and protease inhibitors). Following dosage (BCA Protein Assay, Sigma-Aldrich), proteins were separated on SDS-polyacrylamide gels and transferred to nitrocellulose membrane. Blots were blocked in TBS, 3% BSA, 0.1% Tween-20, and incubated overnight at 4°C with primary antibodies, then for 2 hours with HRP-labeled secondary antibodies. Immunoreactivity was detected using the ECL Western blot detection reagent LumiGLO (KPL) and exposed to Super RX-N films (Fujifilm). Protein expression was normalized to α-actinin, α-tubulin, or the total protein of the corresponding phosphorylated form. Antibodies used are listed in Supplemental Methods.

Polymerase chain reaction. Total RNAs were extracted with the RNeasy Mini Kit (Qiagen), reverse transcribed with the SuperScript III First-Strand Synthesis System (Invitrogen), and amplified with the Power SYBR Green Master Mix (Applied Biosystems) or the Hot Fire-Pol EvaGreen qPCR Mix (Solis BioDyne). Expression of specific spliced or pan transcripts was analyzed by end-point PCR and electrophoresis, or by quantitative PCR with Step One software and normalization to *Actn2* expression. Primers are listed in Supplemental Table 2.

Histology and immunofluorescence. Muscles were frozen in liquid nitrogen–cooled isopentane. Eight-micrometer muscle sections were stained with H&E or NADH, and observed with an upright microscope (DMR, Leica). For immunostaining, sections were unfixed or fixed with 4% paraformaldehyde (PFA), cold acetone, or methanol; for some, microwave antigen retrieval was used. Sections were then blocked in PBS, 3% BSA, incubated sequentially with primary and appropriate secondary fluorescent antibodies (Invitrogen), mounted with Vectashield medium (Vector), and observed with a Leica fluorescent microscope.

GFP-LC3 puncta analysis. For GFP-LC3 detection, mice were perfused with 4% PFA, and muscles were incubated in 30% sucrose overnight. Cryosections were washed and mounted. Images were recorded using a Leica confocal microscope with ×63 or ×100 objectives. The number of GFP-LC3 puncta was counted on the 3D reconstructed images with Imaris (version 8.1.2) software. Seven to twelve image stacks were quantified for each muscle, and the average number of GFP-LC3 puncta per volume unit defined within a single fiber ($20.8 \times 20.8 \times 6.5\ \mu m^3$) was used for statistical analyses. All GFP quantifications were done in a blinded way.

Fluorescence in situ hybridization. FISH was conducted on muscle cryosections as previously described by Batra et al. (68), using a Cy3-CAG_{10} DNA probe. Nuclear foci were observed with a Leica confocal microscope with ×40 and ×100 objectives.

Statistics. Quantitative data are displayed as mean ± SEM of independent samples, with n (number of individual experiments) ≥ 3. Statistical analysis of values was performed using Student's t test or 2-way ANOVA test with Tukey's multiple comparisons test correction, with a 0.05 level of confidence accepted for statistical significance.

Study approval. Muscle biopsies from DM1 patients were obtained from the Neuromuscular Tissue Bank (Department of Neurosciences, University of Padova, Padova, Italy) through the Telethon Network of Genetic Biobanks and the EuroBioBank, in accordance with European recommendation and Italian legislation on ethics. Control and IBM human muscle biopsies were from the Department of Pathology, University Hospital Basel (Basel, Switzerland); their use was approved by the Ethical Committee of the University Hospital Basel. Human fibroblast cell lines were obtained from the platform for immortalization of human cells at the Institut de Myologie (Paris, France). Fibroblasts derived from skin biopsies were obtained from the MyoBank-AFM bank of tissues for research at the Institut de Myologie, a partner in the European Union network EuroBioBank, in accordance with European recommendation and French legislation on ethics. All animal studies were performed in accordance with the European Union guidelines for animal care and approved by the Veterinary Office of the Canton of Basel city (application number 2601).

Author contributions

MB and PC performed most of the experiments, analyzed the data, and wrote the paper with input from all authors. NR, KC, TW, CE, and BE conducted quantitative PCR and Western blot analyses, GFP-LC3 quantification, muscle dissection, cryosections and inorganic staining, and electron microscopy analyses, respectively. SF and CA provided human muscle biopsies. DF developed and provided transduced fibroblasts from DM1 patients. MAR and MS helped conceive the project and edited the manuscript. MS secured funding. PC designed and directed the research project.

Acknowledgments

We thank C.A. Thornton for the generous gift of HSA^{LR} mice, and J. Hench and G. Schweighauser (Institute of Pathology, University of Basel, University Hospital Basel) for their help in preparing electron microscopy samples. We are grateful to S. Lin (Biozentrum, University of Basel) for his technical expertise on muscle force measurement and Imaris software, and to J. Kinter and L. Tintignac (Neuromuscular Research Group, University of Basel, University Hospital Basel) for their constructive comments on the project. We also thank the platform for immortalization of human cells from the Institut de Myologie (Paris, France) for providing human transduced fibroblasts. MHC antibodies, developed by H.M. Blau and S. Schiaffino, were obtained from the Developmental Studies Hybridoma Bank (University of Iowa, Iowa City, Iowa, USA). This work was supported by EuroBioBank and Telethon Network of Genetic Biobanks (grant GTB 12001D to CA), the University of Basel and University Hospital Basel (MS), the University of Basel–Stadt and Basel-Landschaft (MAR), the Neuromuscular Research Association Basel (MS, PC), the Swiss Foundation for Research on Muscle Diseases (MAR, MS), and the Swiss National Science Foundation (PC, MS).

Address correspondence to: Perrine Castets, Biozentrum, University of Basel, Klingelbergstrasse 50/70, CH-4056 Basel, Switzerland. Phone: 41.61.260.22.25; E-mail: perrine.castets@unibas.ch. Or to: Michael Sinnreich, Neuromuscular Research Group, Departments of Neurology and Biomedicine, University of Basel, University Hospital Basel, Klingelbergstrasse 50/70, CH-4056 Basel, Switzerland. Phone: 41.61.265.25.25; E-mail: michael.sinnreich@unibas.ch.

1. Machuca-Tzili L, Brook D, Hilton-Jones D. Clinical and molecular aspects of the myotonic dystrophies: a review. *Muscle Nerve*. 2005;32(1):1–18.
2. Brook JD, et al. Molecular basis of myotonic dystrophy: expansion of a trinucleotide (CTG) repeat at the 3′ end of a transcript encoding a protein kinase family member. *Cell*. 1992;69(2):385.
3. Mahadevan M, et al. Myotonic dystrophy mutation: an unstable CTG repeat in the 3′ untranslated region of the gene. *Science*. 1992;255(5049):1253–1255.
4. Lin X, et al. Failure of MBNL1-dependent post-natal splicing transitions in myotonic dystrophy. *Hum Mol Genet*. 2006;15(13):2087–2097.
5. Mankodi A, et al. Myotonic dystrophy in transgenic mice expressing an expanded CUG repeat. *Science*. 2000;289(5485):1769–1773.
6. Philips AV, Timchenko LT, Cooper TA. Disruption of splicing regulated by a CUG-binding protein in myotonic dystrophy. *Science*. 1998;280(5364):737–741.
7. Mankodi A, et al. Expanded CUG repeats trigger aberrant splicing of ClC-1 chloride channel pre-mRNA and hyperexcitability of skeletal muscle in myotonic dystrophy. *Mol Cell*. 2002;10(1):35–44.
8. Moyer M, Berger DS, Ladd AN, Van Lunteren E. Differential susceptibility of muscles to myotonia and force impairment in a mouse model of myotonic dystrophy. *Muscle Nerve*. 2011;43(6):818–827.
9. Herrendorff R, et al. Identification of plant-derived alkaloids with therapeutic potential for myotonic dystrophy type I. *J Biol Chem*. 2016;291(33):17165–17177.
10. Wheeler TM, et al. Reversal of RNA dominance by displacement of protein sequestered on triplet repeat RNA. *Science*. 2009;325(5938):336–339.
11. Sobczak K, Wheeler TM, Wang W, Thornton CA. RNA interference targeting CUG repeats in a mouse model of myotonic dystrophy. *Mol Ther*. 2013;21(2):380–387.
12. Vignaud A, et al. Progressive skeletal muscle weakness in transgenic mice expressing CTG expansions is associated with the activation of the ubiquitin-proteasome pathway. *Neuromuscul Disord*. 2010;20(5):319–325.
13. Bargiela A, Cerro-Herreros E, Fernandez-Costa JM, Vilchez JJ, Llamusi B, Artero R. Increased autophagy and apoptosis contribute to muscle atrophy in a myotonic dystrophy type 1 Drosophila model. *Dis Model Mech*. 2015;8(7):679–690.
14. Beffy P, et al. Altered signal transduction pathways and induction of autophagy in human myotonic dystrophy type 1 myoblasts. *Int J Biochem Cell Biol*. 2010;42(12):1973–1983.
15. Savkur RS, Philips AV, Cooper TA. Aberrant regulation of insulin receptor alternative splicing is associated with insulin resistance in myotonic dystrophy. *Nat Genet*. 2001;29(1):40–47.
16. Llagostera E, et al. Role of myotonic dystrophy protein kinase (DMPK) in glucose homeostasis and muscle insulin action. *PLoS One*. 2007;2(11):e1134.
17. Denis JA, et al. mTOR-dependent proliferation defect in human ES-derived neural stem cells affected by myotonic dystrophy type 1. *J Cell Sci*. 2013;126(pt 8):1763–1772.
18. Li X, Zhang W, Lv H, Wang ZX, Yuan Y. [Activities of Akt pathway and their correlation with pathological changes in myotonic dystrophy]. *Beijing Da Xue Xue Bao*. 2010;42(5):526–529.
19. Loro E, et al. Normal myogenesis and increased apoptosis in myotonic dystrophy type-1 muscle cells. *Cell Death Differ*. 2010;17(8):1315–1324.
20. Mizushima N, Yamamoto A, Matsui M, Yoshimori T, Ohsumi Y. In vivo analysis of autophagy in response to nutrient starvation using transgenic mice expressing a fluorescent autophagosome marker. *Mol Biol Cell*. 2004;15(3):1101–1111.
21. Suenaga K, et al. Muscleblind-like 1 knockout mice reveal novel splicing defects in the myotonic dystrophy brain. *PLoS One*. 2012;7(3):e33218.
22. Du H, et al. Aberrant alternative splicing and extracellular matrix gene expression in mouse models of myotonic dystrophy. *Nat Struct Mol Biol*. 2010;17(2):187–193.
23. Nakamori M, et al. Splicing biomarkers of disease severity in myotonic dystrophy. *Ann Neurol*. 2013;74(6):862–872.
24. Hart PC, et al. MnSOD upregulation sustains the Warburg effect via mitochondrial ROS and AMPK-dependent signalling in cancer. *Nat Commun*. 2015;6:6053.
25. Lee H, et al. NQO1-induced activation of AMPK contributes to cancer cell death by oxygen-glucose deprivation. *Sci Rep*. 2015;5:7769.
26. Raney MA, Turcotte LP. Evidence for the involvement of CaMKII and AMPK in Ca^{2+}-dependent signaling pathways regulating FA uptake and oxidation in contracting rodent muscle. *J Appl Physiol*. 2008;104(5):1366–1373.
27. Bentzinger CF, et al. Differential response of skeletal muscles to mTORC1 signaling during atrophy and hypertrophy. *Skelet Muscle*. 2013;3(1):6.
28. Bentzinger CF, et al. Skeletal muscle-specific ablation of raptor, but not of rictor, causes metabolic changes and results in muscle dystrophy. *Cell Metab*. 2008;8(5):411–424.
29. Kang SA, et al. mTORC1 phosphorylation sites encode their sensitivity to starvation and rapamycin. *Science*. 2013;341(6144):1236566.
30. Roux PP, et al. RAS/ERK signaling promotes site-specific ribosomal protein S6 phosphorylation via RSK and stimulates cap-dependent translation. *J Biol Chem*. 2007;282(19):14056–14064.
31. Kim J, Kundu M, Viollet B, Guan KL. AMPK and mTOR regulate autophagy through direct phosphorylation of Ulk1. *Nat Cell Biol*. 2011;13(2):132–141.
32. Castets P, et al. Sustained activation of mTORC1 in skeletal muscle inhibits constitutive and starvation-induced autophagy and causes a severe, late-onset myopathy. *Cell Metab*. 2013;17(5):731–744.
33. Masiero E, et al. Autophagy is required to maintain muscle mass. *Cell Metab*. 2009;10(6):507–515.
34. Klionsky DJ, et al. Guidelines for the use and interpretation of assays for monitoring autophagy. *Autophagy*. 2012;8(4):445–544.
35. Ueda H, et al. Decreased expression of myotonic dystrophy protein kinase and disorganization of sarcoplasmic reticulum in skeletal muscle of myotonic dystrophy. *J Neurol Sci*. 1999;162(1):38–50.
36. Swash M, Fox KP. Abnormal intrafusal muscle fibres in myotonic dystrophy: a study using serial sections. *J Neurol Neurosurg Psychiatr*. 1975;38(1):91–99.
37. Ludatscher RM, Kerner H, Amikam S, Gellei B. Myotonia dystrophica with heart involvement: an electron microscopic study of skeletal, cardiac, and smooth muscle. *J Clin Pathol*. 1978;31(11):1057–1064.
38. Laustriat D, et al. In vitro and in vivo modulation of alternative splicing by the biguanide metformin. *Mol Ther Nucleic Acids*. 2015;4:e262.

39. Wheeler TM, Lueck JD, Swanson MS, Dirksen RT, Thornton CA. Correction of ClC-1 splicing eliminates chloride channelopathy and myotonia in mouse models of myotonic dystrophy. *J Clin Invest*. 2007;117(12):3952–3957.
40. Lueck JD, et al. Chloride channelopathy in myotonic dystrophy resulting from loss of posttranscriptional regulation for CLCN1. *Am J Physiol Cell Physiol*. 2007;292(4):C1291–C1297.
41. Charlet-BN, Savkur RS, Singh G, Philips AV, Grice EA, Cooper TA. Loss of the muscle-specific chloride channel in type 1 myotonic dystrophy due to misregulated alternative splicing. *Mol Cell*. 2002;10(1):45–53.
42. Pauly M, et al. AMPK activation stimulates autophagy and ameliorates muscular dystrophy in the mdx mouse diaphragm. *Am J Pathol*. 2012;181(2):583–592.
43. Lee CS, et al. Ligands for FKBP12 increase Ca^{2+} influx and protein synthesis to improve skeletal muscle function. *J Biol Chem*. 2014;289(37):25556–25570.
44. Grumati P, et al. Autophagy is defective in collagen VI muscular dystrophies, and its reactivation rescues myofiber degeneration. *Nat Med*. 2010;16(11):1313–1320.
45. Jones K, et al. GSK3β mediates muscle pathology in myotonic dystrophy. *J Clin Invest*. 2012;122(12):4461–4472.
46. Suzuki T, et al. Inhibition of AMPK catabolic action by GSK3. *Mol Cell*. 2013;50(3):407–419.
47. Inoki K, Zhu T, Guan KL. TSC2 mediates cellular energy response to control cell growth and survival. *Cell*. 2003;115(5):577–590.
48. Castets P, Frank S, Sinnreich M, Rüegg MA. "Get the balance right": pathological significance of autophagy perturbation in neuromuscular disorders. *J Neuromuscul Dis*. 2016;3(2):127–155.
49. Dunne PW, Ma L, Casey DL, Harati Y, Epstein HF. Localization of myotonic dystrophy protein kinase in skeletal muscle and its alteration with disease. *Cell Motil Cytoskeleton*. 1996;33(1):52–63.
50. Kim N, et al. AMPKα2 translocates into the nucleus and interacts with hnRNP H: implications in metformin-mediated glucose uptake. *Cell Signal*. 2014;26(9):1800–1806.
51. Kim DH, Langlois MA, Lee KB, Riggs AD, Puymirat J, Rossi JJ. HnRNP H inhibits nuclear export of mRNA containing expanded CUG repeats and a distal branch point sequence. *Nucleic Acids Res*. 2005;33(12):3866–3874.
52. Zou T, et al. Polyamines modulate the subcellular localization of RNA-binding protein HuR through AMP-activated protein kinase-regulated phosphorylation and acetylation of importin alpha1. *Biochem J*. 2008;409(2):389–398.
53. Wang W, et al. AMP-activated kinase regulates cytoplasmic HuR. *Mol Cell Biol*. 2002;22(10):3425–3436.
54. Finley J. Alteration of splice site selection in the LMNA gene and inhibition of progerin production via AMPK activation. *Med Hypotheses*. 2014;83(5):580–587.
55. Santoro M, et al. Alternative splicing alterations of Ca^{2+} handling genes are associated with Ca^{2+} signal dysregulation in myotonic dystrophy type 1 (DM1) and type 2 (DM2) myotubes. *Neuropathol Appl Neurobiol*. 2014;40(4):464–476.
56. Vihola A, et al. Altered expression and splicing of Ca(2+) metabolism genes in myotonic dystrophies DM1 and DM2. *Neuropathol Appl Neurobiol*. 2013;39(4):390–405.
57. Kimura T, et al. Alternative splicing of RyR1 alters the efficacy of skeletal EC coupling. *Cell Calcium*. 2009;45(3):264–274.
58. Kimura T, et al. Altered mRNA splicing of the skeletal muscle ryanodine receptor and sarcoplasmic/endoplasmic reticulum Ca^{2+}-ATPase in myotonic dystrophy type 1. *Hum Mol Genet*. 2005;14(15):2189–2200.
59. Tang ZZ, et al. Muscle weakness in myotonic dystrophy associated with misregulated splicing and altered gating of Ca(V)1.1 calcium channel. *Hum Mol Genet*. 2012;21(6):1312–1324.
60. Franke C, Hatt H, Iaizzo PA, Lehmann-Horn F. Characteristics of Na^+ channels and Cl^- conductance in resealed muscle fibre segments from patients with myotonic dystrophy. *J Physiol (Lond)*. 1990;425:391–405.
61. Andersen MN, Rasmussen HB. AMPK: a regulator of ion channels. *Commun Integr Biol*. 2012;5(5):480–484.
62. Sukhodub A, et al. AMP-activated protein kinase mediates preconditioning in cardiomyocytes by regulating activity and trafficking of sarcolemmal ATP-sensitive K(+) channels. *J Cell Physiol*. 2007;210(1):224–236.
63. Kaftan E, Marks AR, Ehrlich BE. Effects of rapamycin on ryanodine receptor/Ca(2+)-release channels from cardiac muscle. *Circ Res*. 1996;78(6):990–997.
64. Avila G, Dirksen RT. Rapamycin and FK506 reduce skeletal muscle voltage sensor expression and function. *Cell Calcium*. 2005;38(1):35–44.
65. Brillantes AB, et al. Stabilization of calcium release channel (ryanodine receptor) function by FK506-binding protein. *Cell*. 1994;77(4):513–523.
66. Lopez RJ, et al. Raptor ablation in skeletal muscle decreases Cav1.1 expression and affects the function of the excitation-contraction coupling supramolecular complex. *Biochem J*. 2015;466(1):123–135.
67. Chaouch S, et al. Immortalized skin fibroblasts expressing conditional MyoD as a renewable and reliable source of converted human muscle cells to assess therapeutic strategies for muscular dystrophies: validation of an exon-skipping approach to restore dystrophin in Duchenne muscular dystrophy cells. *Hum Gene Ther*. 2009;20(7):784–790.
68. Batra R, et al. Loss of MBNL leads to disruption of developmentally regulated alternative polyadenylation in RNA-mediated disease. *Mol Cell*. 2014;56(2):311–322.

11 References

Ahmed, S. T., Craven, L., Russell, O. M., Turnbull, D. M. & Vincent, A. E. (2018) Diagnosis and Treatment of Mitochondrial Myopathies. *Neurotherapeutics*.

Allen, D. G., Gervasio, O. L., Yeung, E. W. & Whitehead, N. P. (2010) Calcium and the damage pathways in muscular dystrophy. *Can J Physiol Pharmacol*, 88(2), 83-91.

Allen, D. G., Lamb, G. D. & Westerblad, H. (2008) Skeletal muscle fatigue: cellular mechanisms. *Physiol Rev*, 88(1), 287-332.

Anderson, R. M. & Weindruch, R. (2010) Metabolic reprogramming, caloric restriction and aging. *Trends Endocrinol Metab*, 21(3), 134-41.

Anton, S. & Leeuwenburgh, C. (2013) Fasting or caloric restriction for healthy aging. *Exp Gerontol*, 48(10), 1003-5.

Apostolakos, J., Durant, T. J., Dwyer, C. R., Russell, R. P., Weinreb, J. H., Alaee, F., Beitzel, K., McCarthy, M. B., Cote, M. P. & Mazzocca, A. D. (2014) The enthesis: a review of the tendon-to-bone insertion. *Muscles Ligaments Tendons J*, 4(3), 333-42.

Arnold, A. S., Gill, J., Christe, M., Ruiz, R., McGuirk, S., St-Pierre, J., Tabares, L. & Handschin, C. (2014) Morphological and functional remodelling of the neuromuscular junction by skeletal muscle PGC-1alpha. *Nat Commun*, 5, 3569.

Asahi, M., Sugita, Y., Kurzydlowski, K., De Leon, S., Tada, M., Toyoshima, C. & MacLennan, D. H. (2003) Sarcolipin regulates sarco(endo)plasmic reticulum Ca2+-ATPase (SERCA) by binding to transmembrane helices alone or in association with phospholamban. *Proc Natl Acad Sci U S A*, 100(9), 5040-5.

Axelrod, C. L., Fealy, C. E., Mulya, A. & Kirwan, J. P. (2018) Exercise Training Remodels Human Skeletal Muscle Mitochondrial Fission and Fusion Machinery Towards a Pro-Elongation Phenotype. *Acta Physiol (Oxf)*, e13216.

Baar, E. L., Carbajal, K. A., Ong, I. M. & Lamming, D. W. (2016) Sex- and tissue-specific changes in mTOR signaling with age in C57BL/6J mice. *Aging Cell*, 15(1), 155-66.

Bagherniya, M., Butler, A. E., Barreto, G. E. & Sahebkar, A. (2018) The effect of fasting or calorie restriction on autophagy induction: A review of the literature. *Ageing Res Rev*, 47, 183-197.

Baldwin, K. M., Klinkerfuss, G. H., Terjung, R. L., Mole, P. A. & Holloszy, J. O. (1972) Respiratory capacity of white, red, and intermediate muscle: adaptative response to exercise. *Am J Physiol*, 222(2), 373-8.

Bancroft, J. D. & Cook, H. C. (1984) *Manual of histological techniques*. Edinburgh ; New York: Churchill Livingstone.

Bar-Peled, L. & Sabatini, D. M. (2014) Regulation of mTORC1 by amino acids. *Trends Cell Biol*, 24(7), 400-6.

Barany, M. (1967) ATPase activity of myosin correlated with speed of muscle shortening. *J Gen Physiol*, 50(6), Suppl:197-218.

Baumann, C. W., Kwak, D., Liu, H. M. & Thompson, L. V. (2016) Age-induced oxidative stress: how does it influence skeletal muscle quantity and quality? *J Appl Physiol (1985)*, 121(5), 1047-1052.

Bellinger, A. M., Reiken, S., Carlson, C., Mongillo, M., Liu, X., Rothman, L., Matecki, S., Lacampagne, A. & Marks, A. R. (2009) Hypernitrosylated ryanodine receptor calcium release channels are leaky in dystrophic muscle. *Nat Med*, 15(3), 325-30.

Bentzinger, C. F., Lin, S., Romanino, K., Castets, P., Guridi, M., Summermatter, S., Handschin, C., Tintignac, L. A., Hall, M. N. & Ruegg, M. A. (2013) Differential response of skeletal muscles to mTORC1 signaling during atrophy and hypertrophy. *Skelet Muscle*, 3(1), 6.

Bentzinger, C. F., Romanino, K., Cloetta, D., Lin, S., Mascarenhas, J. B., Oliveri, F., Xia, J., Casanova, E., Costa, C. F., Brink, M., Zorzato, F., Hall, M. N. & Ruegg, M. A. (2008) Skeletal muscle-specific ablation of raptor, but not of rictor, causes metabolic changes and results in muscle dystrophy. *Cell Metab*, 8(5), 411-24.

Berchtold, M. W., Brinkmeier, H. & Muntener, M. (2000) Calcium ion in skeletal muscle: its crucial role for muscle function, plasticity, and disease. *Physiol Rev*, 80(3), 1215-65.

Betts, J. G. D., P.; Johnson, E.; Johnson, J.E.; Korol, O.; Kruse, D.; Poe, B.; Wise, J.A.; Womble, M.; Young, K.A. (2018) *Anatomy and Physiology*, 2018. Available online: https://opentextbc.ca/anatomyandphysiology/chapter/10-2-skeletal-muscle/ [Accessed.

Bjorkoy, G., Lamark, T., Brech, A., Outzen, H., Perander, M., Overvatn, A., Stenmark, H. & Johansen, T. (2005) p62/SQSTM1 forms protein aggregates degraded by autophagy and has a protective effect on huntingtin-induced cell death. *J Cell Biol*, 171(4), 603-14.

Bjorkoy, G., Lamark, T., Pankiv, S., Overvatn, A., Brech, A. & Johansen, T. (2009) Monitoring autophagic degradation of p62/SQSTM1. *Methods Enzymol*, 452, 181-97.

Brancaccio, P., Lippi, G. & Maffulli, N. (2010) Biochemical markers of muscular damage. *Clin Chem Lab Med*, 48(6), 757-67.

Brittsan, A. G., Carr, A. N., Schmidt, A. G. & Kranias, E. G. (2000) Maximal inhibition of SERCA2 Ca(2+) affinity by phospholamban in transgenic hearts overexpressing a non-phosphorylatable form of phospholamban. *J Biol Chem*, 275(16), 12129-35.

Bruss, M. D., Khambatta, C. F., Ruby, M. A., Aggarwal, I. & Hellerstein, M. K. (2010) Calorie restriction increases fatty acid synthesis and whole body fat oxidation rates. *Am J Physiol Endocrinol Metab*, 298(1), E108-16.

Calabria, E., Ciciliot, S., Moretti, I., Garcia, M., Picard, A., Dyar, K. A., Pallafacchina, G., Tothova, J., Schiaffino, S. & Murgia, M. (2009) NFAT isoforms control activity-dependent muscle fiber type specification. *Proc Natl Acad Sci U S A*, 106(32), 13335-40.

Calderon, J. C., Bolanos, P. & Caputo, C. (2014) The excitation-contraction coupling mechanism in skeletal muscle. *Biophys Rev*, 6(1), 133-160.

Cao, S. X., Dhahbi, J. M., Mote, P. L. & Spindler, S. R. (2001) Genomic profiling of short- and long-term caloric restriction effects in the liver of aging mice. *Proc Natl Acad Sci U S A*, 98(19), 10630-5.

Carnio, S., LoVerso, F., Baraibar, M. A., Longa, E., Khan, M. M., Maffei, M., Reischl, M., Canepari, M., Loefler, S., Kern, H., Blaauw, B., Friguet, B., Bottinelli, R., Rudolf, R. & Sandri, M. (2014) Autophagy impairment in muscle induces neuromuscular junction degeneration and precocious aging. *Cell Rep*, 8(5), 1509-21.

Carreras-Sureda, A., Pihan, P. & Hetz, C. (2018) Calcium signaling at the endoplasmic reticulum: fine-tuning stress responses. *Cell Calcium*, 70, 24-31.

Castets, P., Lin, S., Rion, N., Di Fulvio, S., Romanino, K., Guridi, M., Frank, S., Tintignac, L. A., Sinnreich, M. & Ruegg, M. A. (2013) Sustained activation of mTORC1 in skeletal muscle inhibits constitutive and starvation-induced autophagy and causes a severe, late-onset myopathy. *Cell Metab*, 17(5), 731-44.

Chakkalakal, J. V., Stocksley, M. A., Harrison, M. A., Angus, L. M., Deschenes-Furry, J., St-Pierre, S., Megeney, L. A., Chin, E. R., Michel, R. N. & Jasmin, B. J. (2003) Expression of utrophin A mRNA correlates with the oxidative capacity of skeletal muscle fiber types and is regulated by calcineurin/NFAT signaling. *Proc Natl Acad Sci U S A*, 100(13), 7791-6.

Chandrasekar, B., Nelson, J. F., Colston, J. T. & Freeman, G. L. (2001) Calorie restriction attenuates inflammatory responses to myocardial ischemia-reperfusion injury. *Am J Physiol Heart Circ Physiol*, 280(5), H2094-102.

Chantranupong, L., Scaria, S. M., Saxton, R. A., Gygi, M. P., Shen, K., Wyant, G. A., Wang, T., Harper, J. W., Gygi, S. P. & Sabatini, D. M. (2016) The CASTOR Proteins Are Arginine Sensors for the mTORC1 Pathway. *Cell*, 165(1), 153-164.

Chen, H., Detmer, S. A., Ewald, A. J., Griffin, E. E., Fraser, S. E. & Chan, D. C. (2003) Mitofusins Mfn1 and Mfn2 coordinately regulate mitochondrial fusion and are essential for embryonic development. *J Cell Biol*, 160(2), 189-200.

Cheng, S. W., Fryer, L. G., Carling, D. & Shepherd, P. R. (2004) Thr2446 is a novel mammalian target of rapamycin (mTOR) phosphorylation site regulated by nutrient status. *J Biol Chem*, 279(16), 15719-22.

Chin, E. R., Olson, E. N., Richardson, J. A., Yang, Q., Humphries, C., Shelton, J. M., Wu, H., Zhu, W., Bassel-Duby, R. & Williams, R. S. (1998) A calcineurin-dependent transcriptional pathway controls skeletal muscle fiber type. *Genes Dev*, 12(16), 2499-509.

Chuvpilo, S., Avots, A., Berberich-Siebelt, F., Glockner, J., Fischer, C., Kerstan, A., Escher, C., Inashkina, I., Hlubek, F., Jankevics, E., Brabletz, T. & Serfling, E. (1999) Multiple NF-ATc isoforms with individual transcriptional properties are synthesized in T lymphocytes. *J Immunol*, 162(12), 7294-301.

Cipolat, S., Martins de Brito, O., Dal Zilio, B. & Scorrano, L. (2004) OPA1 requires mitofusin 1 to promote mitochondrial fusion. *Proc Natl Acad Sci U S A*, 101(45), 15927-32.

Colman, R. J., Anderson, R. M., Johnson, S. C., Kastman, E. K., Kosmatka, K. J., Beasley, T. M., Allison, D. B., Cruzen, C., Simmons, H. A., Kemnitz, J. W. & Weindruch, R. (2009) Caloric restriction delays disease onset and mortality in rhesus monkeys. *Science*, 325(5937), 201-4.

Colman, R. J., Beasley, T. M., Kemnitz, J. W., Johnson, S. C., Weindruch, R. & Anderson, R. M. (2014) Caloric restriction reduces age-related and all-cause mortality in rhesus monkeys. *Nat Commun*, 5, 3557.

Davis, L. M., Pauly, J. R., Readnower, R. D., Rho, J. M. & Sullivan, P. G. (2008) Fasting is neuroprotective following traumatic brain injury. *J Neurosci Res*, 86(8), 1812-22.

De Andrade, P. B., Neff, L. A., Strosova, M. K., Arsenijevic, D., Patthey-Vuadens, O., Scapozza, L., Montani, J. P., Ruegg, U. T., Dulloo, A. G. & Dorchies, O. M. (2015) Caloric restriction induces energy-sparing alterations in skeletal muscle contraction, fiber composition and local thyroid hormone metabolism that persist during catch-up fat upon refeeding. *Front Physiol*, 6, 254.

DiMauro, S. (2004) Mitochondrial diseases. *Biochim Biophys Acta*, 1658(1-2), 80-8.

Dowling, P., Doran, P. & Ohlendieck, K. (2004) Drastic reduction of sarcalumenin in Dp427 (dystrophin of 427 kDa)-deficient fibres indicates that abnormal calcium handling plays a key role in muscular dystrophy. *Biochem J*, 379(Pt 2), 479-88.

Dutchak, P. A., Estill-Terpack, S. J., Plec, A. A., Zhao, X., Yang, C., Chen, J., Ko, B., Deberardinis, R. J., Yu, Y. & Tu, B. P. (2018) Loss of a Negative Regulator of mTORC1 Induces Aerobic Glycolysis and Altered Fiber Composition in Skeletal Muscle. *Cell Rep*, 23(7), 1907-1914.

Duvel, K., Yecies, J. L., Menon, S., Raman, P., Lipovsky, A. I., Souza, A. L., Triantafellow, E., Ma, Q., Gorski, R., Cleaver, S., Vander Heiden, M. G., MacKeigan, J. P., Finan, P. M., Clish, C. B., Murphy, L. O. & Manning, B. D. (2010) Activation of a metabolic gene regulatory network downstream of mTOR complex 1. *Mol Cell*, 39(2), 171-83.

Egan, B., Hawley, J. A. & Zierath, J. R. (2016) SnapShot: Exercise Metabolism. *Cell Metab*, 24(2), 342-342 e1.

El-Hattab, A. W., Suleiman, J., Almannai, M. & Scaglia, F. (2018) Mitochondrial dynamics: Biological roles, molecular machinery, and related diseases. *Mol Genet Metab*, 125(4), 315-321.

Friday, B. B., Mitchell, P. O., Kegley, K. M. & Pavlath, G. K. (2003) Calcineurin initiates skeletal muscle differentiation by activating MEF2 and MyoD. *Differentiation*, 71(3), 217-27.

Frontera, W. R. & Ochala, J. (2015) Skeletal muscle: a brief review of structure and function. *Calcif Tissue Int*, 96(3), 183-95.

Gaburjakova, M., Gaburjakova, J., Reiken, S., Huang, F., Marx, S. O., Rosemblit, N. & Marks, A. R. (2001) FKBP12 binding modulates ryanodine receptor channel gating. *J Biol Chem*, 276(20), 16931-5.

Ganley, I. G., Lam du, H., Wang, J., Ding, X., Chen, S. & Jiang, X. (2009) ULK1.ATG13.FIP200 complex mediates mTOR signaling and is essential for autophagy. *J Biol Chem*, 284(18), 12297-305.

Garcia-Martinez, J. M. & Alessi, D. R. (2008) mTOR complex 2 (mTORC2) controls hydrophobic motif phosphorylation and activation of serum- and glucocorticoid-induced protein kinase 1 (SGK1). *Biochem J*, 416(3), 375-85.

Gill, J. F., Santos, G., Schnyder, S. & Handschin, C. (2018) PGC-1alpha affects aging-related changes in muscle and motor function by modulating specific exercise-mediated changes in old mice. *Aging Cell*, 17(1).

Gingras, A. C., Raught, B. & Sonenberg, N. (1999) eIF4 initiation factors: effectors of mRNA recruitment to ribosomes and regulators of translation. *Annu Rev Biochem*, 68, 913-63.

Gittings, W., Huang, J., Smith, I. C., Quadrilatero, J. & Vandenboom, R. (2011) The effect of skeletal myosin light chain kinase gene ablation on the fatigability of mouse fast muscle. *J Muscle Res Cell Motil*, 31(5-6), 337-48.

Goberdhan, D. C., Wilson, C. & Harris, A. L. (2016) Amino Acid Sensing by mTORC1: Intracellular Transporters Mark the Spot. *Cell Metab*, 23(4), 580-9.

Golbidi, S., Daiber, A., Korac, B., Li, H., Essop, M. F. & Laher, I. (2017) Health Benefits of Fasting and Caloric Restriction. *Curr Diab Rep*, 17(12), 123.

Goodman, C. A. (2014) The role of mTORC1 in regulating protein synthesis and skeletal muscle mass in response to various mechanical stimuli. *Rev Physiol Biochem Pharmacol*, 166, 43-95.

Gorman, G. S., Chinnery, P. F., DiMauro, S., Hirano, M., Koga, Y., McFarland, R., Suomalainen, A., Thorburn, D. R., Zeviani, M. & Turnbull, D. M. (2016) Mitochondrial diseases. *Nat Rev Dis Primers*, 2, 16080.

Gumerson, J. D., Kabaeva, Z. T., Davis, C. S., Faulkner, J. A. & Michele, D. E. (2010) Soleus muscle in glycosylation-deficient muscular dystrophy is protected from contraction-induced injury. *Am J Physiol Cell Physiol*, 299(6), C1430-40.

Guo, W., Jiang, L., Bhasin, S., Khan, S. M. & Swerdlow, R. H. (2009) DNA extraction procedures meaningfully influence qPCR-based mtDNA copy number determination. *Mitochondrion*, 9(4), 261-5.

Guridi, M., Kupr, B., Romanino, K., Lin, S., Falcetta, D., Tintignac, L. & Ruegg, M. A. (2016) Alterations to mTORC1 signaling in the skeletal muscle differentially affect whole-body metabolism. *Skelet Muscle*, 6, 13.

Guridi, M., Tintignac, L. A., Lin, S., Kupr, B., Castets, P. & Ruegg, M. A. (2015) Activation of mTORC1 in skeletal muscle regulates whole-body metabolism through FGF21. *Sci Signal*, 8(402), ra113.

Gustavsson, M., Verardi, R., Mullen, D. G., Mote, K. R., Traaseth, N. J., Gopinath, T. & Veglia, G. (2013) Allosteric regulation of SERCA by phosphorylation-mediated conformational shift of phospholamban. *Proc Natl Acad Sci U S A*, 110(43), 17338-43.

Gwinn, D. M., Shackelford, D. B., Egan, D. F., Mihaylova, M. M., Mery, A., Vasquez, D. S., Turk, B. E. & Shaw, R. J. (2008) AMPK phosphorylation of raptor mediates a metabolic checkpoint. *Mol Cell*, 30(2), 214-26.

Hara, T., Takamura, A., Kishi, C., Iemura, S., Natsume, T., Guan, J. L. & Mizushima, N. (2008) FIP200, a ULK-interacting protein, is required for autophagosome formation in mammalian cells. *J Cell Biol*, 181(3), 497-510.

Harputlugil, E., Hine, C., Vargas, D., Robertson, L., Manning, B. D. & Mitchell, J. R. (2014) The TSC complex is required for the benefits of dietary protein restriction on stress resistance in vivo. *Cell Rep*, 8(4), 1160-70.

Hempenstall, S., Page, M. M., Wallen, K. R. & Selman, C. (2012) Dietary restriction increases skeletal muscle mitochondrial respiration but not mitochondrial content in C57BL/6 mice. *Mech Ageing Dev*, 133(1), 37-45.

Henriksson, J. (1990) The possible role of skeletal muscle in the adaptation to periods of energy deficiency. *Eur J Clin Nutr*, 44 Suppl 1, 55-64.

Higami, Y., Pugh, T. D., Page, G. P., Allison, D. B., Prolla, T. A. & Weindruch, R. (2004) Adipose tissue energy metabolism: altered gene expression profile of mice subjected to long-term caloric restriction. *FASEB J*, 18(2), 415-7.

Hogan, P. G., Chen, L., Nardone, J. & Rao, A. (2003) Transcriptional regulation by calcium, calcineurin, and NFAT. *Genes Dev*, 17(18), 2205-32.

Holloszy, J. O. (1967) Biochemical adaptations in muscle. Effects of exercise on mitochondrial oxygen uptake and respiratory enzyme activity in skeletal muscle. *J Biol Chem*, 242(9), 2278-82.

Holz, M. K., Ballif, B. A., Gygi, S. P. & Blenis, J. (2005) mTOR and S6K1 mediate assembly of the translation preinitiation complex through dynamic protein interchange and ordered phosphorylation events. *Cell*, 123(4), 569-80.

Hood, D. A., Memme, J. M., Oliveira, A. N. & Triolo, M. (2018) Maintenance of Skeletal Muscle Mitochondria in Health, Exercise, and Aging. *Annu Rev Physiol*.

Hosokawa, N., Sasaki, T., Iemura, S., Natsume, T., Hara, T. & Mizushima, N. (2009) Atg101, a novel mammalian autophagy protein interacting with Atg13. *Autophagy*, 5(7), 973-9.
Houstek, J., Pickova, A., Vojtiskova, A., Mracek, T., Pecina, P. & Jesina, P. (2006) Mitochondrial diseases and genetic defects of ATP synthase. *Biochim Biophys Acta*, 1757(9-10), 1400-5.
Howard, C., Ferrucci, L., Sun, K., Fried, L. P., Walston, J., Varadhan, R., Guralnik, J. M. & Semba, R. D. (2007) Oxidative protein damage is associated with poor grip strength among older women living in the community. *J Appl Physiol (1985)*, 103(1), 17-20.
Inoki, K., Li, Y., Xu, T. & Guan, K. L. (2003) Rheb GTPase is a direct target of TSC2 GAP activity and regulates mTOR signaling. *Genes Dev*, 17(15), 1829-34.
Inoki, K., Li, Y., Zhu, T., Wu, J. & Guan, K. L. (2002) TSC2 is phosphorylated and inhibited by Akt and suppresses mTOR signalling. *Nat Cell Biol*, 4(9), 648-57.
Iqbal, S. & Hood, D. A. (2015) The role of mitochondrial fusion and fission in skeletal muscle function and dysfunction. *Front Biosci (Landmark Ed)*, 20, 157-72.
Ito, N., Ruegg, U. T. & Takeda, S. (2018) ATP-Induced Increase in Intracellular Calcium Levels and Subsequent Activation of mTOR as Regulators of Skeletal Muscle Hypertrophy. *Int J Mol Sci*, 19(9).
Jacinto, E., Loewith, R., Schmidt, A., Lin, S., Ruegg, M. A., Hall, A. & Hall, M. N. (2004) Mammalian TOR complex 2 controls the actin cytoskeleton and is rapamycin insensitive. *Nat Cell Biol*, 6(11), 1122-8.
Jain, A., Lamark, T., Sjottem, E., Larsen, K. B., Awuh, J. A., Overvatn, A., McMahon, M., Hayes, J. D. & Johansen, T. (2010) p62/SQSTM1 is a target gene for transcription factor NRF2 and creates a positive feedback loop by inducing antioxidant response element-driven gene transcription. *J Biol Chem*, 285(29), 22576-91.
Jewell, J. L., Kim, Y. C., Russell, R. C., Yu, F. X., Park, H. W., Plouffe, S. W., Tagliabracci, V. S. & Guan, K. L. (2015) Metabolism. Differential regulation of mTORC1 by leucine and glutamine. *Science*, 347(6218), 194-8.
Johnson, S. C., Rabinovitch, P. S. & Kaeberlein, M. (2013) mTOR is a key modulator of ageing and age-related disease. *Nature*, 493(7432), 338-45.
Jongpiputvanich, S., Sueblinvong, T. & Norapucsunton, T. (2005) Mitochondrial respiratory chain dysfunction in various neuromuscular diseases. *J Clin Neurosci*, 12(4), 426-8.
Jung, C. H., Ro, S. H., Cao, J., Otto, N. M. & Kim, D. H. (2010) mTOR regulation of autophagy. *FEBS Lett*, 584(7), 1287-95.
Jung, J., Genau, H. M. & Behrends, C. (2015) Amino Acid-Dependent mTORC1 Regulation by the Lysosomal Membrane Protein SLC38A9. *Mol Cell Biol*, 35(14), 2479-94.
Kafami, L., Raza, M., Razavi, A., Mirshafiey, A., Movahedian, M. & Khorramizadeh, M. R. (2010) Intermittent feeding attenuates clinical course of experimental autoimmune encephalomyelitis in C57BL/6 mice. *Avicenna J Med Biotechnol*, 2(1), 47-52.
Kalaany, N. Y. & Sabatini, D. M. (2009) Tumours with PI3K activation are resistant to dietary restriction. *Nature*, 458(7239), 725-31.
Kapahi, P., Zid, B. M., Harper, T., Koslover, D., Sapin, V. & Benzer, S. (2004) Regulation of lifespan in Drosophila by modulation of genes in the TOR signaling pathway. *Curr Biol*, 14(10), 885-90.
Kemnitz, J. W., Roecker, E. B., Weindruch, R., Elson, D. F., Baum, S. T. & Bergman, R. N. (1994) Dietary restriction increases insulin sensitivity and lowers blood glucose in rhesus monkeys. *Am J Physiol*, 266(4 Pt 1), E540-7.
Khan, N. A., Nikkanen, J., Yatsuga, S., Jackson, C., Wang, L., Pradhan, S., Kivela, R., Pessia, A., Velagapudi, V. & Suomalainen, A. (2017) mTORC1 Regulates Mitochondrial Integrated Stress Response and Mitochondrial Myopathy Progression. *Cell Metab*, 26(2), 419-428 e5.
Kim, S. G., Buel, G. R. & Blenis, J. (2013) Nutrient regulation of the mTOR complex 1 signaling pathway. *Mol Cells*, 35(6), 463-73.
Kohler, L., Puertollano, R. & Raben, N. (2018) Pompe Disease: From Basic Science to Therapy. *Neurotherapeutics*, 15(4), 928-942.
Komulainen, T., Hautakangas, M. R., Hinttala, R., Pakanen, S., Vahasarja, V., Lehenkari, P., Olsen, P., Vieira, P., Saarenpaa-Heikkila, O., Palmio, J., Tuominen, H., Kinnunen, P.,

Majamaa, K., Rantala, H. & Uusimaa, J. (2015) Mitochondrial DNA Depletion and Deletions in Paediatric Patients with Neuromuscular Diseases: Novel Phenotypes. *JIMD Rep*, 23, 91-100.

Kuo, I. Y. & Ehrlich, B. E. (2015) Signaling in muscle contraction. *Cold Spring Harb Perspect Biol*, 7(2), a006023.

Kwak, H. B. (2013) Exercise and obesity-induced insulin resistance in skeletal muscle. *Integr Med Res*, 2(4), 131-138.

Laganiere, S. & Yu, B. P. (1989) Effect of chronic food restriction in aging rats. II. Liver cytosolic antioxidants and related enzymes. *Mech Ageing Dev*, 48(3), 221-30.

Laplante, M. & Sabatini, D. M. (2009) mTOR signaling at a glance. *J Cell Sci*, 122(Pt 20), 3589-94.

Laplante, M. & Sabatini, D. M. (2012a) mTOR Signaling. *Cold Spring Harb Perspect Biol*, 4(2).

Laplante, M. & Sabatini, D. M. (2012b) mTOR signaling in growth control and disease. *Cell*, 149(2), 274-93.

Le Bourg, E. (2009) Hormesis, aging and longevity. *Biochim Biophys Acta*, 1790(10), 1030-9.

Leonard, J. V. & Schapira, A. H. (2000a) Mitochondrial respiratory chain disorders I: mitochondrial DNA defects. *Lancet*, 355(9200), 299-304.

Leonard, J. V. & Schapira, A. H. (2000b) Mitochondrial respiratory chain disorders II: neurodegenerative disorders and nuclear gene defects. *Lancet*, 355(9201), 389-94.

Lin, J., Wu, H., Tarr, P. T., Zhang, C. Y., Wu, Z., Boss, O., Michael, L. F., Puigserver, P., Isotani, E., Olson, E. N., Lowell, B. B., Bassel-Duby, R. & Spiegelman, B. M. (2002) Transcriptional co-activator PGC-1 alpha drives the formation of slow-twitch muscle fibres. *Nature*, 418(6899), 797-801.

Long, Y. C., Glund, S., Garcia-Roves, P. M. & Zierath, J. R. (2007) Calcineurin regulates skeletal muscle metabolism via coordinated changes in gene expression. *J Biol Chem*, 282(3), 1607-14.

Lopez, R. J., Mosca, B., Treves, S., Maj, M., Bergamelli, L., Calderon, J. C., Bentzinger, C. F., Romanino, K., Hall, M. N., Ruegg, M. A., Delbono, O., Caputo, C. & Zorzato, F. (2015) Raptor ablation in skeletal muscle decreases Cav1.1 expression and affects the function of the excitation-contraction coupling supramolecular complex. *Biochem J*, 466(1), 123-35.

Lowey, S., Waller, G. S. & Trybus, K. M. (1993) Skeletal muscle myosin light chains are essential for physiological speeds of shortening. *Nature*, 365(6445), 454-6.

Luo, C., Burgeon, E., Carew, J. A., McCaffrey, P. G., Badalian, T. M., Lane, W. S., Hogan, P. G. & Rao, A. (1996) Recombinant NFAT1 (NFATp) is regulated by calcineurin in T cells and mediates transcription of several cytokine genes. *Mol Cell Biol*, 16(7), 3955-66.

Macian, F. (2005) NFAT proteins: key regulators of T-cell development and function. *Nat Rev Immunol*, 5(6), 472-84.

Makino, N., Oyama, J., Maeda, T., Koyanagi, M., Higuchi, Y. & Tsuchida, K. (2015) Calorie restriction increases telomerase activity, enhances autophagy, and improves diastolic dysfunction in diabetic rat hearts. *Mol Cell Biochem*, 403(1-2), 1-11.

Manning, B. D., Tee, A. R., Logsdon, M. N., Blenis, J. & Cantley, L. C. (2002) Identification of the tuberous sclerosis complex-2 tumor suppressor gene product tuberin as a target of the phosphoinositide 3-kinase/akt pathway. *Mol Cell*, 10(1), 151-62.

Marques, F. Z., Markus, M. A. & Morris, B. J. (2009) Hormesis as a pro-healthy aging intervention in human beings? *Dose Response*, 8(1), 28-33.

Martin, C. K., Bhapkar, M., Pittas, A. G., Pieper, C. F., Das, S. K., Williamson, D. A., Scott, T., Redman, L. M., Stein, R., Gilhooly, C. H., Stewart, T., Robinson, L., Roberts, S. B. & Comprehensive Assessment of Long-term Effects of Reducing Intake of Energy Phase 2 Study, G. (2016) Effect of Calorie Restriction on Mood, Quality of Life, Sleep, and Sexual Function in Healthy Nonobese Adults: The CALERIE 2 Randomized Clinical Trial. *JAMA Intern Med*, 176(6), 743-52.

Martinez-Lopez, N., Tarabra, E., Toledo, M., Garcia-Macia, M., Sahu, S., Coletto, L., Batista-Gonzalez, A., Barzilai, N., Pessin, J. E., Schwartz, G. J., Kersten, S. & Singh, R. (2017)

System-wide Benefits of Intermeal Fasting by Autophagy. *Cell Metab*, 26(6), 856-871 e5.
Martinuzzi, A., Schievano, G., Nascimbeni, A. & Fanin, M. (1999) McArdle's disease. The unsolved mystery of the reappearing enzyme. *Am J Pathol*, 154(6), 1893-7.
Masoro, E. J. (1998) Hormesis and the antiaging action of dietary restriction. *Exp Gerontol*, 33(1-2), 61-6.
Mattison, J. A., Colman, R. J., Beasley, T. M., Allison, D. B., Kemnitz, J. W., Roth, G. S., Ingram, D. K., Weindruch, R., de Cabo, R. & Anderson, R. M. (2017) Caloric restriction improves health and survival of rhesus monkeys. *Nat Commun*, 8, 14063.
McCay, C. M. C., Mary F. (1935) Prolonging the Life Span. *The Scientific Monthly*, Volume 39(Issue 5), pp. 405-414.
McCullagh, K. J., Calabria, E., Pallafacchina, G., Ciciliot, S., Serrano, A. L., Argentini, C., Kalhovde, J. M., Lomo, T. & Schiaffino, S. (2004) NFAT is a nerve activity sensor in skeletal muscle and controls activity-dependent myosin switching. *Proc Natl Acad Sci U S A*, 101(29), 10590-5.
Meissner, J. D., Freund, R., Krone, D., Umeda, P. K., Chang, K. C., Gros, G. & Scheibe, R. J. (2011) Extracellular signal-regulated kinase 1/2-mediated phosphorylation of p300 enhances myosin heavy chain I/beta gene expression via acetylation of nuclear factor of activated T cells c1. *Nucleic Acids Res*, 39(14), 5907-25.
Menazza, S., Blaauw, B., Tiepolo, T., Toniolo, L., Braghetta, P., Spolaore, B., Reggiani, C., Di Lisa, F., Bonaldo, P. & Canton, M. (2010) Oxidative stress by monoamine oxidases is causally involved in myofiber damage in muscular dystrophy. *Hum Mol Genet*, 19(21), 4207-15.
Meng, S. J. & Yu, L. J. (2010) Oxidative stress, molecular inflammation and sarcopenia. *Int J Mol Sci*, 11(4), 1509-26.
Merrell, A. J. & Kardon, G. (2013) Development of the diaphragm -- a skeletal muscle essential for mammalian respiration. *FEBS J*, 280(17), 4026-35.
Miragoli, M., Sanchez-Alonso, J. L., Bhargava, A., Wright, P. T., Sikkel, M., Schobesberger, S., Diakonov, I., Novak, P., Castaldi, A., Cattaneo, P., Lyon, A. R., Lab, M. J. & Gorelik, J. (2016) Microtubule-Dependent Mitochondria Alignment Regulates Calcium Release in Response to Nanomechanical Stimulus in Heart Myocytes. *Cell Rep*, 14(1), 140-151.
Mitch, W. E. & Goldberg, A. L. (1996) Mechanisms of muscle wasting. The role of the ubiquitin-proteasome pathway. *N Engl J Med*, 335(25), 1897-905.
Mitchell, S. E., Tang, Z., Kerbois, C., Delville, C., Konstantopedos, P., Bruel, A., Derous, D., Green, C., Aspden, R. M., Goodyear, S. R., Chen, L., Han, J. J., Wang, Y., Promislow, D. E., Lusseau, D., Douglas, A. & Speakman, J. R. (2015) The effects of graded levels of calorie restriction: I. impact of short term calorie and protein restriction on body composition in the C57BL/6 mouse. *Oncotarget*, 6(18), 15902-30.
Mizushima, N., Yoshimori, T. & Ohsumi, Y. (2011) The role of Atg proteins in autophagosome formation. *Annu Rev Cell Dev Biol*, 27, 107-32.
Morita, M., Gravel, S. P., Chenard, V., Sikstrom, K., Zheng, L., Alain, T., Gandin, V., Avizonis, D., Arguello, M., Zakaria, C., McLaughlan, S., Nouet, Y., Pause, A., Pollak, M., Gottlieb, E., Larsson, O., St-Pierre, J., Topisirovic, I. & Sonenberg, N. (2013) mTORC1 controls mitochondrial activity and biogenesis through 4E-BP-dependent translational regulation. *Cell Metab*, 18(5), 698-711.
Murphy, M. P. (2009) How mitochondria produce reactive oxygen species. *Biochem J*, 417(1), 1-13.
Odermatt, A., Taschner, P. E., Khanna, V. K., Busch, H. F., Karpati, G., Jablecki, C. K., Breuning, M. H. & MacLennan, D. H. (1996) Mutations in the gene-encoding SERCA1, the fast-twitch skeletal muscle sarcoplasmic reticulum Ca2+ ATPase, are associated with Brody disease. *Nat Genet*, 14(2), 191-4.
Oh, W. J. & Jacinto, E. (2011) mTOR complex 2 signaling and functions. *Cell Cycle*, 10(14), 2305-16.
Omodei, D., Licastro, D., Salvatore, F., Crosby, S. D. & Fontana, L. (2013) Serum from humans on long-term calorie restriction enhances stress resistance in cell culture. *Aging (Albany NY)*, 5(8), 599-606.

Pant, I., Chaturvedi, S., Bala, K. & Kushwaha, S. (2015a) Muscle histopathology in today's era of molecular genetics: Role and limitations. *Ann Indian Acad Neurol*, 18(4), 398-402.

Pant, M., Sopariwala, D. H., Bal, N. C., Lowe, J., Delfin, D. A., Rafael-Fortney, J. & Periasamy, M. (2015b) Metabolic dysfunction and altered mitochondrial dynamics in the utrophin-dystrophin deficient mouse model of duchenne muscular dystrophy. *PLoS One*, 10(4), e0123875.

Parsons, S. A., Wilkins, B. J., Bueno, O. F. & Molkentin, J. D. (2003) Altered skeletal muscle phenotypes in calcineurin Aalpha and Abeta gene-targeted mice. *Mol Cell Biol*, 23(12), 4331-43.

Patel, J. R., Diffee, G. M., Huang, X. P. & Moss, R. L. (1998) Phosphorylation of myosin regulatory light chain eliminates force-dependent changes in relaxation rates in skeletal muscle. *Biophys J*, 74(1), 360-8.

Peng, T., Golub, T. R. & Sabatini, D. M. (2002) The immunosuppressant rapamycin mimics a starvation-like signal distinct from amino acid and glucose deprivation. *Mol Cell Biol*, 22(15), 5575-84.

Periasamy, M., Herrera, J. L. & Reis, F. C. G. (2017) Skeletal Muscle Thermogenesis and Its Role in Whole Body Energy Metabolism. *Diabetes Metab J*, 41(5), 327-336.

Perrie, W. T., Smillie, L. B. & Perry, S. B. (1973) A phosphorylated light-chain component of myosin from skeletal muscle. *Biochem J*, 135(1), 151-64.

Pertille, A., de Carvalho, C. L., Matsumura, C. Y., Neto, H. S. & Marques, M. J. (2010) Calcium-binding proteins in skeletal muscles of the mdx mice: potential role in the pathogenesis of Duchenne muscular dystrophy. *Int J Exp Pathol*, 91(1), 63-71.

Petejova, N. & Martinek, A. (2014) Acute kidney injury due to rhabdomyolysis and renal replacement therapy: a critical review. *Crit Care*, 18(3), 224.

Peterson, T. R., Laplante, M., Thoreen, C. C., Sancak, Y., Kang, S. A., Kuehl, W. M., Gray, N. S. & Sabatini, D. M. (2009) DEPTOR is an mTOR inhibitor frequently overexpressed in multiple myeloma cells and required for their survival. *Cell*, 137(5), 873-86.

Pfluger, P. T., Kabra, D. G., Aichler, M., Schriever, S. C., Pfuhlmann, K., Garcia, V. C., Lehti, M., Weber, J., Kutschke, M., Rozman, J., Elrod, J. W., Hevener, A. L., Feuchtinger, A., Hrabe de Angelis, M., Walch, A., Rollmann, S. M., Aronow, B. J., Muller, T. D., Perez-Tilve, D., Jastroch, M., De Luca, M., Molkentin, J. D. & Tschop, M. H. (2015) Calcineurin Links Mitochondrial Elongation with Energy Metabolism. *Cell Metab*, 22(5), 838-50.

Phillips, T. & Leeuwenburgh, C. (2005) Muscle fiber specific apoptosis and TNF-alpha signaling in sarcopenia are attenuated by life-long calorie restriction. *FASEB J*, 19(6), 668-70.

Picard, M., White, K. & Turnbull, D. M. (2013) Mitochondrial morphology, topology, and membrane interactions in skeletal muscle: a quantitative three-dimensional electron microscopy study. *J Appl Physiol (1985)*, 114(2), 161-71.

Piccio, L., Stark, J. L. & Cross, A. H. (2008) Chronic calorie restriction attenuates experimental autoimmune encephalomyelitis. *J Leukoc Biol*, 84(4), 940-8.

Powers, R. W., 3rd, Kaeberlein, M., Caldwell, S. D., Kennedy, B. K. & Fields, S. (2006) Extension of chronological life span in yeast by decreased TOR pathway signaling. *Genes Dev*, 20(2), 174-84.

Powers, S. K., Ji, L. L., Kavazis, A. N. & Jackson, M. J. (2011) Reactive oxygen species: impact on skeletal muscle. *Compr Physiol*, 1(2), 941-69.

Prins, D. & Michalak, M. (2011) Organellar calcium buffers. *Cold Spring Harb Perspect Biol*, 3(3).

Rabanal-Ruiz, Y., Otten, E. G. & Korolchuk, V. I. (2017) mTORC1 as the main gateway to autophagy. *Essays Biochem*, 61(6), 565-584.

Radak, Z., Chung, H. Y., Koltai, E., Taylor, A. W. & Goto, S. (2008) Exercise, oxidative stress and hormesis. *Ageing Res Rev*, 7(1), 34-42.

Rakus, D., Gizak, A., Deshmukh, A. & Wisniewski, J. R. (2015) Absolute quantitative profiling of the key metabolic pathways in slow and fast skeletal muscle. *J Proteome Res*, 14(3), 1400-11.

Rambold, A. S., Cohen, S. & Lippincott-Schwartz, J. (2015) Fatty acid trafficking in starved cells: regulation by lipid droplet lipolysis, autophagy, and mitochondrial fusion dynamics. *Dev Cell*, 32(6), 678-92.

Ranieri, M., Brajkovic, S., Riboldi, G., Ronchi, D., Rizzo, F., Bresolin, N., Corti, S. & Comi, G. P. (2013) Mitochondrial fusion proteins and human diseases. *Neurol Res Int*, 2013, 293893.

Ravel-Chapuis, A., Belanger, G., Cote, J., Michel, R. N. & Jasmin, B. J. (2017) Misregulation of calcium-handling proteins promotes hyperactivation of calcineurin-NFAT signaling in skeletal muscle of DM1 mice. *Hum Mol Genet*, 26(12), 2192-2206.

Rebsamen, M., Pochini, L., Stasyk, T., de Araujo, M. E., Galluccio, M., Kandasamy, R. K., Snijder, B., Fauster, A., Rudashevskaya, E. L., Bruckner, M., Scorzoni, S., Filipek, P. A., Huber, K. V., Bigenzahn, J. W., Heinz, L. X., Kraft, C., Bennett, K. L., Indiveri, C., Huber, L. A. & Superti-Furga, G. (2015) SLC38A9 is a component of the lysosomal amino acid sensing machinery that controls mTORC1. *Nature*, 519(7544), 477-81.

Redman, L. M., Heilbronn, L. K., Martin, C. K., Alfonso, A., Smith, S. R., Ravussin, E. & Pennington, C. T. (2007) Effect of calorie restriction with or without exercise on body composition and fat distribution. *J Clin Endocrinol Metab*, 92(3), 865-72.

Redman, L. M., Martin, C. K., Williamson, D. A. & Ravussin, E. (2008) Effect of caloric restriction in non-obese humans on physiological, psychological and behavioral outcomes. *Physiol Behav*, 94(5), 643-8.

Redza-Dutordoir, M. & Averill-Bates, D. A. (2016) Activation of apoptosis signalling pathways by reactive oxygen species. *Biochim Biophys Acta*, 1863(12), 2977-2992.

Ribas, V., Garcia-Ruiz, C. & Fernandez-Checa, J. C. (2014) Glutathione and mitochondria. *Front Pharmacol*, 5, 151.

Rice, K. M. & Blough, E. R. (2006) Sarcopenia-related apoptosis is regulated differently in fast- and slow-twitch muscles of the aging F344/N x BN rat model. *Mech Ageing Dev*, 127(8), 670-9.

Rios, E. & Brum, G. (1987) Involvement of dihydropyridine receptors in excitation-contraction coupling in skeletal muscle. *Nature*, 325(6106), 717-20.

Robert, V., Massimino, M. L., Tosello, V., Marsault, R., Cantini, M., Sorrentino, V. & Pozzan, T. (2001) Alteration in calcium handling at the subcellular level in mdx myotubes. *J Biol Chem*, 276(7), 4647-51.

Robertson, L. T. & Mitchell, J. R. (2013) Benefits of short-term dietary restriction in mammals. *Exp Gerontol*, 48(10), 1043-8.

Robin, G. & Allard, B. (2012) Dihydropyridine receptors actively control gating of ryanodine receptors in resting mouse skeletal muscle fibres. *J Physiol*, 590(23), 6027-36.

Rocha, A. G., Franco, A., Krezel, A. M., Rumsey, J. M., Alberti, J. M., Knight, W. C., Biris, N., Zacharioudakis, E., Janetka, J. W., Baloh, R. H., Kitsis, R. N., Mochly-Rosen, D., Townsend, R. R., Gavathiotis, E. & Dorn, G. W., 2nd (2018) MFN2 agonists reverse mitochondrial defects in preclinical models of Charcot-Marie-Tooth disease type 2A. *Science*, 360(6386), 336-341.

Rochon, J., Bales, C. W., Ravussin, E., Redman, L. M., Holloszy, J. O., Racette, S. B., Roberts, S. B., Das, S. K., Romashkan, S., Galan, K. M., Hadley, E. C., Kraus, W. E. & Group, C. S. (2011) Design and conduct of the CALERIE study: comprehensive assessment of the long-term effects of reducing intake of energy. *J Gerontol A Biol Sci Med Sci*, 66(1), 97-108.

Romanello, V., Guadagnin, E., Gomes, L., Roder, I., Sandri, C., Petersen, Y., Milan, G., Masiero, E., Del Piccolo, P., Foretz, M., Scorrano, L., Rudolf, R. & Sandri, M. (2010) Mitochondrial fission and remodelling contributes to muscle atrophy. *EMBO J*, 29(10), 1774-85.

Romanello, V. & Sandri, M. (2015) Mitochondrial Quality Control and Muscle Mass Maintenance. *Front Physiol*, 6, 422.

Romanino, K., Mazelin, L., Albert, V., Conjard-Duplany, A., Lin, S., Bentzinger, C. F., Handschin, C., Puigserver, P., Zorzato, F., Schaeffer, L., Gangloff, Y. G. & Ruegg, M. A. (2011) Myopathy caused by mammalian target of rapamycin complex 1 (mTORC1)

inactivation is not reversed by restoring mitochondrial function. *Proc Natl Acad Sci U S A*, 108(51), 20808-13.
Rosenberg, H., Pollock, N., Schiemann, A., Bulger, T. & Stowell, K. (2015) Malignant hyperthermia: a review. *Orphanet J Rare Dis*, 10, 93.
Rusecka, J., Kaliszewska, M., Bartnik, E. & Tonska, K. (2018) Nuclear genes involved in mitochondrial diseases caused by instability of mitochondrial DNA. *J Appl Genet*, 59(1), 43-57.
Russell, A. P., Foletta, V. C., Snow, R. J. & Wadley, G. D. (2014) Skeletal muscle mitochondria: a major player in exercise, health and disease. *Biochim Biophys Acta*, 1840(4), 1276-84.
Russell, D. M., Atwood, H. L., Whittaker, J. S., Itakura, T., Walker, P. M., Mickle, D. A. & Jeejeebhoy, K. N. (1984) The effect of fasting and hypocaloric diets on the functional and metabolic characteristics of rat gastrocnemius muscle. *Clin Sci (Lond)*, 67(2), 185-94.
Safdar, A., Little, J. P., Stokl, A. J., Hettinga, B. P., Akhtar, M. & Tarnopolsky, M. A. (2011) Exercise increases mitochondrial PGC-1alpha content and promotes nuclear-mitochondrial cross-talk to coordinate mitochondrial biogenesis. *J Biol Chem*, 286(12), 10605-17.
Sakuma, K., Aoi, W. & Yamaguchi, A. (2014) The intriguing regulators of muscle mass in sarcopenia and muscular dystrophy. *Front Aging Neurosci*, 6, 230.
Sakuma, K., Nishikawa, J., Nakao, R., Watanabe, K., Totsuka, T., Nakano, H., Sano, M. & Yasuhara, M. (2003) Calcineurin is a potent regulator for skeletal muscle regeneration by association with NFATc1 and GATA-2. *Acta Neuropathol*, 105(3), 271-80.
Sakuma, K. & Yamaguchi, A. (2010) The functional role of calcineurin in hypertrophy, regeneration, and disorders of skeletal muscle. *J Biomed Biotechnol*, 2010, 721219.
Sancak, Y., Thoreen, C. C., Peterson, T. R., Lindquist, R. A., Kang, S. A., Spooner, E., Carr, S. A. & Sabatini, D. M. (2007) PRAS40 is an insulin-regulated inhibitor of the mTORC1 protein kinase. *Mol Cell*, 25(6), 903-15.
Sandow, A. (1952) Excitation-contraction coupling in muscular response. *Yale J Biol Med*, 25(3), 176-201.
Sandri, M. (2010) Autophagy in skeletal muscle. *FEBS Lett*, 584(7), 1411-6.
Sanz, A., Caro, P. & Barja, G. (2004) Protein restriction without strong caloric restriction decreases mitochondrial oxygen radical production and oxidative DNA damage in rat liver. *J Bioenerg Biomembr*, 36(6), 545-52.
Sardiello, M., Palmieri, M., di Ronza, A., Medina, D. L., Valenza, M., Gennarino, V. A., Di Malta, C., Donaudy, F., Embrione, V., Polishchuk, R. S., Banfi, S., Parenti, G., Cattaneo, E. & Ballabio, A. (2009) A gene network regulating lysosomal biogenesis and function. *Science*, 325(5939), 473-7.
Saucerman, J. J. & Bers, D. M. (2008) Calmodulin mediates differential sensitivity of CaMKII and calcineurin to local Ca2+ in cardiac myocytes. *Biophys J*, 95(10), 4597-612.
Saxton, R. A. & Sabatini, D. M. (2017) mTOR Signaling in Growth, Metabolism, and Disease. *Cell*, 168(6), 960-976.
Schiaffino, S. & Reggiani, C. (2011) Fiber types in mammalian skeletal muscles. *Physiol Rev*, 91(4), 1447-531.
Schieke, S. M., Phillips, D., McCoy, J. P., Jr., Aponte, A. M., Shen, R. F., Balaban, R. S. & Finkel, T. (2006) The mammalian target of rapamycin (mTOR) pathway regulates mitochondrial oxygen consumption and oxidative capacity. *J Biol Chem*, 281(37), 27643-52.
Schwaller, B. (2010) Cytosolic Ca2+ buffers. *Cold Spring Harb Perspect Biol*, 2(11), a004051.
Schwaller, B., Dick, J., Dhoot, G., Carroll, S., Vrbova, G., Nicotera, P., Pette, D., Wyss, A., Bluethmann, H., Hunziker, W. & Celio, M. R. (1999) Prolonged contraction-relaxation cycle of fast-twitch muscles in parvalbumin knockout mice. *Am J Physiol*, 276(2 Pt 1), C395-403.
Scott, I. & Youle, R. J. (2010) Mitochondrial fission and fusion. *Essays Biochem*, 47, 85-98.

Selsby, J. T., Morine, K. J., Pendrak, K., Barton, E. R. & Sweeney, H. L. (2012) Rescue of dystrophic skeletal muscle by PGC-1alpha involves a fast to slow fiber type shift in the mdx mouse. *PLoS One*, 7(1), e30063.

Semsarian, C., Wu, M. J., Ju, Y. K., Marciniec, T., Yeoh, T., Allen, D. G., Harvey, R. P. & Graham, R. M. (1999) Skeletal muscle hypertrophy is mediated by a Ca2+-dependent calcineurin signalling pathway. *Nature*, 400(6744), 576-81.

Sena, L. A. & Chandel, N. S. (2012) Physiological roles of mitochondrial reactive oxygen species. *Mol Cell*, 48(2), 158-67.

Settembre, C., Di Malta, C., Polito, V. A., Garcia Arencibia, M., Vetrini, F., Erdin, S., Erdin, S. U., Huynh, T., Medina, D., Colella, P., Sardiello, M., Rubinsztein, D. C. & Ballabio, A. (2011) TFEB links autophagy to lysosomal biogenesis. *Science*, 332(6036), 1429-33.

Shaw, J. P., Utz, P. J., Durand, D. B., Toole, J. J., Emmel, E. A. & Crabtree, G. R. (1988) Identification of a putative regulator of early T cell activation genes. *Science*, 241(4862), 202-5.

Shaw, R. J., Bardeesy, N., Manning, B. D., Lopez, L., Kosmatka, M., DePinho, R. A. & Cantley, L. C. (2004) The LKB1 tumor suppressor negatively regulates mTOR signaling. *Cancer Cell*, 6(1), 91-9.

Shepherd, R. K., Checcarelli, N., Naini, A., De Vivo, D. C., DiMauro, S. & Sue, C. M. (2006) Measurement of ATP production in mitochondrial disorders. *J Inherit Metab Dis*, 29(1), 86-91.

Shimobayashi, M. & Hall, M. N. (2016) Multiple amino acid sensing inputs to mTORC1. *Cell Res*, 26(1), 7-20.

Shkryl, V. M., Martins, A. S., Ullrich, N. D., Nowycky, M. C., Niggli, E. & Shirokova, N. (2009) Reciprocal amplification of ROS and Ca(2+) signals in stressed mdx dystrophic skeletal muscle fibers. *Pflugers Arch*, 458(5), 915-28.

Sousa, J. S., D'Imprima, E. & Vonck, J. (2018) Mitochondrial Respiratory Chain Complexes. *Subcell Biochem*, 87, 167-227.

Stankovic, M., Mladenovic, D., Ninkovic, M., Vucevic, D., Tomasevic, T. & Radosavljevic, T. (2013) Effects of caloric restriction on oxidative stress parameters. *Gen Physiol Biophys*, 32(2), 277-83.

Stojanovski, D., Koutsopoulos, O. S., Okamoto, K. & Ryan, M. T. (2004) Levels of human Fis1 at the mitochondrial outer membrane regulate mitochondrial morphology. *J Cell Sci*, 117(Pt 7), 1201-10.

Stull, J. T., Kamm, K. E. & Vandenboom, R. (2011) Myosin light chain kinase and the role of myosin light chain phosphorylation in skeletal muscle. *Arch Biochem Biophys*, 510(2), 120-8.

Stupka, N., Plant, D. R., Schertzer, J. D., Emerson, T. M., Bassel-Duby, R., Olson, E. N. & Lynch, G. S. (2006) Activated calcineurin ameliorates contraction-induced injury to skeletal muscles of mdx dystrophic mice. *J Physiol*, 575(Pt 2), 645-56.

Stupka, N., Schertzer, J. D., Bassel-Duby, R., Olson, E. N. & Lynch, G. S. (2008) Stimulation of calcineurin Aalpha activity attenuates muscle pathophysiology in mdx dystrophic mice. *Am J Physiol Regul Integr Comp Physiol*, 294(3), R983-92.

Summermatter, S., Baum, O., Santos, G., Hoppeler, H. & Handschin, C. (2010) Peroxisome proliferator-activated receptor {gamma} coactivator 1{alpha} (PGC-1{alpha}) promotes skeletal muscle lipid refueling in vivo by activating de novo lipogenesis and the pentose phosphate pathway. *J Biol Chem*, 285(43), 32793-800.

Talmadge, R. J., Otis, J. S., Rittler, M. R., Garcia, N. D., Spencer, S. R., Lees, S. J. & Naya, F. J. (2004) Calcineurin activation influences muscle phenotype in a muscle-specific fashion. *BMC Cell Biol*, 5, 28.

Tarnopolsky, M. A. (2016) Metabolic Myopathies. *Continuum (Minneap Minn)*, 22(6, Muscle and Neuromuscular Junction Disorders), 1829-1851.

Tee, A. R., Manning, B. D., Roux, P. P., Cantley, L. C. & Blenis, J. (2003) Tuberous sclerosis complex gene products, Tuberin and Hamartin, control mTOR signaling by acting as a GTPase-activating protein complex toward Rheb. *Curr Biol*, 13(15), 1259-68.

Thedieck, K., Polak, P., Kim, M. L., Molle, K. D., Cohen, A., Jeno, P., Arrieumerlou, C. & Hall, M. N. (2007) PRAS40 and PRR5-like protein are new mTOR interactors that regulate apoptosis. *PLoS One*, 2(11), e1217.

Tipton, K. D., Hamilton, D. L. & Gallagher, I. J. (2018) Assessing the Role of Muscle Protein Breakdown in Response to Nutrition and Exercise in Humans. *Sports Med*, 48(Suppl 1), 53-64.

Treves, S., Jungbluth, H., Muntoni, F. & Zorzato, F. (2008) Congenital muscle disorders with cores: the ryanodine receptor calcium channel paradigm. *Curr Opin Pharmacol*, 8(3), 319-26.

Usuki, F., Yasutake, A., Umehara, F. & Higuchi, I. (2004) Beneficial effects of mild lifelong dietary restriction on skeletal muscle: prevention of age-related mitochondrial damage, morphological changes, and vulnerability to a chemical toxin. *Acta Neuropathol*, 108(1), 1-9.

Vallejo-Illarramendi, A., Toral-Ojeda, I., Aldanondo, G. & de Munain, A. L. (2014) Dysregulation of calcium homeostasis in muscular dystrophies. *Expert Reviews in Molecular Medicine*, 16.

Vander Haar, E., Lee, S. I., Bandhakavi, S., Griffin, T. J. & Kim, D. H. (2007) Insulin signalling to mTOR mediated by the Akt/PKB substrate PRAS40. *Nat Cell Biol*, 9(3), 316-23.

Ventura-Clapier, R., Garnier, A. & Veksler, V. (2008) Transcriptional control of mitochondrial biogenesis: the central role of PGC-1alpha. *Cardiovasc Res*, 79(2), 208-17.

Verweij, M., van Ginhoven, T. M., Mitchell, J. R., Sluiter, W., van den Engel, S., Roest, H. P., Torabi, E., Ijzermans, J. N., Hoeijmakers, J. H. & de Bruin, R. W. (2011) Preoperative fasting protects mice against hepatic ischemia/reperfusion injury: mechanisms and effects on liver regeneration. *Liver Transpl*, 17(6), 695-704.

Vogel, H. (2001) Mitochondrial myopathies and the role of the pathologist in the molecular era. *J Neuropathol Exp Neurol*, 60(3), 217-27.

Webster, C., Silberstein, L., Hays, A. P. & Blau, H. M. (1988) Fast muscle fibers are preferentially affected in Duchenne muscular dystrophy. *Cell*, 52(4), 503-13.

Wei, L., Varsanyi, M., Dulhunty, A. F. & Beard, N. A. (2006) The conformation of calsequestrin determines its ability to regulate skeletal ryanodine receptors. *Biophys J*, 91(4), 1288-301.

Weidberg, H., Shpilka, T., Shvets, E., Abada, A., Shimron, F. & Elazar, Z. (2011) LC3 and GATE-16 N termini mediate membrane fusion processes required for autophagosome biogenesis. *Dev Cell*, 20(4), 444-54.

Weindruch, R., Walford, R. L., Fligiel, S. & Guthrie, D. (1986) The retardation of aging in mice by dietary restriction: longevity, cancer, immunity and lifetime energy intake. *J Nutr*, 116(4), 641-54.

Westerblad, H., Bruton, J. D. & Katz, A. (2010) Skeletal muscle: energy metabolism, fiber types, fatigue and adaptability. *Exp Cell Res*, 316(18), 3093-9.

Westermann, B. (2012) Bioenergetic role of mitochondrial fusion and fission. *Biochim Biophys Acta*, 1817(10), 1833-8.

Wheeler, D. G., Barrett, C. F., Groth, R. D., Safa, P. & Tsien, R. W. (2008) CaMKII locally encodes L-type channel activity to signal to nuclear CREB in excitation-transcription coupling. *J Cell Biol*, 183(5), 849-63.

Winey, M., Meehl, J. B., O'Toole, E. T. & Giddings, T. H., Jr. (2014) Conventional transmission electron microscopy. *Mol Biol Cell*, 25(3), 319-23.

Wolfson, R. L., Chantranupong, L., Saxton, R. A., Shen, K., Scaria, S. M., Cantor, J. R. & Sabatini, D. M. (2016) Sestrin2 is a leucine sensor for the mTORC1 pathway. *Science*, 351(6268), 43-8.

Xu, J., Ji, J. & Yan, X. H. (2012) Cross-talk between AMPK and mTOR in regulating energy balance. *Crit Rev Food Sci Nutr*, 52(5), 373-81.

Yang, L., Licastro, D., Cava, E., Veronese, N., Spelta, F., Rizza, W., Bertozzi, B., Villareal, D. T., Hotamisligil, G. S., Holloszy, J. O. & Fontana, L. (2016) Long-Term Calorie Restriction Enhances Cellular Quality-Control Processes in Human Skeletal Muscle. *Cell Rep*, 14(3), 422-428.

Yoshida, M., Minamisawa, S., Shimura, M., Komazaki, S., Kume, H., Zhang, M., Matsumura, K., Nishi, M., Saito, M., Saeki, Y., Ishikawa, Y., Yanagisawa, T. & Takeshima, H. (2005) Impaired Ca2+ store functions in skeletal and cardiac muscle cells from sarcalumenin-deficient mice. *J Biol Chem*, 280(5), 3500-6.

Youle, R. J. & van der Bliek, A. M. (2012) Mitochondrial fission, fusion, and stress. *Science*, 337(6098), 1062-5.

Yu, B. P. & Chung, H. Y. (2001) Stress resistance by caloric restriction for longevity. *Ann N Y Acad Sci*, 928, 39-47.

Zhao, H., Tang, M., Liu, M. & Chen, L. (2018) Glycophagy: An emerging target in pathology. *Clin Chim Acta*, 484, 298-303.

Zhi, G., Ryder, J. W., Huang, J., Ding, P., Chen, Y., Zhao, Y., Kamm, K. E. & Stull, J. T. (2005) Myosin light chain kinase and myosin phosphorylation effect frequency-dependent potentiation of skeletal muscle contraction. *Proc Natl Acad Sci U S A*, 102(48), 17519-24.

Zorov, D. B., Juhaszova, M. & Sollott, S. J. (2014) Mitochondrial reactive oxygen species (ROS) and ROS-induced ROS release. *Physiol Rev*, 94(3), 909-50.

Zuchner, S., Mersiyanova, I. V., Muglia, M., Bissar-Tadmouri, N., Rochelle, J., Dadali, E. L., Zappia, M., Nelis, E., Patitucci, A., Senderek, J., Parman, Y., Evgrafov, O., Jonghe, P. D., Takahashi, Y., Tsuji, S., Pericak-Vance, M. A., Quattrone, A., Battaloglu, E., Polyakov, A. V., Timmerman, V., Schroder, J. M. & Vance, J. M. (2004) Mutations in the mitochondrial GTPase mitofusin 2 cause Charcot-Marie-Tooth neuropathy type 2A. *Nat Genet*, 36(5), 449-51.